# SHEAR STRENGTH ASSESSMENT OF A MANUFACTURED WELL-GRADED SAND

**by**

© Riju Chandra Saha

A Thesis Submitted to the

School of Graduate Studies

In partial fulfillment of the requirements for the degree of

**Master of Engineering**

**Faculty of Engineering and Applied Science**

Memorial University of Newfoundland

**January 2021**

St. John's Newfoundland and Labrador Canada

## ABSTRACT

Granular materials, such as sand, are commonly used to backfill buried structures due to its free-draining property and higher shearing resistance. Conventional analysis of soil-structure interaction is performed assuming soil parameters based on typical values available in published literature. Most of the soil parameters available in the literature were obtained from various laboratory tests with standard and natural soils. However, the use of natural soil is gradually decreasing due to the scarcity of material and environmental considerations. Engineers often require replacing natural sand with locally manufactured sand as a backfill material for buried structures. This thesis presents a laboratory investigation of the strength and deformation behavior of a locally manufactured sand which is classified as well-graded clean sand. Considering the various factors on which the strength parameters of soil depend, a series of direct shear tests and triaxial tests are performed with varying density, normal stress, moisture content, shear displacement rate. As the soil used as a backfill for the buried structure is usually moist (unsaturated), the entire test program focuses on investigating the behavior of moist sand. The conventional test apparatus is used in this study as the special apparatus typical used in the research with unsaturated soil is not readily available to the practicing engineer. The study reveals that the conventional test apparatus can reasonably be used to estimate the design parameters for moist sand. For the manufactured sand used in this study, the effect of capillary suction on the shear strength parameters is found to be less significant. While the strength parameters depend on the degree of saturation, these depend extensively on the dry density of the soil with a higher angle of internal friction for the soil with higher dry density.

## ACKNOWLEDGMENTS

First of all, I would like to thank the Almighty God for giving me the opportunity to be a part of the geotechnical research group at the Memorial University of Newfoundland. I have interacted with several individuals who contributed to my research throughout my master's program. It is my opportunity to acknowledge them.

I would like to express my utmost gratitude to my supervisor Dr. Ashutosh Sutra Dhar, for his continuous guidance, support. His technical skill and personal experience made me able to think reasonably about geotechnical problems. I would also like to express my sincere gratitude to Dr. Bipul Hawlader for sharing his geotechnical expertise. I am also thankful to him for the opportunity to explore geotechnical engineering through his 'Soil Properties and Behavior' course, which was instrumental for the success of this research.

I highly appreciate the laboratory support given by Anup Fouzder, Mahmud Amer Al Tarhouni, lab technologist, especially Shawn Organ, and my research groupmates Auchib Reza, Suprio Das, Sudipta Chakraborty, and Tanmoy Sinha. I am also thankful to my friend Rayhan Bin Ahmed for providing me moral support throughout my research period.

I gratefully acknowledge the financial support provided by the Collaborative Research and Development Grant program of the Natural Science and Engineering Research Council of Canada, Innovate NL program of the Government of Newfoundland and Labrador, Fortis BC Energy Inc., and the School of Graduate Studies of Memorial University.

Finally, I am greatly indebted to my parents for their unconditional support and continuous encouragement to overcome the hardship of these two years of my graduate study.

## Table of Contents

## List of Figures

## List of Tables

## List of Symbols

$\sigma$ normal stress

$\tau$ shear stress

$\sigma'$ effective normal stress

$c'$ effective cohesion

$\emptyset'$ effective angle of internal friction

$u_w$ pore water pressure

$\sigma_1'$ major principal effective stresses

$\sigma_3'$ minor principal effective stresses

$\emptyset_p$ peak shearing resistance

$\emptyset_\mu$ interparticle sliding resistance at contact

$\emptyset_f$ resistance against particle crushing and rearrangement

$\emptyset_{cv}$ shearing resistance at constant volume

$\psi_{max}$ maximum dilatancy angle

$p'$ mean effective stress

$e$ void ratio

$D_r$ relative density

$(\sigma - u_a)$ net normal stress

$u_a$ pore air pressure

$(u_a - u_w)$ matric suction

$\chi$ effective stress parameter

$\sigma_s$ suction stress

$G_s$ specific gravity of soil particles

$\theta$ volumetric water content

$\theta_s$ saturated volumetric water content

$\alpha$ air entry value

$D_{50}$ mean particle size

$C_u$ coefficient of uniformity

$C_c$ coefficient of curvature

# CHAPTER 1 Introduction

## 1.1 Background and Motivation

The selection of backfill material is an important design consideration for buried structures. The granular material is considered more suitable than the cohesive material as the backfill material for buried structures (Zornberg and Mitchell 1994). As the most granular materials have adequate porosity to allow water to flow, these drain more freely than cohesive materials (Selig 1990). As a result, pore water pressure cannot build up within the soil and around the structures. However, natural sources of granular materials are dwindling worldwide due to extensive construction activities using these materials. Besides, suitable granular materials are sometimes not available near the construction sites, requiring importing materials from different areas. Importing materials can increase construction costs significantly. To limit the construction cost, coarse-grained materials manufactured through mechanically crushing rocks are being used in various construction works. However, the behaviors of the manufactured granular materials are not well-known.

The stability of buried structures is controlled by soil-structure interaction, where the soil surrounding the structures plays a vital role. The mechanical behavior of the soil and the structural material is required for investigating the soil-structure interaction. While the strength and deformation behaviors of structural materials, such as concrete, metal, plastic, etc., can be reasonably predicted using well-defined tests, the complex nature of soil makes it difficult to predict the behaviors accurately. The soil properties are generally estimated

based on information available in published literature for soil-structure interaction analysis (Cheuk et al. 2008; Jung et al. 2013; Roy et al. 2016). However, the studies using different soil models often provide significantly different behavior of the structures, demonstrating the need for correctly modeling the soil behavior. Researchers employed different types of laboratory tests such as direct shear tests, triaxial tests, simple shear tests, etc., for determining soil parameters specific to the problems. Most of the test results available in the literature are for standard sands, such as silica sand, Fraser River Sand, Chiba sand, Cornell sand, RMS graded sand, and others (Robert 2017; Weerasekara 2011). The data on the strength and deformation of sand locally manufactured through the crushing of rocks is very limited.

On the other hand, the shear strength of the soil is conventionally assessed using the Mohr-Coulomb theory, assuming the soil as saturated or dry (for coarse-grained soil) condition. However, the soil around structures buried at shallow depth is typically moist and unsaturated. Therefore, the application of the parameters from conventional tests for assessing soil-pipeline interaction in moist and unsaturated soil may lead to erroneous results. Jung et al. (2006) and Al-Khazaali and Vanapalli (2019) revealed that the axial pullout force of pipe in unsaturated sand could be higher than that in saturated sand. Large scale experiments on soil-pipeline interaction conducted with Cornell sand and Tokyo gas sand also suggests that the variation of moisture content of the soil around the pipelines should be taken into consideration as the presence of moisture affects strength parameters of soil and soil-pipeline interaction (Robert 2010). To deal with the unsaturated soil, researchers employed different methods through modification of conventional direct shear

or triaxial test apparatus for testing of moist sands. This approach is usually complicated and time-consuming yet not flawless (Bai and Liu 2012; Al-Khazaali and Vanapalli 2019). Besides, the specialized equipment used in the research for unsaturated soil is usually not available in the geotechnical engineering laboratories commonly used in engineering practice.

The motivation of the current study is to address the limitations identified above and investigate the strength and deformation behavior of a locally manufactured sand using conventional direct shear test and triaxial test apparatus.

## 1.2 Objectives and Scope

The overall objective of this research is to characterize the strength and deformation behavior of a locally manufactured sand under various conditions using the conventional test apparatus. The specific objectives of the study are to:

- Develop shear strength parameters for a well-graded manufactured sand under dry, saturated, and unsaturated (moist) conditions.
- Interpretation of the behavior of unsaturated sand using laboratory tests conducted using the conventional test apparatus.
- Examine variation of strength parameters of sand under various conditions, including test types, stress levels, moisture contents, densities, and loading rates.
- Validate the behavior of the manufactured sand through comparison with standard silica sand.

The research objectives are achieved through the following activities.

- Conduct a series of direct shear tests on samples of a manufactured sand and a standard silica sand with various moisture conditions, including dry conditions, various stress levels, various densities, and various shear displacement rates.
- Compare the shear strength and deformation behaviors of the manufactured sand with those for the silica sand using the results from the direct shear tests.
- Conduct a series of triaxial tests on the manufactured sand under saturated and unsaturated conditions with various moisture contents.

### 1.3 Thesis Framework

The outcome of this research is presented in this thesis in five chapters.

**Chapter 1** presents the background of the problem, objectives, and significant contributions to the research work.

**Chapter 2** is a literature review that presents theoretical aspects of the shear strength of sand and previous studies on the shear strength assessment of saturated and unsaturated soils.

**Chapter 3** presents the details of the direct shear testing program undertaken along with findings. Some part of the work presented in this chapter has been published as two conference papers: one in the CSCE Annual Conference held at Laval, (Greater Montreal), Canada on June 12–14, 2019, and the other in the 72$^{nd}$ Canadian geotechnical conference held at St. John's, Newfoundland, Canada on September 29–October 2, 2019.

**Chapter 4** presents the details of the triaxial testing program. A version of the chapter has been published in the 73rd Canadian geotechnical conference, held virtually on September 13–16, 2020.

**Chapter 5** presents a comparative study of the direct shear test and triaxial test to investigate the effect of moisture on the shear strength parameter at constant densities.

**Chapter 6** presents the overall summary of the study with recommendations and suggestions for future works.

### 1.4 Significant Contributions

Various aspects of a manufactured sand are investigated in this research. The following presents a list of contributions to the behavior of the sand that resulted from the study.

- Determined the shear strength parameters and deformation behavior of a manufactured sand.
- Identified a methodology to determine the shear strength parameter for partially saturated sand using conventional direct shear and triaxial equipment.
- Identified the difference in the behavior of the manufactured sand and a standard silica sand.

**Conference Papers**

- Saha, R. C., Dhar, A. S., Muntakim, A. H., and Hawlader, B.C. 2019. Strength and Deformation Behaviour of a Local Sand. CSCE Annual Conference, Laval, (Greater Montreal), Canada, June 12–14.
- Saha, R. C., Dhar, A. S., and Hawlader, B.C. 2019. Shear Strength Assessment of a Well-Graded Clean Sand. 72nd Canadian Geotechnical Conference, St. John's, Newfoundland, September 29–October 2.
- Saha, R. C., Dhar, A. S., and Hawlader, B.C. 2020. "Assessment of shear strength parameters of moist sand using triaxial tests." 73rd Canadian Geotechnical Conference (GeoVirtual2020), September 13–16.

## 1.5 Co-Authorships

All the research presented in the conference papers has been conducted by the author of this thesis, Riju Chandra Saha, under the supervision of Dr. Ashutosh Dhar. The first draft of the manuscript is also prepared by Riju Chandra Saha, and subsequently revised based on the co-authors' feedback and the peer-review process.

## 1.6 References

Al-Khazaali, M., and Vanapalli, S. K. 2019. "Axial Force-Displacement Behaviour of a Buried Pipeline in Saturated and Unsaturated Sand." *Geotechnique* 69 (11): 986–1003. https://doi.org/10.1680/jgeot.17.P.116.

Bai, F. Q., and Liu, S. H. 2012. “Measurement of the Shear Strength of an Expansive Soil by Combining a Filter Paper Method and Direct Shear Tests.” *Geotechnical Testing Journal* 35 (3): 451–459. https://doi.org/10.1520/GTJ103342.

Cheuk, C Y., White, D.J., and Bolton, M. D. 2008. “Uplift Mechanisms of Pipes Buried in Sand.” *Journal of Geotechnical and Geoenvironmental Engineering* 134 (2).

Jung, J. K., O’Rourke, T. D., and Olson, N. A. 2013. “Lateral Soil-Pipe Interaction in Dry and Partially Saturated Sand.” *Journal of Geotechnical and Geoenvironmental Engineering* 139 (12).

Robert, D. 2010. “Soil–Pipeline Interaction in Unsaturated Soils.” The Doctoral Thesis. The University of Cambridge. https://doi.org/https://doi.org/10.17863/CAM.11686.

Robert, D. 2017. “A Modified Mohr-Coulomb Model to Simulate the Behavior of Pipelines in Unsaturated Soils.” *Computers and Geotechnics* 91: 146–160.

Roy, K., Hawlader, B., Kenny, S., and Moore, I. 2016. “Finite Element Modeling of Lateral Pipeline–Soil Interactions in Dense Sand.” *Canadian Geotechnical Journal* 53 (3): 490-504.

Selig, E.T. 1990. “Soil Properties for Plastic Pipe Installations.” In *Buried Plastic Pipe Technology*, edited by George S. Buczala and Michael J. Cassady, 141–158. West Conshohocken, PA: American Society for Testing and Materials.

Weerasekara, L. 2011. “Pipe-Soil Interaction Aspects in Buried Extensible Pipes.” The Doctoral Thesis. The University of British Columbia.

Zornberg, J.G., and Mitchell, J. K. 1994. “Reinforced Soil Structures with Poorly Draining Backfills. Part I: Reinforcement Interactions and Functions.” *Geosynthetics International* 1 (2): 103–147.

# CHAPTER 2 Literature Review

## 2.1 General

The variabilities of shear strength and deformation parameters of soil have inspired researchers to investigate the behavior of various soils under different conditions. Extensive experimental research was conducted in the past to understand soil behavior, and further research is still ongoing. Researchers have established different shear strength theories based on the conditions of the soil, whether it is saturated or unsaturated. Different correlations of the shear strength parameters with the factors affecting the shear strength parameters were developed, including test conditions, soil densities, confining pressures, moisture contents, particle sizes, strain rates, and others. This chapter provides an overview of the shear strength of soil, different shear strength theories, and experimental investigations conducted to assess the shear strength of the soil.

## 2.2 Shear Strength

The shear strength of the soil is generally expressed in terms of two basic parameters: cohesion and internal friction. The cohesion represents the contribution of interparticle attraction to the shear strength, which is independent of the normal stress. The internal friction represents the contribution of the interparticle friction, which depends on the normal stress.

## 2.3 Shear Strength Theory

The widely accepted theory for the strength assessment of soil is the Mohr-Coulomb failure criteria, which defines the shear strength on a slip plane as the sum of cohesion and a contribution of internal friction. This is expressed as a linear relationship (Eq. (2.1)) between normal stress ($\sigma$) and shear stress ($\tau$) at the failure plane (slip plane) with cohesion as the intercept on the shear stress axis and angle of internal friction ($\emptyset$) as the slope of failure envelope (Tinoco 1967).

$$\tau = c + \sigma \tan \emptyset \quad [2.1]$$

The shear strength and failure envelope of saturated soil are generally expressed in the effective stress framework (Eq. (2.2)), proposed by Terzaghi (1936).

$$\tau_f = c' + \sigma' \tan \emptyset' \quad [2.2]$$

where effective normal stress, $\sigma'$ is the difference between total normal stress ($\sigma$) and pore water pressure ($u_w$), $c'$ is the effective cohesion, and $\emptyset'$ is the effective angle of internal friction. The effective stress failure envelope (Eq. (2.2)) can be expressed in terms of the major ($\sigma_1'$) and minor ($\sigma_3'$) principal effective stresses as in Eq. (2.3).

$$\sigma_1' = \sigma_3' \tan^2(45° + \emptyset'/2) + 2c' \tan(45° + \emptyset'/2) \quad [2.3]$$

Figure 2-1 shows the Mohr-Coulomb failure line (failure envelope) in the effective stress framework for a soil element at failure under various levels of stresses shown using Mohr circles. The failure envelope is tangent to the Mohr circles, indicating different sets of major and minor principal stresses at the failure of the soil element. As seen in the figure, for higher minor principal stress, the diameter of the Mohr circle corresponding to failure

is larger, and the shear strength of the soil is higher. The difference between the major principal stress and the minor principal stress (i.e., the diameter of the Mohr circle) is termed as the deviatoric stress.

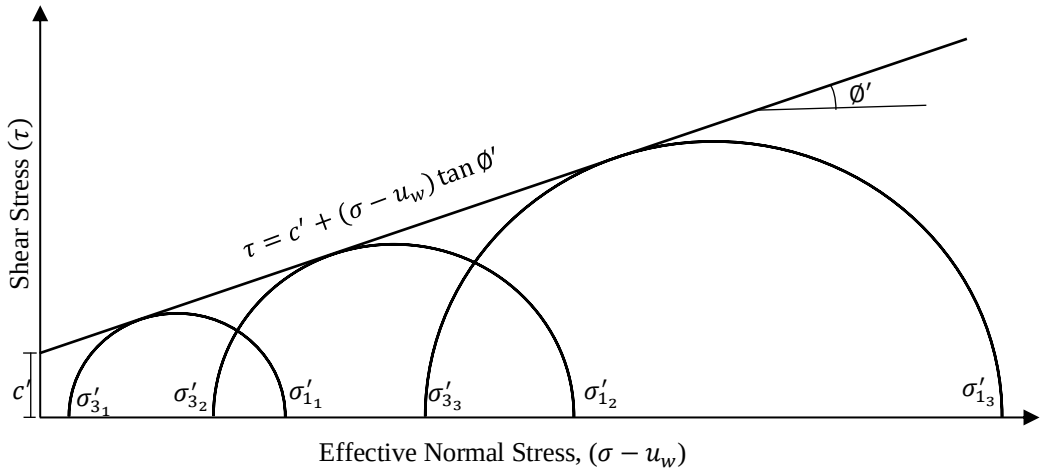


**Figure 2-1**: Mohr-Coulomb failure envelope for saturated soil

The effective cohesion for normally compacted saturated sand is zero, and the Mohr-Coulomb failure envelop passes through the origin in shear stress versus normal stress plot. The shear strength of the sand is mostly contributed by the interparticle friction, represented by the angle of internal friction. In conventional Mohr-Coulomb's theory, the angle of internal friction of soil is assumed to be constant independently of the stress level. However, it has been reported in the literature that the angle of internal friction depends on the stress levels and a few other factors. The effects of various factors such as mineralogy, grain size, grain shape, grain size distribution, density, stress state, stress path, drainage on the shear strength and deformation of soil were investigated by various researchers (Rowe 1962; Terzaghi et al. 1996; Marschi et al., 1972; Lade and Nam 2009; Lee and Seed 1967).

### 2.3.1 Influence of Particle Size

Some studies on the effects of particle size showed that the shear strength of soil increases with the increase of particle size (Kolbuszewski and Frederick 1963; Zolkov and Wiseman 1965). Contrary to these observations, Kirkpatric (1965) and Marschi et al. (1972) observed a decrease in shear strength with the increase in particle size. No significant influence of particle size on the shear strength of granular soils was found in Holtz and Gibbs (1956) and Selig and Roner (1987). Wang et al. (2013) conducted triaxial tests on five different gravel mixtures with a maximum particle size of 10 mm. They showed that the shearing resistance increases with an increase in mean particle size and gravel content.

### 2.3.2 Influence of Density and Stress

In general, the frictional resistance of soil is achieved from the interparticle rolling friction, interparticle sliding friction, and particle interlocking (Terzaghi et al. 1996). The interlocking necessitates volume expansion (dilatancy) for dense sand and grain fracture/crushing at high stresses. Figure 2-2 shows different mechanisms contributing to the angle of internal friction of sand (Rowe 1962). The figure shows that the peak shearing resistance ($\emptyset_p$) of dense sand is contributed by interparticle sliding resistance at contact ($\emptyset_\mu$), resistance against particle crushing and rearrangement ($\emptyset_f$), and dilation (expansion of volume) due to overriding of particle ($\psi$).

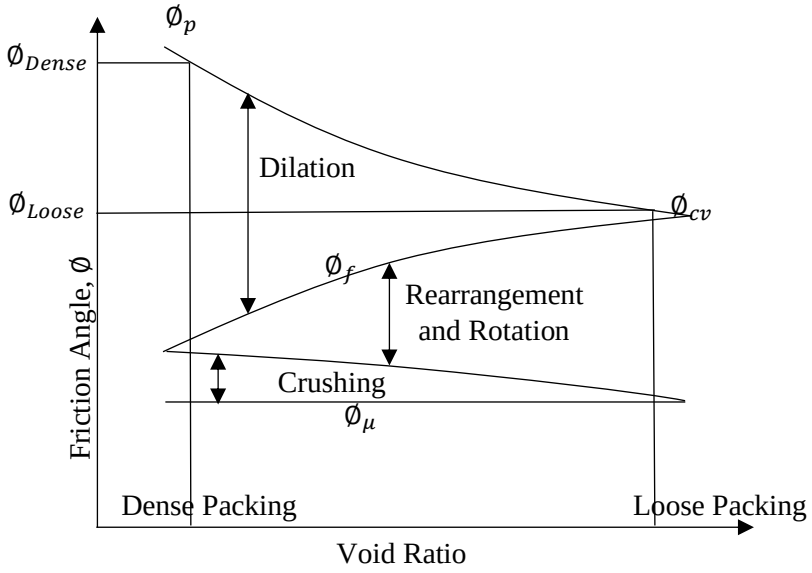


**Figure 2-2**: Components of friction angle (after Rowe 1962)

As seen in Figure 2-2, the peak friction angle decreases with the increase of void ratio (i.e., a decrease of density). In dense sand, the particles have a limited scope of particle rearrangement, and the particles are forced to overriding each other when subjected to shearing stress, which causes dilation. The dilation causes an increase in the angle of internal friction. A high void ratio (and low density) in loose sand allows the rearrangement of particles, causing contraction rather than dilation. The effects of dilation in dense sand diminish gradually with the decrease of density, and thus the angle of internal friction is reduced. The contribution of resistance against particle crushing to the angle of internal friction reduces with the decrease of the density of the soil.

The sand finally fails through shearing at a constant volume known as the "critical state". The frictional resistance at the critical state in dense sand is less than the peak frictional resistance, which occurs due to the effects of dilation. The contribution of the

dilation is not present in loose sand. Bolton (1986) established a correlation (Eq. (2.4)) among the peak frictional angle ($\emptyset_p$), critical state frictional angle ($\emptyset_{cv}$) and maximum dilatancy angle ($\psi_{max}$).

$$\emptyset_p - \emptyset_{cv} = \alpha\psi_{max} \begin{cases} \alpha = 0.8 \; for \; plane \; strain \; condition \\ \alpha = 0.48 \; for \; triaxial \; condition \end{cases} \quad [2.4]$$

Stress level also affects the shearing resistance of the soil. In general, the shearing resistance is higher at higher stresses. However, the rate of increase of shearing resistance with the increase of stress depends on the magnitudes of the confining stress. Lee and Seed (1967) demonstrated how the contributions of different factors to the shearing resistance change with confining (normal) stress at the same density of the soil (shown in Figure 2-3). Figure 2-3 shows that the contribution of the sliding resistance to the rate of increase of shear strength (dash line) is constant with the normal stress. The contribution of soil dilation is high at a low normal stress level. High confining pressure reduces the dilation by restricting the relative movement of the particles. As a result, the contribution of the dilation is reduced. The dotted area in Figure 2-3 shows the contribution of dilation to the shear strength that changes from positive at the low normal stresses to negative at the high normal stresses.

At high confining pressure, particle breakage can occur, promoting the contraction of soil during shearing, which increases the shearing resistance (as seen in Figure 2-2). The particle breakage is usually insignificant at low confining pressure. Thus, the dashed area showing the contribution of particle crushing and rearrangement resistance in Figure 2-3

indicates a lower contribution at the lower stress level and a higher contribution at the higher stress level. However, the rate of decrease of shear strength due to restricting dilation at high normal stress levels is higher than the rate of increase of the shear strength due to particle crushing and rearrangement resistance. As a result, the overall rate of increase of shear strength (the total shearing resistance is shown using the dotted line in Figure 2-3) is higher at the lower normal stresses than the rate of increase at the higher normal stresses.

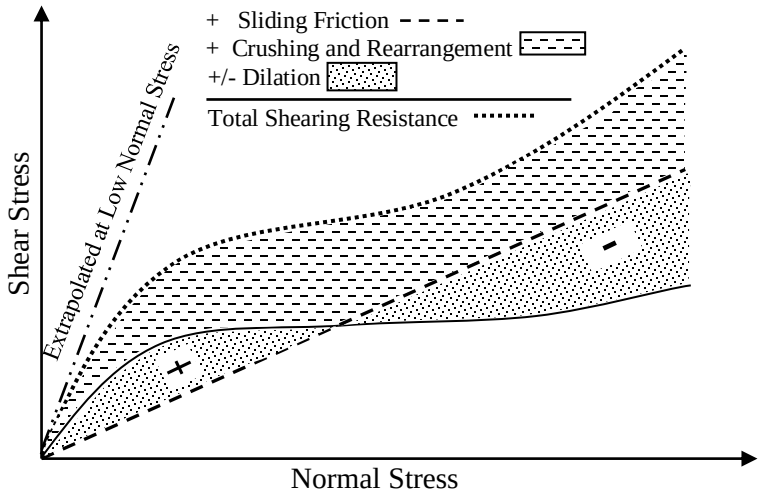


**Figure 2-3**: Effect of normal stress on the component on shearing resistance (after Lee and Seed 1967)

Researchers have been investigating the effects of density and confining pressure on the strength and deformation properties of soil over a few decades. Marschi et al. (1969) reported a decrease of the angle of internal friction of rockfill material by about 10º with an increase of confining pressure from 200 kPa to 4500 kPa. They also found a reduction

of the shear strength parameter with a decrease in initial density, which is higher at lower confining pressures. Been and Jefferies (1985) incorporated mean stress and void ratio into a state parameter '$\Psi$' to interpret the dependency of strength and dilatancy of sand on density and confining stress. A correlation between the state parameter ($\Psi$) and the angle of internal friction was developed from drained and undrained triaxial tests on Kogyuk sand with varying density and stress levels. Mashiri et al. (2015) expressed state parameter $\Psi$ as a function of effective mean stress and the void ratio (Eq. (2.5)).

$$\Psi = e - [e_{csl} - (\lambda \ln p')] \quad [2.5]$$

Where $e =$ void ratio at mean stress $p'$, and $e_{csl}$ and $\lambda$ are the parameters from the critical state line in $e - \ln p'$ space.

Bolton (1986) established an empirical relation (Eq. (2.6)) of the angle of internal friction with the relative density and the mean effective stress.

$$\emptyset_p - \emptyset_{cv} = 3[I_D(1 - \ln p') - 1] \quad [2.6]$$

Where, $\emptyset_p$ = angle of internal friction corresponding to peak shearing strength; $\emptyset_{cv}$ = angle of internal friction corresponding to constant volume shearing, $I_D$ = Initial Relative Density; $p'$ = mean effective stress.

Wan and Guo (1999) conducted consolidated drained tests on an Ottawa sand with five void ratios ranging from 0.5 to 0.8 and confining pressures from 100 to 10000 kPa. The peak behavior of stress–strain curves are only seen in dense sand with void ratios of 0.5

and 0.6. Peak shear stress was found to increase with density. However, the peak shear strain decreased with density. Beyond the peak shear stress, a post–peak softening was observed. Both initial contraction and dilatant behavior were observed in the dense sand, while contraction was only observed in the loose condition of the sand. However, the increase of confining pressure at the same void ratio was found to suppress dilation when the post–peak softening was insignificant. A similar scenario was also reported in Guo and Su (2007), where the suppression of dilation was found to be significant in angular sand than in round sand.

Yang and Li (2004) conducted triaxial tests on Toyura sand with varying relative density ranging from 5% to 90% and varying confining pressures from 50 to 2000 kPa. The critical state stress ratio (at failure) was found to be the same at all confining pressures, while the critical void ratios were different for different confining pressures (Figure 2-4). Figure 2-4a shows that the curves for stress ratios for three different confining pressures meet at failure, but the post–peak degradation of stress ratio is only seen in low confining stress of 50 and 500 kPa. However, the peak stress ratio for low confining stress of 50 kPa is obtained at earlier axial strain than the other confining stresses. Figure 2-4b shows the void ratio to decrease with the increase of stress until failure for 2000 kPa of confining pressure. However, at lower confining pressures, the void ratio slightly decreases initially and then increased until failure. Thus, the void ratios at failure (critical state void ratio) are different. As seen in Figure 2-4b, the increase of void ratio (dilatancy) was higher at lower confining pressure, which was also higher for the higher density of the soil (Yang and Li, 2004).

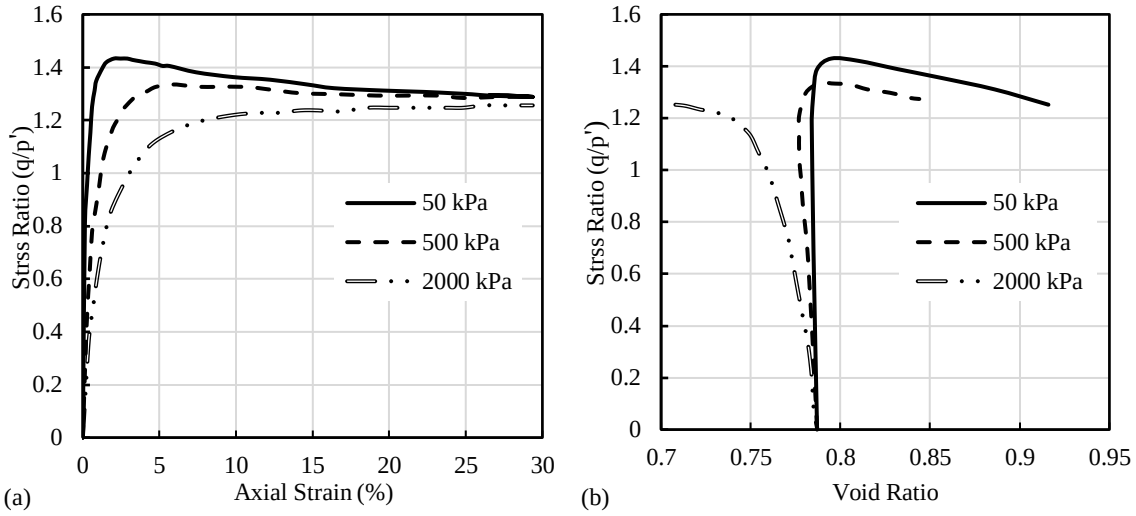


**Figure 2-4**: Effect of confining pressure for Toyura sand with 50% relative density on (a) Critical stress ratio (b) Critical void Ratio (after Yang and Li 2004)

Xiao et al. (2014) conducted large-scale triaxial tests on rockfill material and found that the peak friction angle increases with the increase in density and the decrease in confining pressure. The critical state friction angle is affected more significantly by the initial confining pressure than the initial density. However, strain–softening is more significant at lower confining pressure, whereas strain–hardening is more significant in lower density or higher confining pressure.

Duncan et al. (2014) established an empirical relation (Eq. (2.7)) of the peak friction angle as a function of gradation, density, and confining pressure from 125 triaxial tests on sands and gravel (Marschi et al., 1972; Becker et al. 1972).

$$\emptyset' = A + B(D_r) - [C + D(D_r)]\log_{10}(\frac{\sigma'_N}{P_a}) \quad [2.7]$$

Where, $\emptyset'$ is the effective angle of internal friction, $D_r$ is the relative density, $\sigma'_N$ is the effective normal stress in Pascal, A is the parameter that accounts for the particle size and gradation (i.e., a higher value for gravels and lower value for uniform sand), B is the parameter accounting for the decrease of friction angle with the increase in density, C is the parameter accounting for the greater effect of logarithmic reduction of friction angle with the increase in normal stress on gravels than on sands, D is a constant.

### 2.3.3 Effect of Strain Rate

As loads are often applied to the soil at various rates, researchers investigated the effect of the rate of loading on the shear strength of the soil. A study showed that the angle of internal friction of uniform dense Cambria sand increases about 4.7° with changing of strain rate from 0.0042 %/min to 0.74 %/min in an undrained triaxial test (Yamamuro and Lade 1993). A similar type of effect of strain rate was found in drained triaxial compression tests of a crushed coral sand (Lade and Nam 2009). However, no significant effect of strain rate was observed on Hostun and Toyura sands (Matsushita et al. 1999). The inertia of the material plays a role at a very high strain rate, and there can be a change in the material response due to strain rate change (Matsushita et al. 1999; Abrantes and Yamamuro 2002). The strain rate effect on the shear strength is an active area of research requiring further attention.

### 2.3.4 Shear Strength of Unsaturated Soil

The shear strength is conventionally assessed, assuming the soil is saturated. However, the soil near the ground surface is typically unsaturated, which cannot be assessed using

the theories developed for saturated soil. For unsaturated soil, the Mohr-Coulomb failure criteria can be applied, accounting for the contribution of matric suction to the shear strength due to the presence of pore air pressure ($u_a$) in pore space in addition to the pore water pressure. Bishop (1959) modified the effective stress framework of Terzaghi (1936) for the unsaturated soil by introducing the contribution of matric suction to the effective stress as the combination of net normal stress ($\sigma - u_a$) and matric suction ($u_a - u_w$) (Eq. (2.8)). This is known as single stress state approach as the net normal stress, and matric suction works as a single variable.

$$\tau_f = c' + \left[(\sigma - u_a)_f + \chi_f (u_a - u_w)_f\right] \tan \emptyset' \quad [2.8]$$

In Eq. (2.8), $\chi$ is the effective stress parameter with the value from zero for dry soil to unity for fully saturated soil. It represents the existence of a capillary force in pore space filled with air and water. Jennings and Burland (1962) revealed that the determination of the effective stress parameter is very complex and not well established. Khalili and Khabbaz (1998) proposed an empirical equation (Eq. (2.9)) based on 13 soils for the determination of $\chi$.

$$\chi = \left[\frac{(u_a - u_w)_f}{(u_a - u_w)_b}\right]^{-0.55} \quad [2.9]$$

where $(u_a - u_w)_f$ and $(u_a - u_w)_b$ are matric suction at specimen failure and air entry state, respectively. Air entry state is defined as the state of soil where matric suction of soil exceeds a specified value and the ingress of air into the soil is promoted.

This single stress state approach has the limitation of interpreting the dilative behavior of unsaturated soil. Fredlund and Morgenstern (1977) presented two stress state approach (Eq. (2.10)) for unsaturated soil by implementing matric suction and net normal stress as two different stress variables and additional angle of internal friction $\emptyset^b$ which accounts for only the contribution of matric suction to the shear strength.

$$\tau_f = c' + (\sigma - u_a)_f \tan \emptyset' + (u_a - u_w)_f \tan \emptyset^b \quad [2.10]$$

$\emptyset^b$ is equal to $\emptyset'$ at air entry value of soil or at lower matric suction after that. The angle of internal friction for suction, $\emptyset^b$ generally decreases nonlinearly with the increase of matric suction (Gan et al. 1988a). The traditional two-dimensional Mohr-Coulomb failure envelope can be extended into three-dimension using the above equation (Eq. (2.10)) by implanting the new axis of matric suction (Figure 2-5), Fredlund and Morgenstern (1977). Figure 2-5 shows that the radius of the Mohr circle is increased when it is translated along with matric suction $(u_a - u_w)$ axis and apparent cohesion becomes the summation of effectice cohesion $(c')$ and capilary cohesion $((u_a - u_w) \tan \emptyset^b)$ arising from the capillary effect of unsaturated soil.

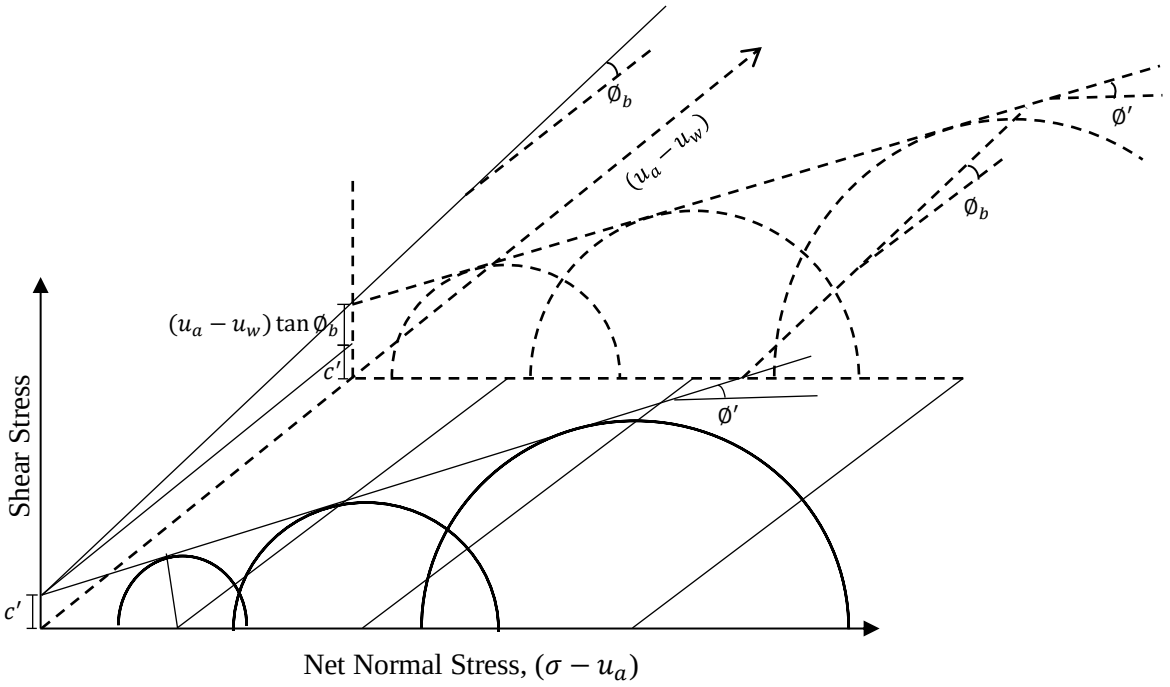


**Figure 2-5**: Extended Mohr-Coulomb failure envelope for unsaturated soil (after Fredlund and Morgenstern 1977)

As stated earlier, most of the experimental investigations of sand were conducted using the test apparatus suitable for testing saturated and dry soils. Test setups for unsaturated soil are different from those for saturated soil due to the requirement of controlling matric suction. Donald (1956) first introduced the mechanism of testing unsaturated soil through direct shear testing of fine sands and coarse silts. In this test, pore air pressure was maintained zero gauge pressure by exposing the upper part of the shear box into the atmosphere, whereas the pore water pressure was maintained negative by applying negative water head through a membrane and porous stone in the lower part connected to a constant head water tube. The method is found suitable for matric suction of up to 101

kPa. For higher matric suctions, an axis translation technique was adopted by the researchers (Hilf 1956; Bishop and Donald 1961). The method includes a ceramic disk that has a high air entry value (greater than the matric suction). The ceramic disk is installed at the bottom of the sample that prevents the passage of air from the sample to the pore water measuring system connected at the bottom of the sample. The pore air pressure in the sample is increased by an external air pressure system connected to the coarse porous disc at the top of the sample. The increase of air pressure translates the negative pore-water pressure into positive pore water pressure. Thus, the matric suction of the samples can be controlled at values higher than 101 kPa.

However, the modification of conventional triaxial and direct shear by integrating the axis translation technique for testing unsaturated soil is very complex and requires skilled personnel. It is also time-consuming to conduct tests under desired matric suction by controlling pore air pressure and water pressure independently. To avoid the difficulties, researchers proposed using indirect approaches without modifying the test equipment (Vanapalli et al. 1996; Fredlund et al. 1996; Khalili and Khabbaz 1998). In the indirect approaches, suction related information is separately obtained from the Soil Water Characteristic Curve (SWCC) of the soil, which can be developed using different methods (i.e., the Filter paper method, Hanging column method, Tensiometer, Psychrometer, or others). Then, the shear strength of unsaturated soil with respect to suction is predicted from the extension of the total stress approach accumulating the SWCC data, saturated soil property, and conventional shear strength test data (Fredlund and Rahardjo 1993).

Bai and Liu (2012) successfully employed the combination of the filter paper method for SWCC and the conventional direct shear test to characterize the shear strength of expansive soil. The matric suction of the sample was estimated from the SWCC at a moisture content, which was used in the direct shear test. The contribution of matric suction to shear strength ($\tan \emptyset_b$) was determined from the slope of the shear strength versus the matric suction curve. A nonlinear failure envelope for the shear strength versus matric suction was observed at each normal stress. The value of $\emptyset_b$ is found to be close to the effective friction angle, $\emptyset'$ at lower matric suction.

A similar methodology was adopted for the shear strength characterization of unsaturated kaolin at different matric suction in Oh et al. (2008). Matric suction at different moisture contents was determined separately through psychrometer tests. A conventional triaxial test was performed by shearing the unsaturated kaolin sample at different moisture contents immediately after the application of confining pressure. A consolidated undrained test was also performed to obtain the shear strength of saturated kaolin, which was used to find $\emptyset_b$. The study showed that the suction has a greater effect on the angle of internal friction than the cohesion. The rate of increase of shear strength due to suction was decreased with an increase in confining pressure at higher suction.

Xing et al. (2016) presented a modified form of equation (Eq. (2.11)) for the shear strength of the unsaturated soil where the parameters related to matric suction (i.e., $\chi$ of Eq. (2.8) and $\tan \phi_b$ of Eq. (2.10)) were replaced by suction stress, $\sigma_s$. A series of conventional consolidated undrained triaxial tests were conducted on unsaturated soil, and the suction stress was found from the effective stress path. They also plotted the suction

from SWCC obtained using the tensiometer test for the soil at different moisture contents and determined $\chi$ and $\tan\phi_b$ from the slope of effective cohesion $c'$ versus $(u_a - u_w)$. There was logarithmic decrease of effective cohesion with moisture content. The effective angle of internal friction did not change significantly with the change of moisture content.

$$\tau_f = (\sigma - u_a - \sigma_s)_f \tan \emptyset' \quad [2.11]$$

Where $\sigma_s = \frac{c'}{\tan \emptyset'}$

Lu and Likos (2006) used earlier a similar concept of the suction stress defined as the isotropic interparticle stress (termed as "isotropic tensile stress") arising from capillary mechanisms in unsaturated sand. They stated it to have an equivalent meaning of the "apparent cohesion" of soil. The isotropic tensile strength ($\sigma_{tia}$) can be obtained through a linear extension of the M-C failure envelope with total stress Mohr circles (Figure 2-6). In Figure 2-6, the effective stress Mohr circles are drawn to the right of the total-stress Mohr circles as the negative pore pressure or suction in unsaturated soil increases the effective stress, making it higher than the total stress.

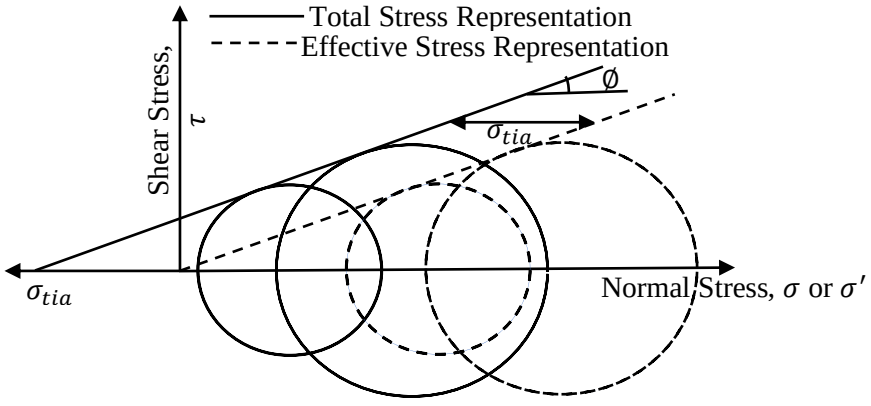


**Figure 2-6**: Isotropic tensile strength relating the total stress and effective stress frameworks (after Lu et al. 2009)

The isotropic tensile stress, $\sigma_{tia}$ (or the suction stress) can be considered additive to the total stresses to define effective stresses for assessing the shear strength within the effective stress framework (see Figure 2-6). Thus, suction stress can be used to define the shear strength behavior of unsaturated sand under various suction conditions. In this approach, the angle of internal friction is assumed to be independent of matric suction, which is consistent with the results of direct shear tests of unsaturated silty sands (Edodaski and Chiba sands) reported in Gallage and Uchimura (2016).

## 2.4 Summary

This chapter presents a summary of major developments of shear strength theory and the previous experimental characterization of shear strength of soil considering the effect of density, confining pressure, moisture content, strain rate, and particle size. It reveals that most of these studies were with standard and known soils such as Silica sand, Ottawa sand, Toyura sand. Though the effects of density, confining pressure on the shear strength of soil are well documented, there is limited information regarding the combined effects of density, moisture content, and confining pressure. For unsaturated soil, complex methods are generally required for the determination of shear strength parameters. The development of simplified methods for assessing the shear strength of unsaturated soil is a subject of further research and investigation.

## 2.5 References

Abrantes, A. E., and Yamamuro, J. A. 2002. "Experimental and Data Analysis Techniques Used for High Strain Rate Tests on Cohesionless Soil." *Geotechnical Testing Journal*

25 (2): 128–141.

Bai, F. Q., and Liu, S. H. 2012. “Measurement of the Shear Strength of an Expansive Soil by Combining a Filter Paper Method and Direct Shear Tests.” *Geotechnical Testing Journal* 35 (3): 451–459. https://doi.org/10.1520/GTJ103342.

Becker, E., Chan, C. K., and Seed, H.B. 1972. “Strength and Deformation Characteristics of Rockfil Materials in Plane Strain and Triaxial Compression Tests.” Report No. TE-72-3, Dept. of Civil Eng., Univ. of California, Berkeley.

Been, K., and Jefferies, M. G. 1985. “A State Parameter for Sands.” *Geotechnique* 35 (2): 99–112.

Bishop, A. W. 1959. “The Principle of Effective Stress.” *Tecknik Ukeblad* 106 (39): 859–863.

Bishop, A. W., and Donald, I. B. 1961. “The Experimental Study of Partly Saturated Soil in the Triaxial Apparatus.” In *5th International Conference on Soil Mechanics and Foundation Engineering*, 13–21. Paris.

Bolton, M. D. 1986. “The Strength and Dilatancy of Sands.” *Geotechnique* 36 (I): 65–78.

Donald, I. B. 1956. “Shear Strength Measurements in Unsaturated, Non-Cohesive Soils with Negative Pore Pressure.” In *2nd Australia and New Zealand Conference on Soil Mechanics and Foundation Engineering*, 200–205.

Duncan, J. M., Wright, S. G., and Brandon, T. L. 2014. *Soil Strength and Slope Stability*. 2nd ed. John Wiley & Sons, Incorporated.

Fredlund, D. G., Morgenstern, N. R. 1977. “Stress State Variables for Unsaturated Soils.” *Journal of Geotechnical Engineering Division, American Society of Civil Engineers*, 103 (5): 447–466.

Fredlund, D. G., Xing, A., Fredlund, M. D., and. Barbour, S. L. 1996. “The Relationship of the Unsaturated Soil Shear Strength to the Soil-Water Characteristic Curve.” *Canadian Geotechnical Journal* 33 (3): 440–448.

Fredlund, D.G., and Rahardjo, H. 1993. *Soil Mechanics for Unsaturated Soils*. New York: John Wiley & Sons, Incorporated.

Gallage, C., and Uchimura, T. 2016. “Direct Shear Testing on Unsaturated Silty Soils to Investigate the Effects of Drying and Wetting on Shear Strength Parameters at Low Suction.” *Journal of Geotechnical and Geoenvironmental Engineering* 142 (3): 1–9. https://doi.org/10.1061/(ASCE)GT.1943-5606.0001416.

Gan, K. J., and Fredlund, D. G., and Rahardjo, H. 1988a. “Determination of Shear Strength Parameters for Unsaturated Soil Using Direct Shear Test.” *Canadian Geotechnical Journal* 25 (3): 500-510.

Guo, P., and Su, X. 2007. “Shear Strength, Interparticle Locking, and Dilatancy of Granular Materials.” *Canadian Geotechnical Journal* 44 (5): 579–591. https://doi.org/10.1139/T07-010.

Hilf, J. W. 1956. “An Investigation of Pore Pressures in Compacted Cohesive Soil.” Technical Memorandum 654, U .S .B .R., USA.

Holtz, W.G., and Gibbs, H.J. 1956. “Triaxial Shear Tests on Pervious Gravelly Soils.”

*Journal of the Soil Mechanics and Foundations Division* 82 (1): 1–22.

Jennings, J. E., and Burland, J. B. 1962. "Limitations to the Use of Effective Stresses in Partly Saturated Soils." *Geotechnique* 2: 125–144.

Khalili, N., and Khabbaz, M. H. 1998. "A Unique Relationship for the Determination of the Shear Strength of Unsaturated Soils." *Geotechnique* 48 (5): 681–687.

Kirkpatric, W. M. 1965. "Effects of Grain Size and Grading on the Shearing Behaviour of Granular Materials." In *6th International Conference on Soil Mechanics and Foundation Engineering*, 273–277.

Kolbuszewski, J., and Frederick, M.R. 1963. "The Significance of Particle Shape and Size on the Mechanical Behavior of Granular Materials." In *European Conference on Soil Mechanics and Foundation Engineering*, 253–263.

Lade, P. V., and Nam, J. 2009. "Strain Rate , Creep , and Stress Drop-Creep Experiments on Crushed Coral Sand." *Journal of Geotechnical and Geoenvironmental Engineering* 135 (7): 941–954.

Lee, K.L., and Seed, H.B. 1967. "Drained Strength Characteristics of Sands." *Journal of the Soil Mechanics and Foundation Division,* 93 (6): 117–141.

Lu, N., Kim, T. Sture, S., and Likos, W. J. 2009. "Tensile Strength of Unsaturated Sand." *Journal of Geotechnical and Geoenvironmental Engineering* 135 (12): 1410–1419.

Lu, N., and Likos, W.J. 2006. "Suction Stress Characteristic Curve for Unsaturated Soil." *Journal of Geotechnical and Geoenvironmental Engineering* 132 (2): 131–142.

Marschi, N.D., Chan, H. B., Seed, C. K., and. Duncan, J.M. 1969. “Strength and Deformation Characteristics of Rockfill Materials.” Report TE-69-5, Civil Engineering Dept., Univ. of California, California.

Marschi, N. D., Chan, H. B., and Seed, C. K. 1972. “Evaluation of Properties of Rockfill Material.” *Journal of the Soil Mechanics and Foundations Division* 98 (1): 95–114.

Mashiri, M. S., Vinod, J. S., Sheikh, M. N., and Tsang, H. 2015. “Shear Strength and Dilatancy Behaviour of Sand – Tyre Chip Mixtures.” *Soils and Foundations* 55 (3): 517–528. https://doi.org/10.1016/j.sandf.2015.04.004.

Matsushita, M., Tatsuoka, F., Koseki, J., Cazacliu, B., Benedetto, H., and Yasin, S. J. M. 1999. “Time Effects on the Pre Peak Deformation Properties of Sands.” In *Second Int. Conf. on Pre-Failure Deformation Characteristics of Geomaterials*, edited by M. Jamiolkowski, R. Lancelotta, and D. Lo Presti, 681–89. Balkema, Rotterdam.

Oh, W. T., Garga, V. K., and Vanapalli, S. K. 2008. “Shear Strength Characteristics of Statically Compacted Unsaturated Kaolin.” *Canadian Geotechnical Journal* 45 (7): 910–22. https://doi.org/10.1139/T08-032.

Rowe, P. W. 1962. “The Stress Dilatancy Relation for Static Equilibrium of an Assembly of Particles in Contact.” In *Proceeding Royal Society*, 269A, 500–527.

Selig, E. T., and Roner. C. J. 1987. “Effect of Particle Characteristics on Behaviour of Granular Material.” *Transportation Research Record* 1131: 1–6.

Terzaghi, K. 1936. “The Shear Resistance of Saturated Soils.” In *Ist International Conference Soil Mechanics and Foundation Engineering, Cambridge*, MA, 1, 54-56.

Terzaghi, K., Peck, R.B., and Mesri, G. 1996. *Soil Mechanics in Engineering Practice*. John Wiley and Sons, Inc., New York.

Tinoco, F H. 1967. “Shear Strength of Granular Materials.” Doctoral Thesis. Iowa State University.

Vanapalli, S. K., Fredlund, D. G., Pufahl, D. E., and Clifton, A. W. 1996. “Model for the Prediction of Shear Strength Respect to Soil Suction.” *Canadian Geotechnical Journal* 33 (3): 379–392.

Wan, R.G., and Guo, P.J. 1999. “A Pressure and Density Dependent Dilatancy Model For Granular Materials.” *Soils And Foundations, Japanese Geotechnical Society* 39 (6): 1–12.

Wang, J., Zhang, H., Tang, S., and Liang, Y. 2013. “Effects of Particle Size Distribution on Shear Strength of Accumulation Soil.” *Journal of Geotechnical and Geoenvironmental Engineering* 139 (11): 1994–1997.

Xiao, Y., Liu, H., Chen, Y., and Jiang, J. 2014. “Strength and Deformation of Rockfill Material Based on Large-Scale Triaxial Compression Tests. I: Influences of Density and Pressure.” *Journal of Geotechnical and Geoenvironmental Engineering* 140 (12): 1–16. https://doi.org/10.1061/(ASCE)GT.1943-5606.0001176.

Xing, X., Li, T., and Fu, Y. 2016. “Determination of the Related Strength Parameters of Unsaturated Loess with Conventional Triaxial Test.” *Environmental Earth Sciences* 75 (1): 1–11. https://doi.org/10.1007/s12665-015-4797-5.

Yamamuro, J. A., and Lade, P. V. 1993. “Effects of Strain Rate on Instability of Granular

Soils." *Geotechnical Testing Journal* 16 (3): 304–13.

Yang, J., and Li, X. S. 2004. "State-Dependent Strength of Sands from the Perspective of Unified Modeling J." *Journal of Geotechnical and Geoenvironmental Engineering* 130 (2): 186–98. https://doi.org/10.1061/(ASCE)1090-0241(2004)130.

Zolkov, E., and Wiseman. G. 1965. "Engineering Properties of Dune and Beach Sands and the Influence of Stress History." In *6th International Conference on Soil Mechanics and Foundation Engineering*, 134–38.

# CHAPTER 3 Sand Characterization using Direct Shear Tests

## 3.1 General

The direct shear test is the most commonly used test method for the determination of shear strength parameters of sand. Extensive studies are available in the literature conducting direct shear tests to assess the shear strength and deformation behavior considering the effects of specimen size, grain size, density, normal stress, moisture content, strain rate, etc.

Through a series of direct shear tests on standard Ottawa sand with variable void ratios and normal stresses, Taylor (1948) revealed that the angle of internal friction of the sand decreases with the increase in void ratio and decrease in density. At each void ratio, the angle of internal friction decreases with the increase of normal stress. The decrease of shearing resistance with the increase of normal stress is attributed to the reduction of the interparticle friction coefficient due to the breakage of particles at contacts and polishing the particle surfaces with the increase of interparticle contact forces. As a result, the shearing resistance from the interparticle sliding and rolling friction is reduced (Duncan et al. 2014; Terzaghi et al. 1996). However, the void ratio has a more dominant impact on reducing the angle of internal friction than the normal stress.

Wei et al. (2018) conducted direct shear tests on soil-rock mixtures with variable moisture content from 3% to 13%. They found that the ratio of shear stress to normal stress (i.e., shear stress ratio) decreases with an increase of the normal stress. However, the shear

stress ratio decreases gradually with the increase of moisture content up to 8%. The direct shear tests were also conducted at various shear displacement rates (2, 5, 10, & 20 mm/min) under four different normal stresses (100 kPa, 200 kPa, 400 kPa & 800 kPa), Wei et al. (2018). It revealed that the stress ratio increases with the increase in the shear displacement rate. However, beyond the rate of 10 mm/min, the change in stress ratio was negligible. The direct shear test was also conducted on five gravel mixtures with maximum particle size from 20 mm to 60 mm and normal stresses from 100 to 250 kPa (Wang et al. 2013). The results showed a reduction of stress ratio with the increase of the normal stress and an increase of angle of internal friction with mean particle size and gravel contents.

The current study focuses on the characterization of sand locally manufactured through the crushing of bedrocks in eastern Newfoundland (Avalon zone). The bedrock in the region comprises limestone and bimodal volcanic rocks (Natural Resources 2004). A laboratory test program is undertaken to account for the effects of density, normal stress, rate of loading, and water contents on the behavior of the sand. This chapter represents the details of the index property tests and direct shear tests conducted on sand samples. A triaxial test program employed in this effort is discussed in Chapter 4. The direct shear test program is divided into two segments. The first test program was designed for comparison of the behavior of the soil with standard silica sand at low-stress levels (12.5 kPa – 50 kPa). Tests were conducted at a constant shearing rate of 1 mm/min. The moisture content in the soil was varied up to around 3%. A total of 69 direct shear tests have been completed in this test program. The second test program was designed to conduct a more elaborate study of the behavior of the sand. In this test program, both moisture content and normal stress

were varied over a wider range. The rate of shearing is also varied. A total of 80 direct shear tests have been completed in this test program.

### 3.2 Test Equipment

The direct shear test apparatus (Figure 3-1) used in this study utilizes a pneumatic loading concept for applying the vertical load to the sample. Two pneumatic pistons are there. A small diameter rolling diaphragm piston is used in low load mode, which can apply loads from 4 lbs. (17.8 N) up to 100 lbs. (444.82 N). Another is a larger diameter piston used in high load mode that can be used to apply loads up to 1500 lbs (6672.33 N). The direct shear frame is supplied with dial indicators to measure vertical and shear displacements. The device includes 2.5" (63.5 mm) diameter shear rings, porous stones, drainage plates, and a water chamber. The arrangement allows a specimen thickness of 26 mm. The test facility has the capacity of applying a maximum shear displacement of 0.8" (20.32 mm) at a shear displacement rate from 0.0025 mm/min to 7.62 mm/min.


**Figure 3-1**: Direct shear device

### 3.3 Test Material

A locally manufactured sand and silica sand were used in the overall test program. Figure 3-2 shows the grain size distribution of the sands. It reveals the local sand are well-graded clean sand with the mean particle size ($D_{50}$) of 0.742 mm, the uniformity coefficient ($C_u$) of 5.81, and the coefficient of curvature ($C_c$) of 2.04. It has a fines content of around 1.3% and gravel content of around 0.87%. The silica sand is poorly graded sand with the median particle size ($D_{50}$) of 0.22 mm, the uniformity coefficient ($C_u$) of 2.04, and the coefficient of curvature ($C_c$) of 1.09. Two types of samples are extracted from the local sand, which is denoted as sample A and sample B. Sample A consists of particles passing the #4 sieve (opening 4.76 mm), and sample B consists of particles passing the #8 sieve (opening 2.38 mm). The local sand contains more than 99% of particles passing the #4 sieve and 82% of particles passing the #8 sieve. Materials passing the #4 sieve are selected to meet the requirement of direct shear box size relative to maximum particle size according to the ASTM D3080 standard. Materials passing the #8 sieve are selected to investigate the effect of removing coarser particles for use in the triaxial test (discussed in Chapter 4). Particles passing the #8 sieve can only be used in the triaxial test facility at MUN's Geotechnical laboratory. Therefore, the applicability of removing coarser particles was examined. The silica sand is denoted as sample C. Samples A, B, and C are used in the first test program (Test Program 1). Sample A is only used in the second test program (Test Program 2).

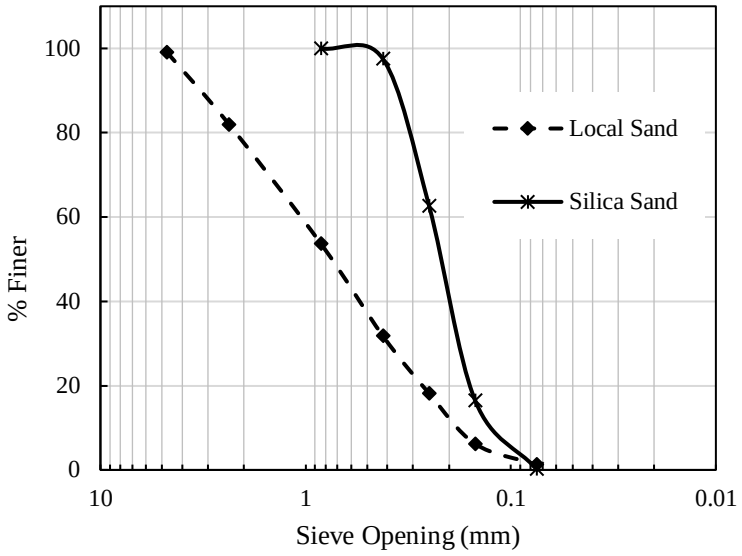


**Figure 3-2**: Grain size distribution of local sand & silica sand

A Standard Proctor compaction test was conducted for each of the samples. The compaction curves are shown in Figure 3-3. In Figure 3-3, the dry densities are the maximum at the zero moisture content (dry condition), which are 18.8 kN/m$^3$ and 15.5 kN/m$^3$ for the local sand (samples A and B) and the silica sand (sample C), respectively. In cohesionless soil, the unit weight can be the maximum at the dry condition when the particles can roll over each other during compaction/vibration. With the addition of water, capillary actions may prohibit particle movements. The effect of capillary tension at lower moisture content dominates the lubrication effect of the water, resulting in lower dry unit weight. At higher moisture contents, the capillary action diminishes, which causes an increase in the dry unit weight. The maximum standard Proctor dry densities (SPMDD) under wet conditions are 18 kN/m$^3$ and 15.1 kN/m$^3$ for the local sand and the silica sand, respectively. The corresponding optimum moisture contents (OMC) of the sands are

10.4% and 15%, respectively. Note that the SPMDD does not represent the maximum unit weight of the soil.

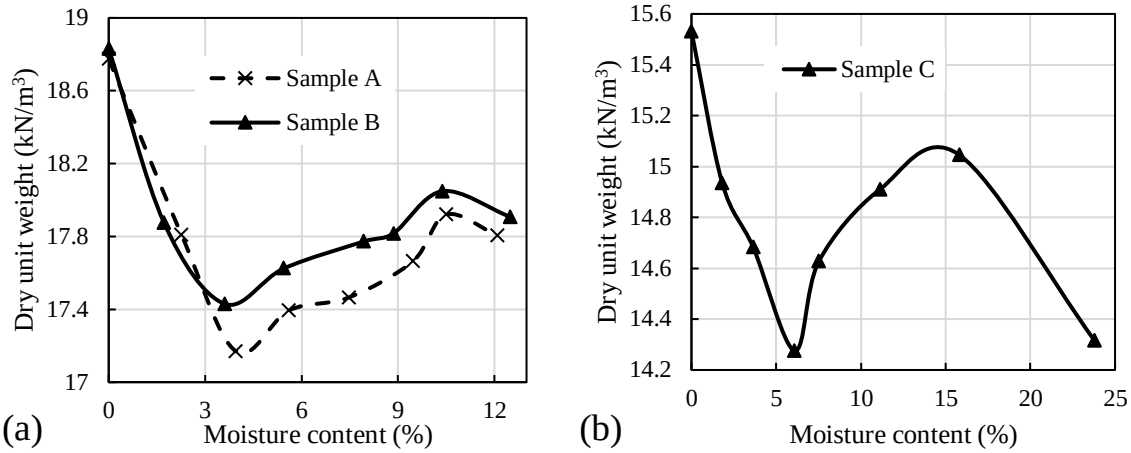


**Figure 3-3**: Results of standard proctor compaction tests: a) Sample A & Sample B, and b) Sample C

A modified Proctor compaction test was also conducted for the local sand (Sample A). The modified Proctor maximum dry density (MPMDD) was obtained as 20 kN/m$^3$, which is higher than SPMDD due to the use of higher compaction energy, which also occurred at zero moisture content. The increase of the density with compaction efforts is further examined through performing compaction following the modified Proctor test procedure but with 50, 75, and 100 blows per each layer. The resulting increase in the maximum density (at zero moisture content) is shown in Figure 3-4. It shows that the increase in density beyond 20.5 kN/m$^3$ is very less. A maximum dry density of 20.7 kN/m$^3$ was obtained using 100 blows per layer.

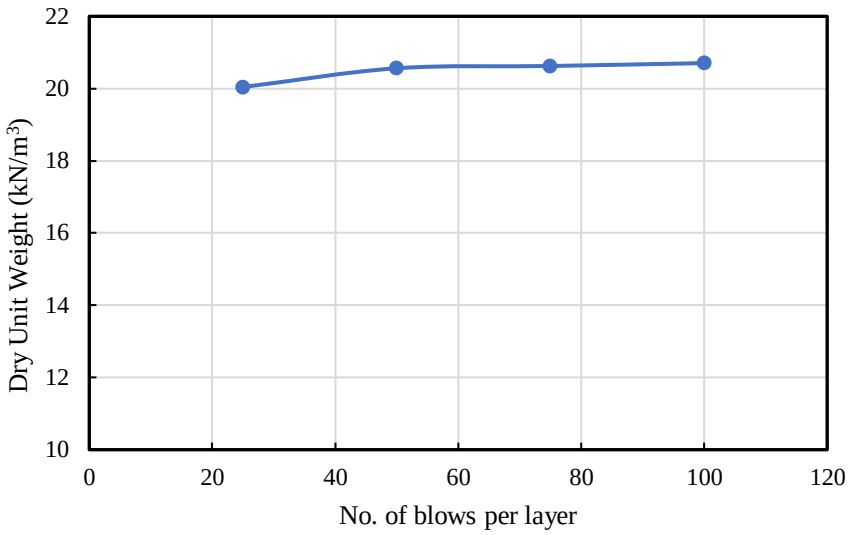


**Figure 3-4:** Increase of density with compaction efforts

As the major focus of the study is to investigate the behavior of the soil in moist conditions, the soil-moisture characteristic of the sand has also been examined. The unsaturated moist soil is subjected to suction that binds the particles together and contributes to the strength and deformation behaviors. The suction in the unsaturated soil depends on the grain-size distribution, relative density, and the degree of saturation of the soil. Jung et al. (2016) presented different grain-size distribution zones depending on the suction effects on the buried pipe. The zones are identified as negligible, low, moderate, and high potential for suction effects depending on the increasing trend of lateral soil-pipe reaction force for soils with different grain size distributions. The grain-size distributions of the soils (Sample A and Sample B) are plotted with the suction effect zones in Figure 3-5. It reveals that Sample A predominantly falls within the low suction effect zones and Sample B (passing #8 Sieve) falls near the boundary of low and moderate suctions zones. However, Sample C (silica sand) falls in the zone of moderate to high suction effects.

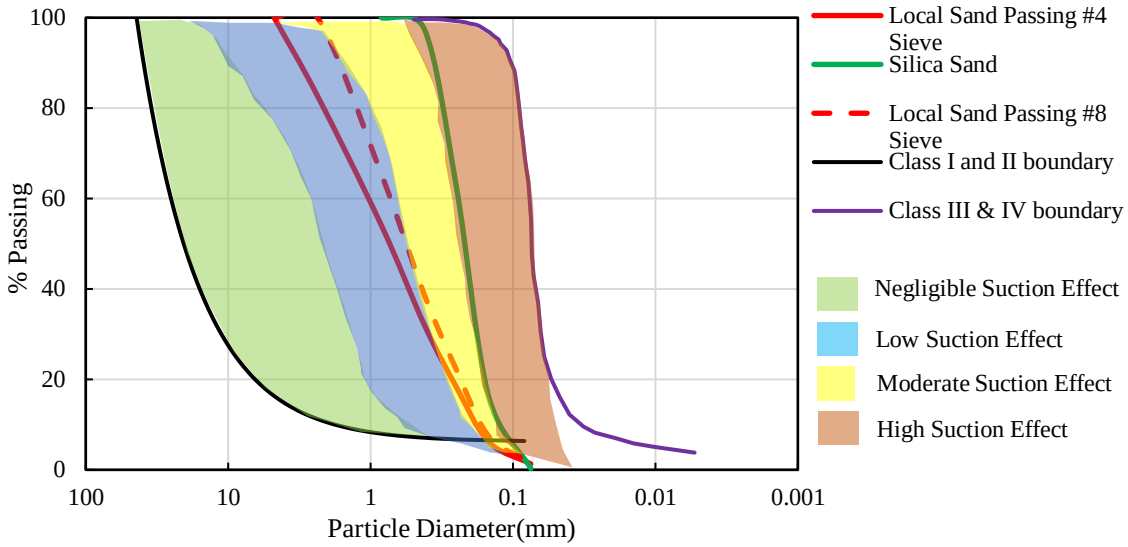


**Figure 3-5**: Suction effect zones based on the grain-size distribution (After Jung et al. 2016)

The locally manufactured sand is expected to have the minimum effect of suction as it falls in the zone of low suction effect (Figure 3-5). Soil water characteristics of soil are often used to predict the suction force in partially saturated soil (Fredlund et al. 1996; Vanapalli et al. 1996; Khalili and Khabbaz 1998; Oh et al. 2008). The soil water characteristics of the local sand are examined here using the filter paper method. The Whatman grade 42 filter paper was used for this purpose.

### 3.4 Soil Water Characteristics

Soil water characteristics were studied for two different densities of the sand to investigate the changes in matric suction in the soil with moisture content. A Whatman grade 42 filter paper was placed in the soil at different moisture contents within a steel container, as shown in Figure 3-6. To ensure constant density (i.e., dry unit weight) for each moisture content,

a fixed amount of dry soil is mixed each time thoroughly with a desired amount of water. Half of the soil is placed and compacted inside the container up to half its height, and the filter paper is placed on top of the layer. The remaining half of the soil is then placed and compacted to the full height of the container. The Whatman filter paper was sandwiched between two larger pore sized filter paper to protect it from direct contact with soil particles before placing. The container was then closed with a lid and inserted inside a Ziploc bag to make it fully airtight. The container was kept inside a temperature-controlled room for seven days. After seven days, the moisture content of the Whatman filter paper was measured. Using the moisture content, the matric suction of the sample was obtained from the calibration curve in ASTM D5298-10 (2010).

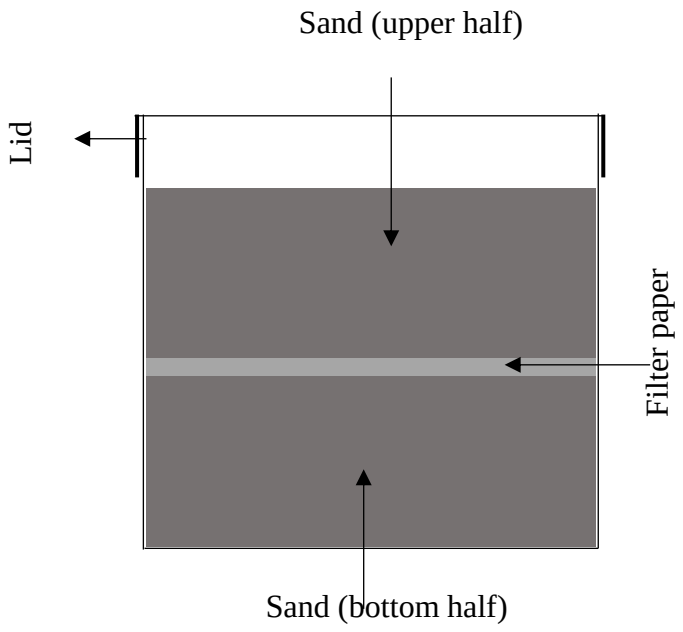


**Figure 3-6**: Suction measurement through filter paper

Figure 3-7 shows the matric suctions measured for the sand at two dry unit weights (17 kN/m$^3$ and 18.5 kN/m$^3$). The matric suctions are examined against the gravimetric moisture content and degree of saturation in the figure. The solid lines are the results for the dry density of 17 kN/m$^3$, and the dotted lines are for the dry density of 18.5 kN/m$^3$. The figure shows that the soil-moisture characteristics are almost the same for the two levels of density considered. The matric suction of the soil is negligible at the moisture content of around 8.5%, which corresponds to the degree of saturation of around 51%. The soil suction increases with the reduction of moisture content and the decrease of the degree of saturation. The maximum suctions of 93 kPa, and 95.5 kPa were observed for the soil with dry unit weights of 17 kN/m$^3$ and 18.5 kN/m$^3$ at the moisture contents of 1.22% and 1.04%, respectively. The corresponding degrees of saturation is 6% and 7%, respectively.

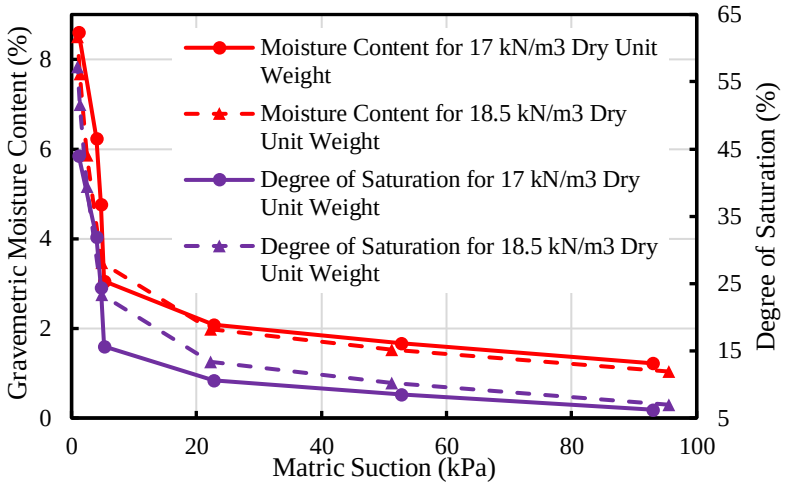


**Figure 3-7**: Soil-Water characteristic curve for sand

The experimental data of matric suction was used to fit with Van Genuchten's (1980) model (Eq. (3.1)).

$$\theta = \frac{\theta_s}{\left[1+\left(\psi/\alpha\right)^n\right]^m} \quad [3.1]$$

Where $\theta$ is the volumetric water content, $\theta_s$ is the saturated volumetric water content, $\psi$ is the matric suction, and $\alpha$ (air entry value), $n, m$ are model-fitting parameter. The value of $\alpha, n, m$ obtained from fitting the experimental data with the model for the dry unit weights of 17 kN/m$^3$ and 18.5 kN/m$^3$. The volumetric water contents are calculated using the specific gravity ($G_s$) of the soil determined from tests (i.e., $G_s$ = 2.63). The resulting parameters are shown in Table 3-1. A comparison of Van Genuchten's model with experimental data is shown in Figure 3-8.

**Table 3-1**: SWCC fitting parameter

| Dry unit weight (kN/m$^3$) | Value of SWCC fitting parameter | | |
|---|---|---|---|
| | $\alpha(kPa)$ | m | n |
| 17 | 0.300 | 0.429 | 1.139 |
| 18.5 | 0.364 | 0.378 | 1.357 |

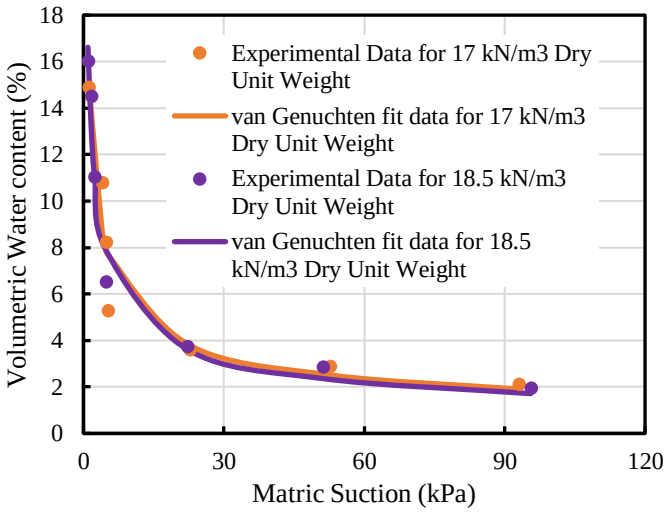


**Figure 3-8**: Comparisons of the best fit SWCC models with lab data.

### 3.5 Sample Preparation for Direct Shear Tests

Samples for the direct shear tests are prepared with different moisture contents and compaction levels. The samples are compacted to three compaction levels: high compaction, medium compaction, and no compaction denoted as H, M, and N, respectively. To achieve high compaction, the sample is poured into the shear box in three layers with a spoon. Each layer is compacted with 25 blows of a free-falling temping rod from a height of 40–50 mm. The temper was moved within the box to apply the same compaction energy over the whole surface. For the medium compacted soil, 4 blows were applied in each layer. After compaction, the volume and mass of the soil sample used in the shear box are measured to determine the unit weight. The other sample is prepared by filling the shear boxes with the soil spread uniformly over the porous stone without compaction. The moist samples are prepared by placing the soil in the shear box immediately after uniform mixing of the soil with predetermined amounts of moisture. The soil was thoroughly mixed to ensure uniformity in the moisture contents. A prepared sample is shown in Figure 3-9. After completion of each test, the actual moisture content of each soil sample is determined through oven-drying. Note that although the same compaction efforts were applied, the unit weights of the soil were different as the moisture contents were different.

As mentioned earlier, two test programs were undertaken to investigate the soil behavior. Table 3-2 shows the detailed test plan for Test Program 1. In this program, Sample A, Sample B, and Sample C are considered at the dry condition and at three different target moisture contents (1%, 2%, and 3%, respectively). The actual moisture

contents of the sand are determined after the tests. Three levels of compaction (high, medium, and no compaction) are considered for the dry soil, and two levels of compaction (high and no compaction) are considered for the moist soil to investigate the effect of compactions. The average densities measured during the tests for each compaction level are shown in Table 3-2. A shear displacement rate of 1 mm/min is applied in each test.

Table 3-3 shows the test plan for Test Program 2. In this test program, sample A with high and no compaction are considered under a wide range of normal stresses. The shear displacement rate is also varied from 0.25 mm/min to 1.5 mm/min.

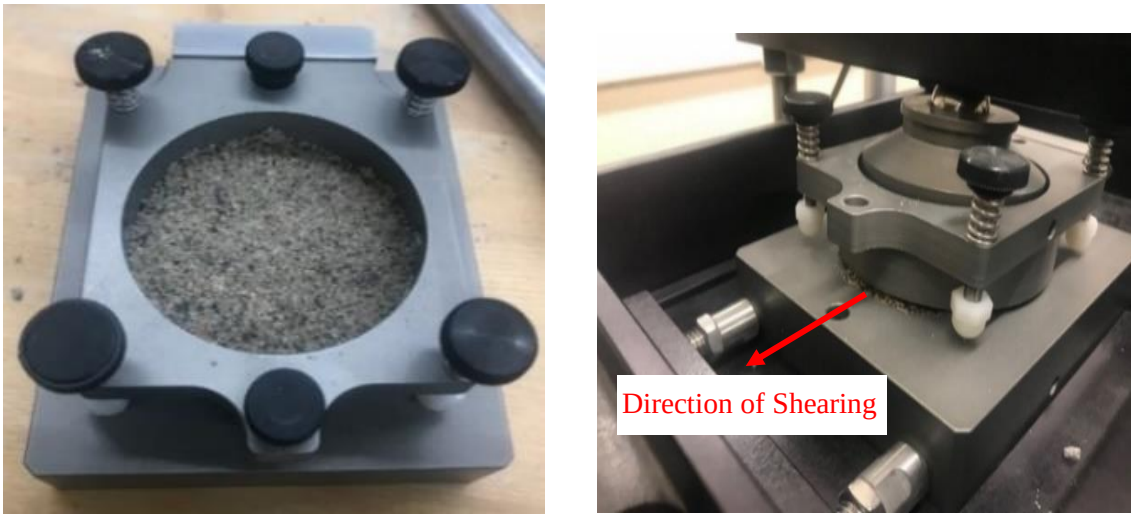


(a) Prepared sample (b) Shearing of Specimen

**Figure 3-9**: Test setup for direct shear tests

**Table 3-2**: Test program 1

| Test No | Sand Sample Type | Actual Moisture (%) | Compaction Status | Sample ID | Normal stress (kPa) |
|---|---|---|---|---|---|
| 1–3 | Sample A (Local sand particle passing #4 sieve) | 0 | High Compaction | AH0 | 12.5, 25, 50 |
| 4–6 | | | Medium Compaction | AM0 | |
| 7–9 | | | No Compaction | AN0 | |
| 10–12 | | 0.80 | High Compaction | AH1 | |
| 13–15 | | 1.25 | No Compaction | AN1 | |
| 16–18 | | 1.20 | High Compaction | AH2 | |
| 19–21 | | 2.0 | No Compaction | AN2 | |
| 22–24 | | 2.6 | High Compaction | AH3 | |
| 25–27 | | 2.7 | No Compaction | AN3 | |
| 28–30 | Sample B (Local sand particle passing #8 sieve) | 0 | High Compaction | BH0 | |
| 31–33 | | | Medium Compaction | BM0 | |
| 34–36 | | | No Compaction | BN0 | |
| 37–39 | | 0.8 | High Compaction | BH1 | |
| 40–42 | | 1.2 | No Compaction | BN1 | |
| 43–45 | | 1.9 | High Compaction | BH2 | |
| 46–48 | | 1.50 | No Compaction | BN2 | |
| 49–51 | | 2.5 | High Compaction | BH3 | |
| 52–54 | | 3.00 | No Compaction | BN3 | |
| 55–57 | Sample C (Silica sand) | 0 | High Compaction | CH0 | |
| 58–60 | | | Medium Compaction | CM0 | |
| 61–63 | | | No Compaction | CN0 | |
| 64–66 | | 1.5 | High Compaction | CH1 | |
| 67–69 | | 3 | High Compaction | CH2 | |
| A = Local Sand particle passing #4 sieve, B = Local Sand particle passing #8 sieve, C = Silica Sand, H = High compaction, M = Medium compaction, N = No compaction, 0 = Dry Sample, 1, 2 & 3 = Predetermined moisture levels | | | | | |

**Table 3-3**: Test program 2

| Test No | Moisture Content (%) | Compaction | Dry Unit Weight ($kN/m^3$) | Shear Displacement Rate (mm/min) | Normal stress (kPa) |
|---|---|---|---|---|---|
| 1–6 | 0 | High compaction | 18.95 | 1 | 12.5, 25, 50, 100, 200, & 400 |
| 7–12 | 1.5 | | 17.39 | | |
| 13–18 | 3 | | 16.98 | | |
| 19–24 | 6 | | 17.23 | | |
| 25–30 | 0 | No compaction | 16.13 | | |
| 31–36 | 1.5 | | 12.67 | | |
| 37–42 | 3 | | 11.60 | | |
| 43–48 | 6 | | 11.49 | | |
| 49–52 | 0 | High compaction | 19.05 | 0.25 | 50, 100, 200, & 400 |
| 53–56 | | | | 0.5 | |
| 57–60 | | | | 1 | |
| 61–64 | | | | 1.5 | |
| 65–68 | | No compaction | 16.20 | 0.25 | |
| 69–72 | | | | 0.5 | |
| 73–76 | | | | 1 | |
| 77–80 | | | | 1.5 | |

### 3.6 Results from Test Program 1

The objective of Test Program 1 is to examine the behavior of the sands at low-stress levels in the range of 12.5 kPa to 50 kPa. Low stresses are typically expected at a shallow depth, such as backfill around the buried structures. Tests are conducted in dry conditions and moist conditions with the target moisture contents between 1% and 3%. The moist soils are in unsaturated condition and are expected to possess tensile strength and cohesion. Conventionally, the cohesion of soil is neglected in modeling the soil behavior using the Mohr-Coulomb failure theory. However, a nonzero value of cohesion may be of importance in some situations. In this test program, the shear strength parameters, including

cohesion and the angle of internal friction for the dry and moist soils, are examined, as discussed below.

### 3.6.1 Shear Strength Parameters

To examine the effect of moisture content on the strength parameters, the maximum shear stresses from the direct shear tests are plotted against the normal stresses in Figure 3-10. Linear regression equations with the data showed an intercept on the vertical axis, indicating a nonzero cohesion even for the dry sand. Cohesion is sometimes expected in dry sand due to interlocking between the particles (Lu and Likos 2013). However, the magnitude of the cohesion (intercept on the vertical axis) ranges from a minimum value of 0.2 kPa for the AH0 sample to a maximum value of 7.9 kPa for the AH3 sample, which is practically negligible, considering the uncertainties involved in the measurements and data interpretations. Thus, the apparent cohesion for the moist soil at the water contents considered (1% to 3%) is negligible. The apparent cohesion in unsaturated granular material predominantly results from the capillary force due to negative pore-water pressure and surface tension (Lu et al. 2007). At very low moisture contents, air voids in the granular soil may be connected, causing the air pressure to be the same as the atmospheric pressure in the direct shear tests. As a result, the negative pore-water pressures and the apparent cohesion can be negligible. Ravindran and Gratchev (2020) also reported a lower apparent cohesion at lower moisture content for a gravelly/sandy soil that increased initially and then decreases with the increase of water content. The slopes of the lines in Figure 3-10 are different (indicating different friction angle) due to the differences in the densities of the soil, as discussed later. As mentioned earlier, although the same compaction efforts

were applied for the soil samples at different moisture contents, the dry densities of the soil were different.

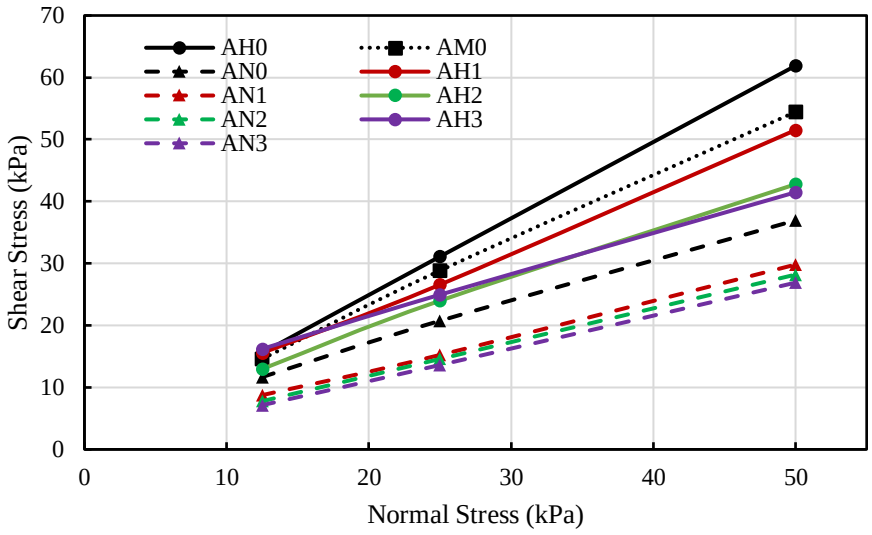


**Figure 3-10**: Shear stress–Normal stress plot for sample A

### 3.6.2 Stress-Deformation Response

Since the apparent cohesion of sand is negligible for the sand, the shear strength of the soil depends exclusively on the normal stress for each condition (i.e., stress level, density, and water content). The ratio of the shear strength to the normal stress (called herein as "stress ratio") is therefore examined here against the shear displacements. The volumetric strain is examined in term of a dilation rate, defined as the ratio of the vertical displacement change ($dv$) to the horizontal displacement change ($du$) (i.e., Dilation rate $= \frac{dv}{du}$), after Simoni and Houlsby (2006).

Figure 3-11 shows the variation of stress ratios with horizontal displacement for four conditions of sample A subjected to high compaction. As seen in the figure, the peak stress

ratio is not significantly affected by the level of normal stress for the dry sample (Figure 3-11 (a)). However, for the moist samples, the peak stress ratio decreases with the increase of normal stress. The peak stress ratio is around 1.2 for the dry sand, which corresponds to a peak friction angle of 50°. For the moist sand, the peak stress ratio varies from 0.8 to 1.25. These correspond to friction angle variations from 38° to 51°, with the lowest value for the normal stress of 50 kPa and the highest value for the normal stress of 12.5 kPa. It is also to be noted that post–peak degradation of the stress ratio is higher for the dry sand, where the post–peak degradation is not significant for the moist sands. This is due to higher densities of the dry sand samples than the moist sand samples prepared using the same compaction efforts. For the dry sand, the stress ratio is reduced from a peak value of 1.2 to the critical state value of around 0.7. Thus, the critical state friction angle for the soil is 35°. The peak and post–peak behavior observed for the dry sand is commonly reported in the literature (Al Tarhouni et al. 2017). However, the behavior of moist sand has not been extensively investigated to examine the behaviors.

For the moist samples, the peak stress ratio is higher for soil AH1 having around 0.8% of moisture content than for AH2, having around 1.2% of moisture content at each of the stress levels considered. The shear strength is higher again for soil AH3 having a moisture content of around 2.6%. As mentioned earlier, although a similar approach of soil compaction is used in each of the tests, the degree of compaction of the soil samples in the test box might be different due to the presence of different moisture contents, which is

found to contribute to the behavior of the moist soil (discussed later in section 3.7.4).

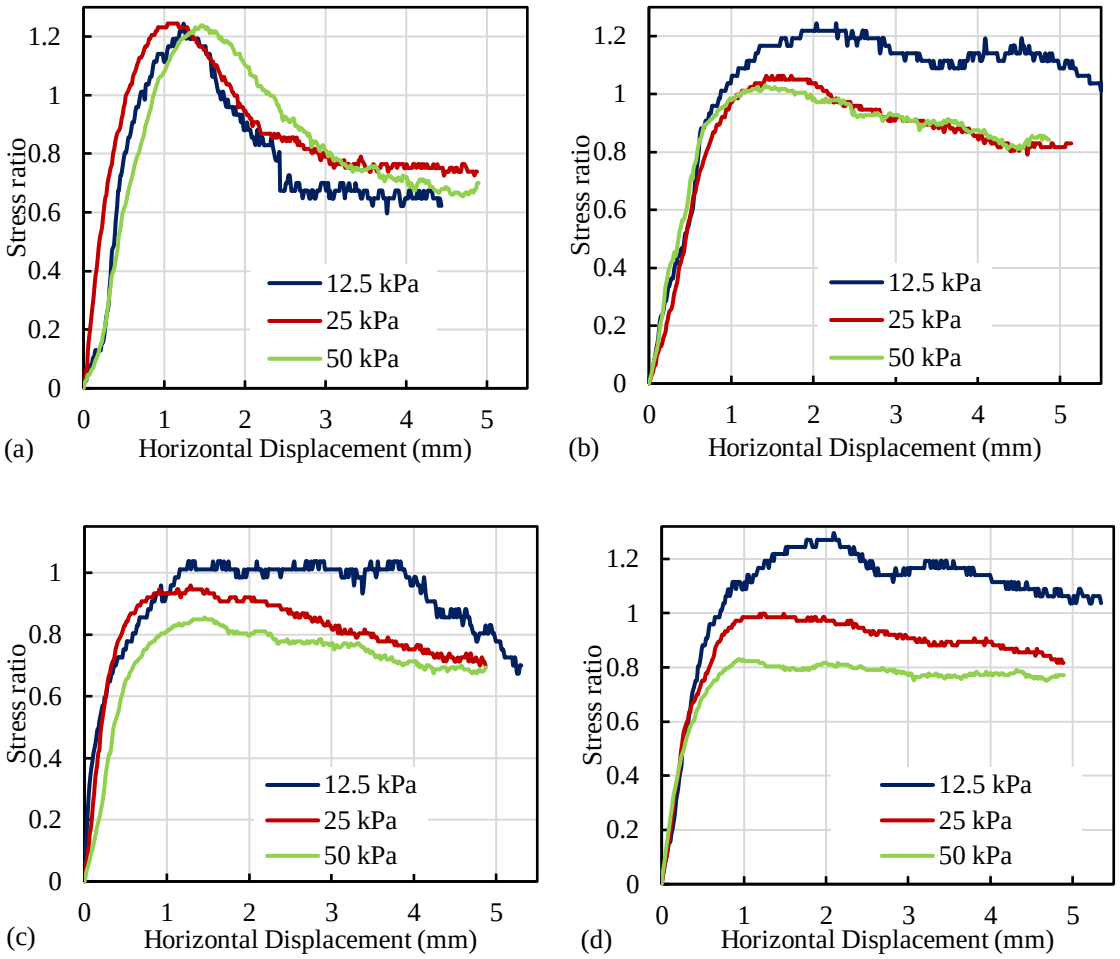


**Figure 3-11**: Variation of stress ratio for dense condition of sample A: a) AH0, b) AH1, c) AH2, and d) AH3

Figure 3-12 plots the calculated dilation rate against the horizontal displacement for the four conditions of sample A subjected to high compaction. Each of the highly compacted samples experiences dilation, although post–peak degradation of stress ratio is not observed for the moist sample (shown in Figure 3-12). The mechanism of post–peak shear stress and soil dilation for the moist samples require further investigation. In general, the

peak dilation rate is almost the same in all three normal stresses for the dry sample, which is 0.48. There is a rapid drop-in dilation rate after reaching the peak. For the moist samples, there are differences in the peak dilation rate at different normal stresses for sample AH2. The difference is not significant for the other samples (AH1 and AH3). After the peak values, the dilation rate decreases gradually with the increase in horizontal displacement for each of the tests. The dilation angle for each of the samples eventually reaches almost zero, which is essentially the critical state. However, the critical state stress ratio is not constant for the moist samples, as shown in Figure 3-11.

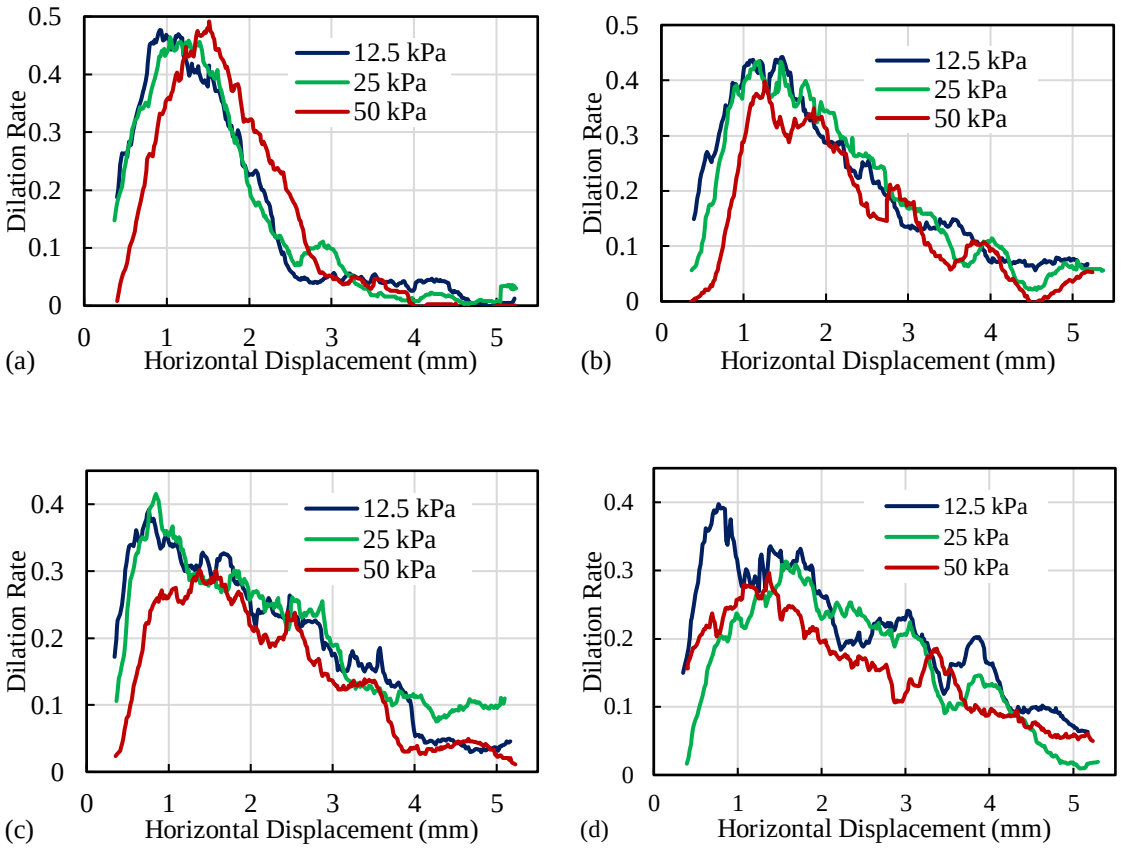


**Figure 3-12**: Dilation rates for dense condition of sample A: a) AH0, b) AH1, c) AH2, and d) AH3

Figure 3-13 shows the variation of stress ratio with horizontal displacement for sample A prepared without compaction. For the loose condition of the soil, no post–peak degradation in the stress ratio is observed in any of the samples, as expected. As seen in Figure 3-13 (b-d), the peak stress ratio is almost the same for all normal stresses for the moist samples. The peak ratios are 0.6, 0.55, and 0.5 for samples AN1, AN2, and AN3, respectively, which correspond to the friction angles of 31°, 29° and 26.5°, respectively. The moisture contents in these samples are 1.25%, 2.0%, and 2.7%, respectively. The friction angles for the loose soils are 30% to 40% less than the peak friction angles for the dense soils discussed above.

For the loose dry sand, the stress ratio appears to decrease with the increase of normal stress. The peak stress ratio for the dry sample (AN0) varies from 0.69 to 0.88 (Figure 3-13(a)), corresponding to the friction angle variations from 34.5° to 41°. The higher value is for the normal stress of 12.5 kPa, and the lower value is for the normal stress of 50 kPa. It is to be noted that, as discussed above, the critical state friction angle for the soil in the dense condition is 35°. Thus, the critical state friction angle for the dense soil appears to be the same as the peak friction angle of the loose soil at 50 kPa, which is consistent with the concept of the critical state friction angle. However, for the low normal stress of 12.5 kPa, the friction angle in the loose condition is significantly higher than the critical state friction angle. Thus, the concept of critical state friction angle may not be applicable at the low confining pressure of the soil. Al Tarhouni et al. (2017) also questioned the critical state friction angle of sand at low confining pressure from direct simple shear and triaxial tests.

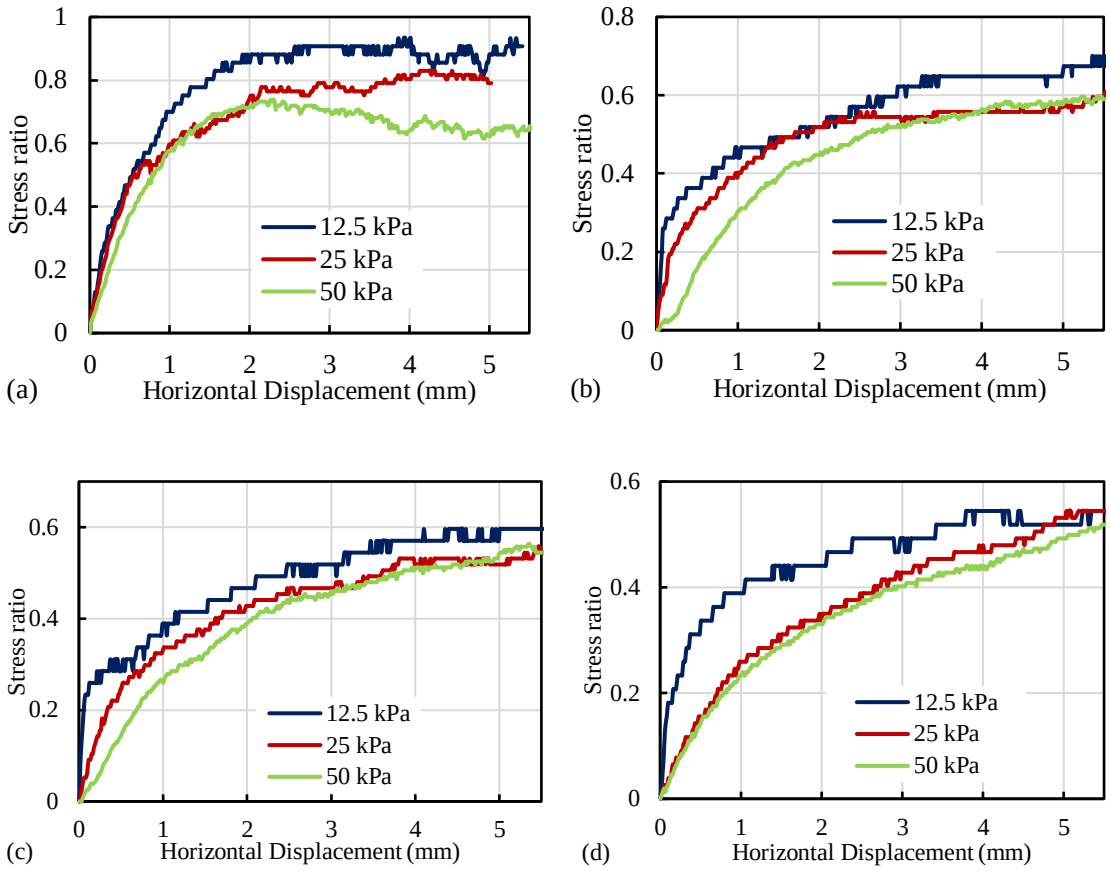


**Figure 3-13**: Variation of stress ratio for loose condition of sample A: a) AN0, b) AN1, c) AN2, and d) AN3

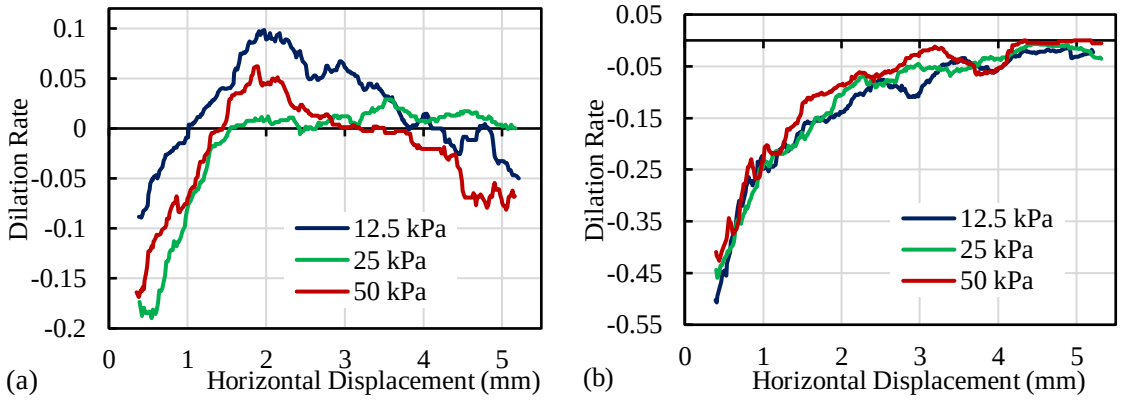

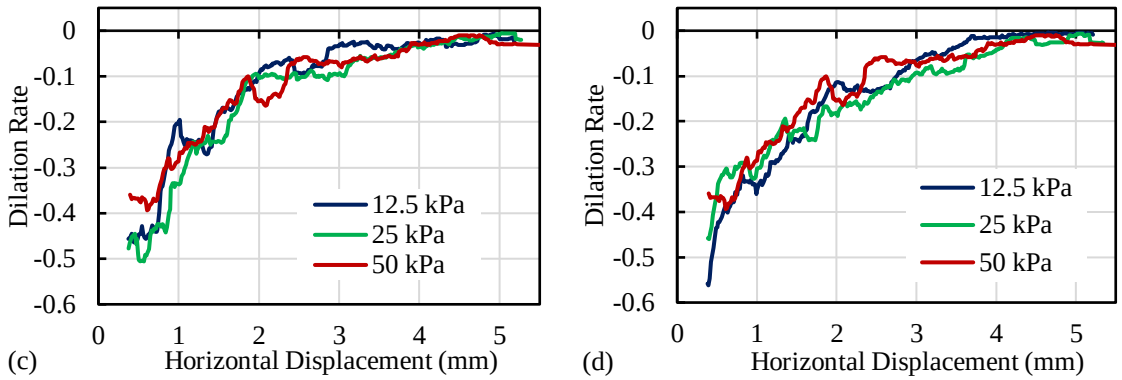


**Figure 3-14**: Dilation rates for loose condition of sample A: a) AN0, b) AN1, c) AN2, and d) AN3

The dilation rate for the loose soil is generally negative, indicating a decrease of volume during the direct shear tests, as shown in Figure 3-14. As the shearing of soil occurs at constant volume, the dilation rates become zero at the point of shear failure. However, the increase in the volume of the soil (positive dilation rate) is observed in the dry sample during shearing (Figure 3-14(a)). It shows that although the dilation rate is negative at the beginning, it increases with the increase of horizontal displacement and reaches the maximum value at the horizontal displacement of around 2 mm. The stress ratio is also peak at the same horizontal displacement (i.e., 2 mm).

Figure 3-15 and Figure 3-16 show the results of direct shear tests for sample B subjected to high compaction. The figures show similar responses to those observed for sample A. The peak stress ratio is the highest for the lowest (12.5 kPa) normal stress except for sample BH1. The peak stress ratio generally reduces with the increase of the normal stress. The magnitudes of the peak stress ratio are different from different tests, likely due

to the differences in the densities of the soil. The dilation rate increases initially with the horizontal displacement and then decreases after reaching the peak.

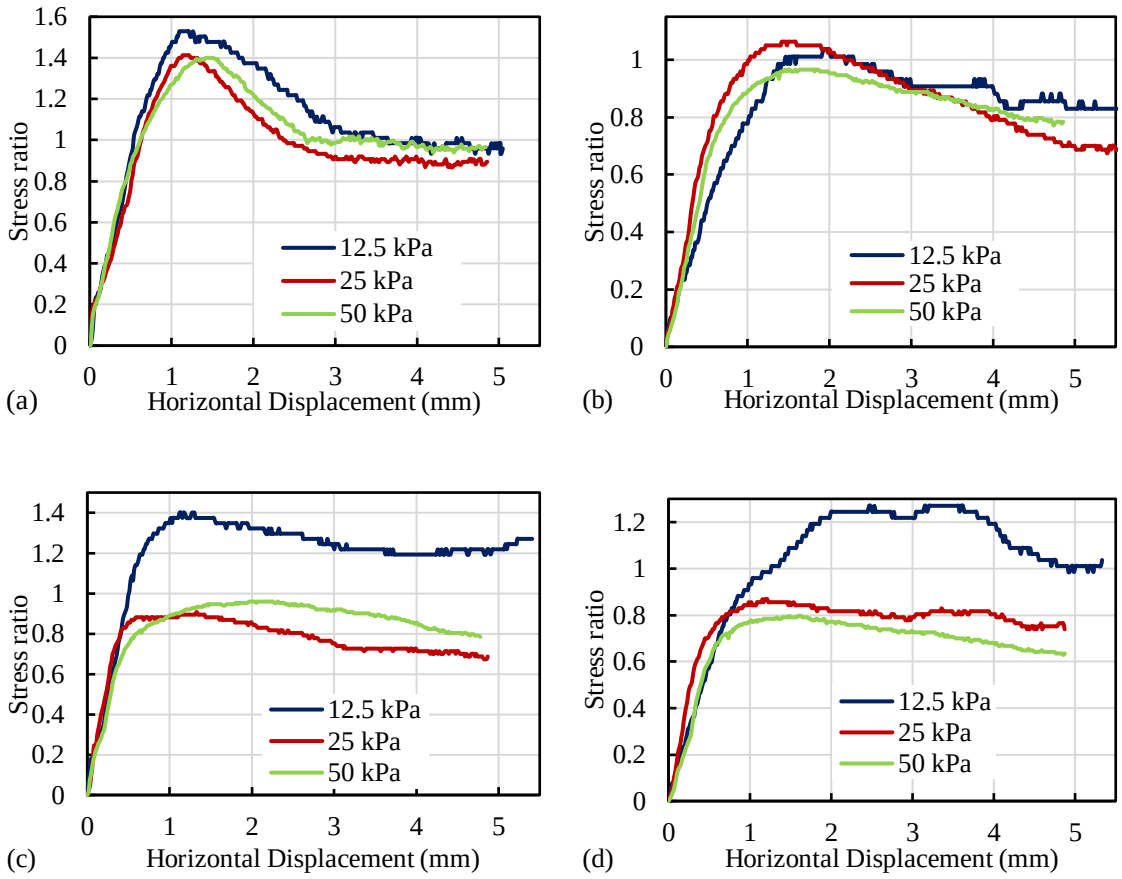


**Figure 3-15**: Variation of stress ratio for dense condition of sample B: a) BH0, b) BH1, c) BH2, and d) BH3

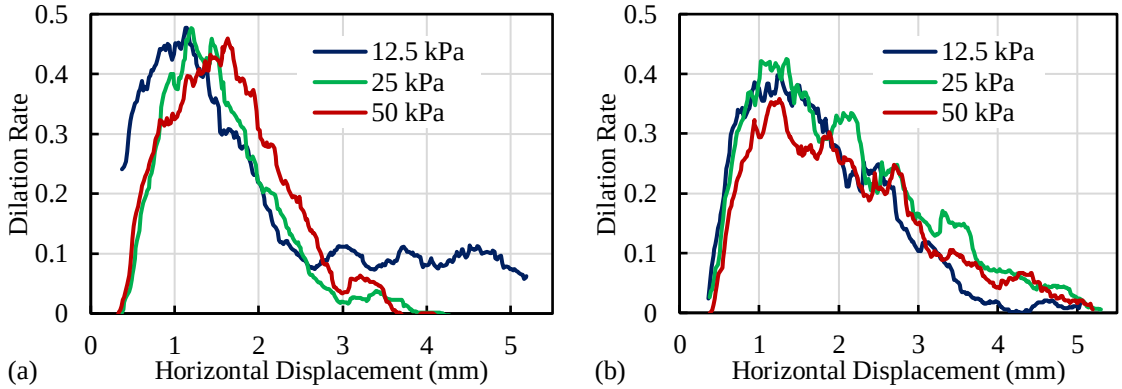

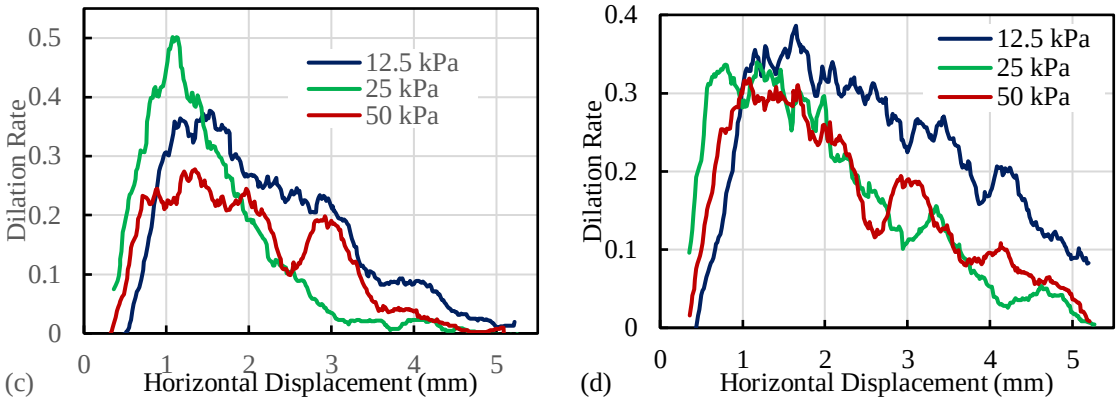


**Figure 3-16**: Variation of dilation rate for dense condition of sample B: a) BH0, b) BH1, c) BH2, and d) BH3

The stress–deformation behavior of the uncompacted sample B is shown in Figure 3-17 and Figure 3-18. The effect of normal stress and moisture content on the variation of stress ratio and dilation rate with horizontal displacement is similar to those of the uncompacted sample A. The moist samples (BN1, BN2, and BN3) reach their peak stress ratio at higher horizontal displacement than the dry sample (BN0). The dilation rate for moist sample B is negative at the initial horizontal displacement and reaches gradually close to zero at the final horizontal displacement.

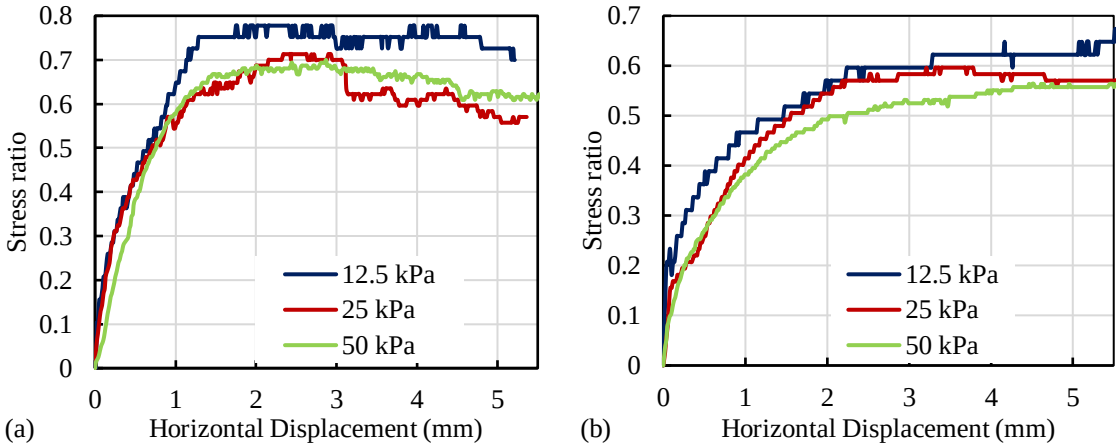

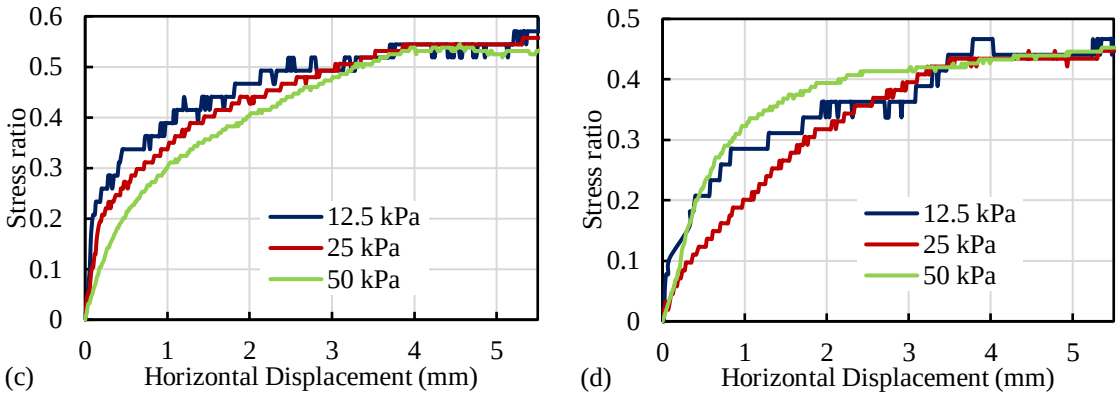


**Figure 3-17**: Variation of stress ratio for loose condition of sample B: a) BN0, b) BN1, c) BN2, and d) BN3

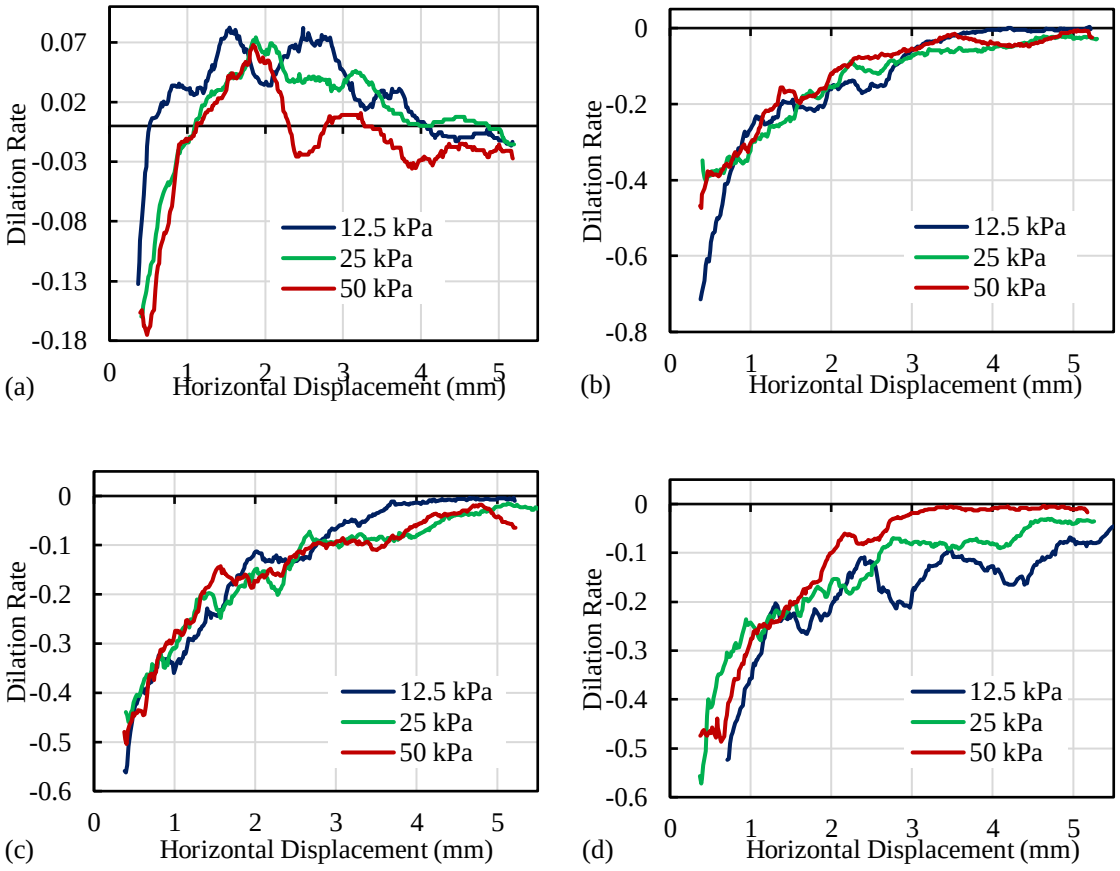


**Figure 3-18**: Variation of dilation rate for loose condition of sample B: a) BN0, b) BN1, c) BN2, and d) BN3

Figure 3-19 and Figure 3-20 present the variation of stress ratio and dilation rate with horizontal displacement for compacted and uncompacted sample C under three different moisture contents. The greater difference in peak stress ratio for the compacted sample C among three normal stresses due to the presence of moisture is similar to those for the compacted sample A and Sample B. However, there is less difference in peak stress ratio for the dry compacted sample C for three normal stresses than those for the dry compacted sample A and sample B. The peak dilation rate is higher for the compacted sample than for the uncompacted sample.

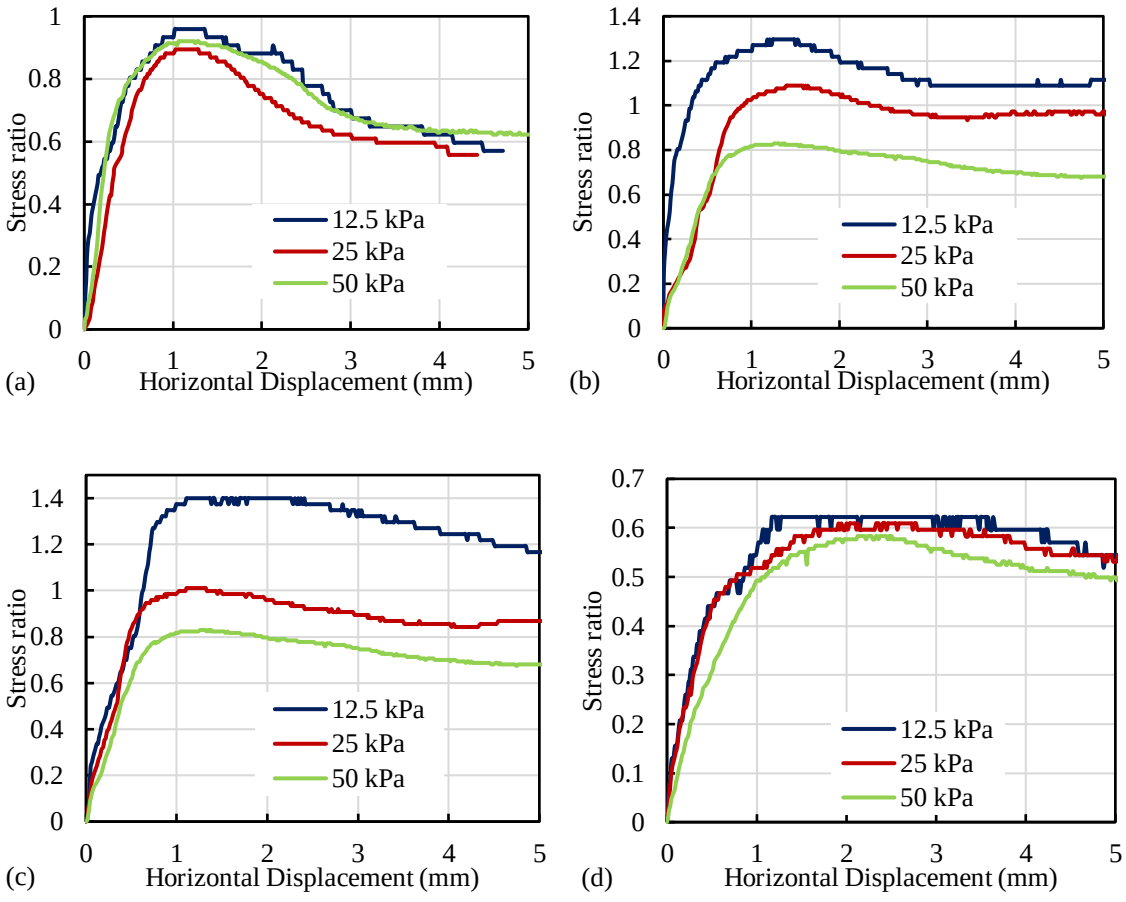


**Figure 3-19**: Variation of stress ratio for sample C: a) CH0, b) CH1, c) CH2, and d) CN0

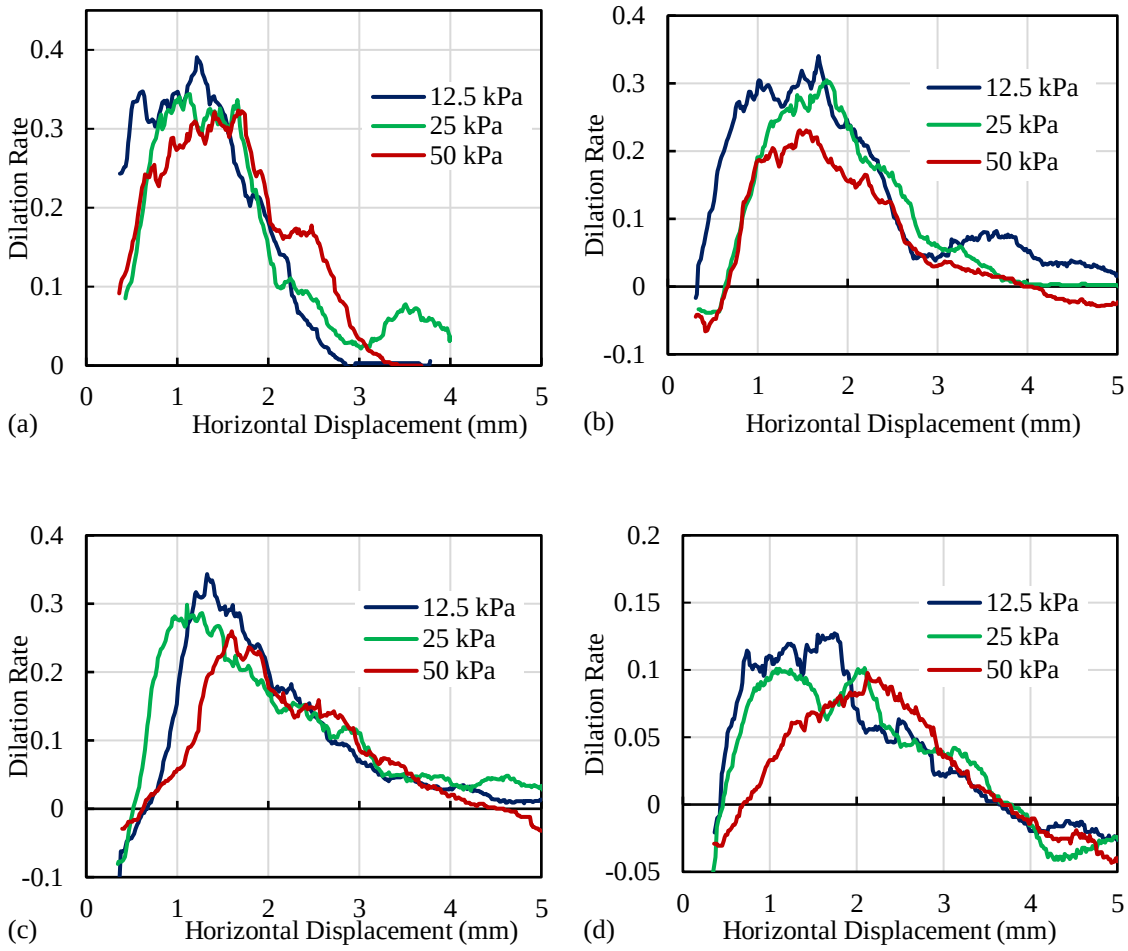


**Figure 3-20**: Variation of dilation rate for sample C: a) CH0, b) CH1, c) CH2, and d) CN0

### 3.6.3 Peak Stress Ratio

As discussed earlier, the peak stress ratios obtained from different tests are found to be different. The stress ratios generally depend on the stress levels, water contents, and the densities of the soil. To examine the effect of stress levels, the peak stress ratios for various soils are plotted against normal stress in Figure 3-21. The figure reveals that the stress ratio is generally the highest at the normal stress of 12.5 kPa. The changes in the stress ratios are not significant beyond the normal stress of 25 kPa. In general, the stress ratio is the

highest for the dry soils and decreases with the increase in water content, except for the silica sand. Tiwari & Al-Adhadh (2014) demonstrated for well-graded sand that the friction angle can decrease for changing from dry state to saturated state at the same relative density, which is likely due to the effect of lubrication around the soil particle by the water. However, the test results presented here can also depend on the density of the soil, as discussed below.

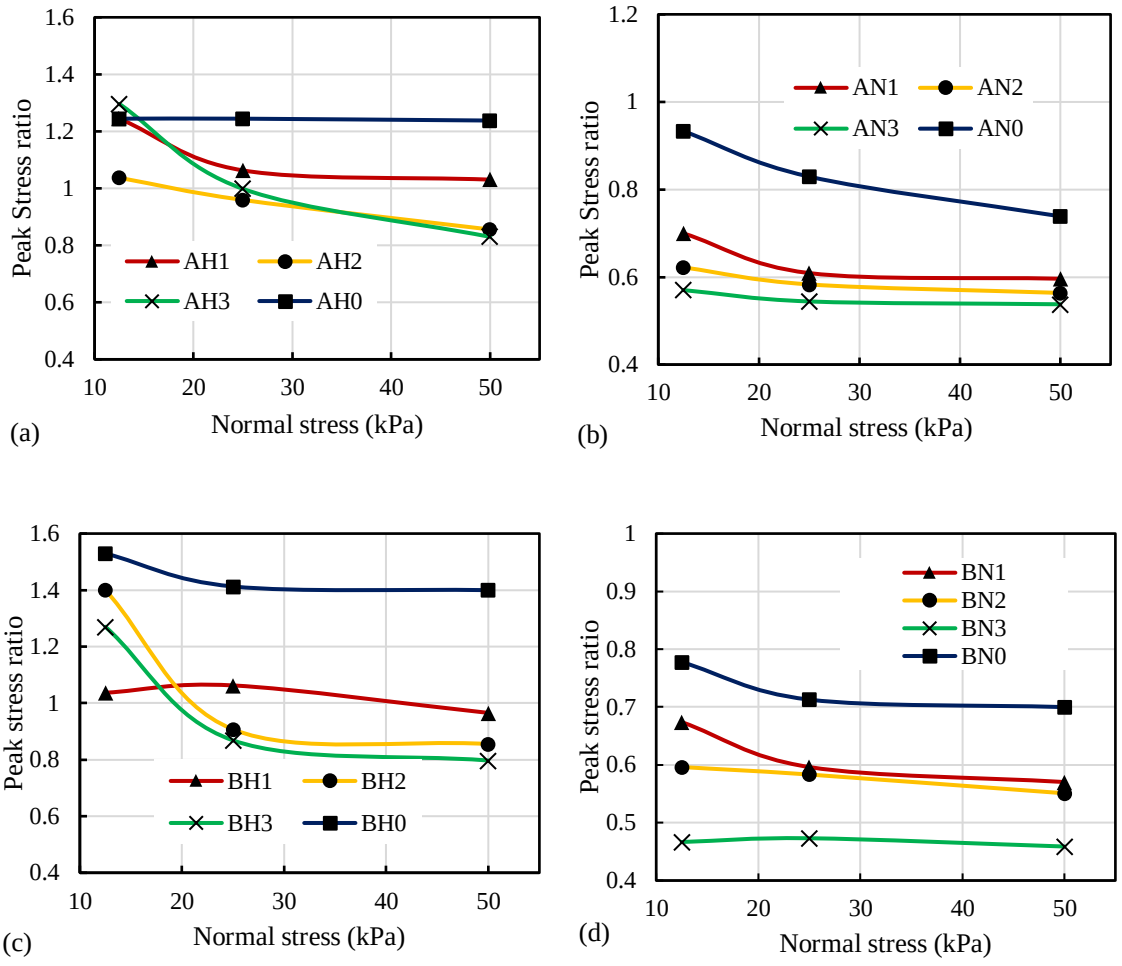

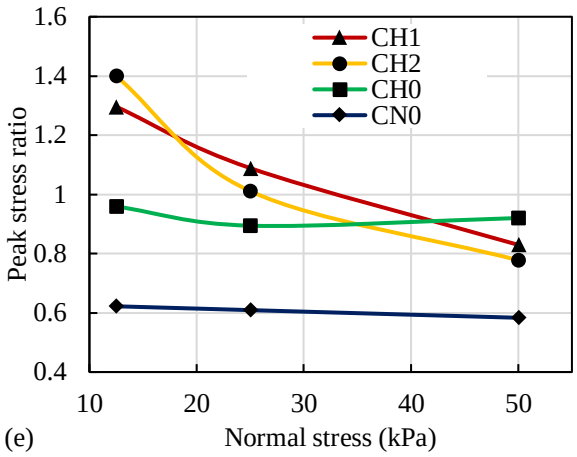


**Figure 3-21**: Peak stress ratio against normal stress: a) Dense sample A, b) Loose sample A, c) Dense sample B, d) Loose sample B, and e) Sample C

To examine the effect of water contents, the peak stress ratio at various normal stresses are plotted against the water contents in Figure 3-22. Since the dry densities of the soil in the shear box are also expected to be different even under the same compaction effort, the calculated dry unit weights of the soil are also plotted against the moisture contents in this figure. It shows that the peak stress ratio and the dry unit weight of the soils decrease with the increase of moisture content. Thus, the reduction of the peak stress ratio with moisture content has a strong correlation with the reduction of the dry density. While both dry density and the water content are expected to contribute to the peak stress ratio of the soil, the contribution of each parameter could not be separated from this test program.

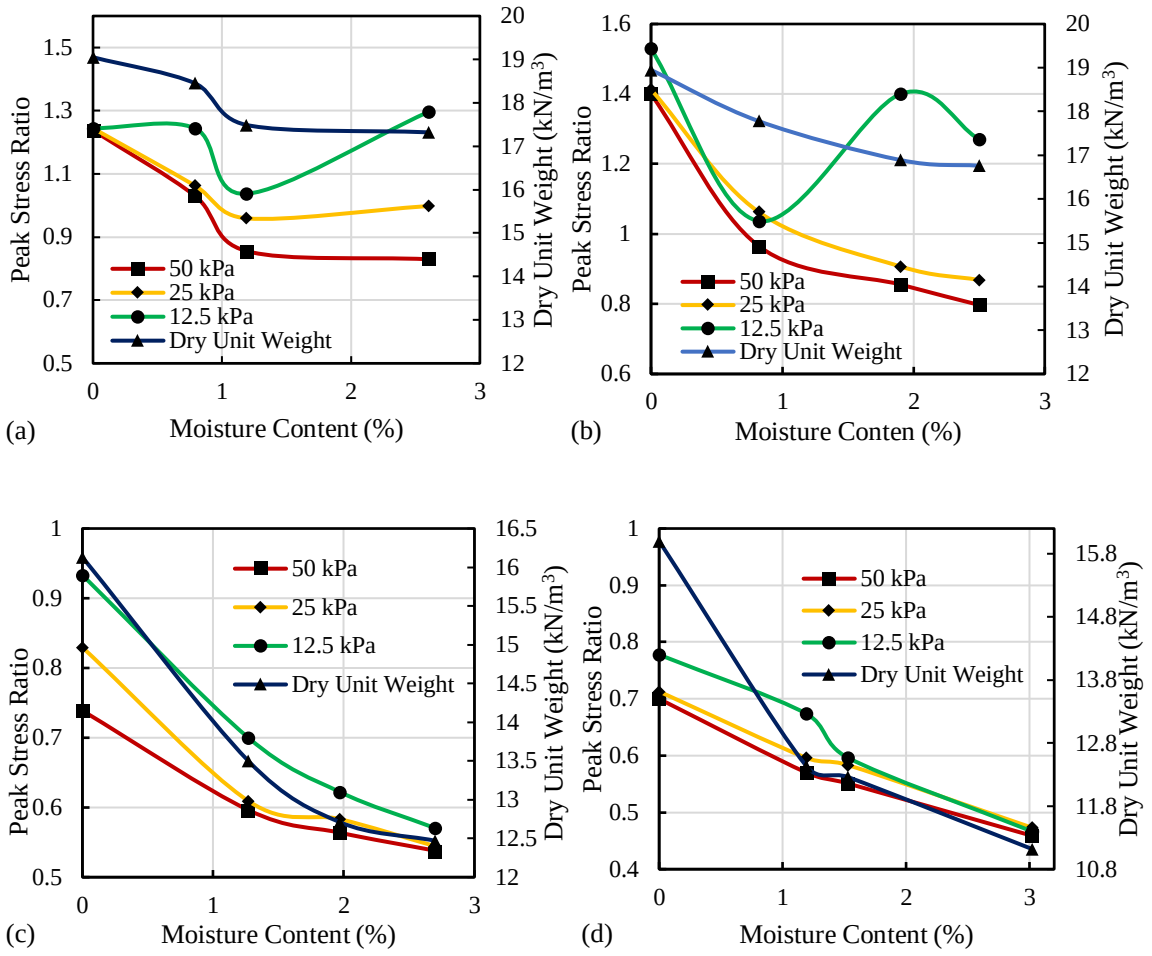


**Figure 3-22**: The peak stress ratio with dry unit weight: a) Compacted Sample A, b) Compacted Sample B, c) Uncompacted Sample A, d) Uncompacted Sample B

### 3.7 Results from Test Program 2

In test program 2, 48 tests are used to examine the effects of confining pressure, dry unit weight, and moisture content on the shear strength of soil (Sample A), and 32 tests are used to explore the effect of shear displacement rate on the behavior of the soil. The stress–displacement response, peak stress ratio, and angle of internal friction are examined.

### 3.7.1 Stress–Deformation Response

Figure 3-23 shows the changes in stress ratio with horizontal displacement for the compacted samples for different normal stresses. Each sand sample was tested at six normal stresses. As seen in the figure, the peak stress ratio is again the highest for 12.5 kPa of normal stress that reduces with the increase of the normal stress. The reduction of peak stress ratio with the increase in normal stress is more for the moist samples than for the dry samples. The peak stress ratio is reduced from 1.2 to 1.1 for increasing of normal stress from 12.5 kPa to 400 kPa for dry samples, whereas for the moist samples, the peak stress ratio is reduced from 1.6 to 0.7 (Figure 3-23 (d)), showing the effect of the moisture contents. It is also to be noted that post–peak degradation of the stress ratio is significant for the dry sand. Al Tarhouni et al. (2017) demonstrated similar peak and post–peak behavior for dense silica sand.

For the dry sand samples, the stress ratio is reduced from the peak value of around 1.2 to the critical state value of around 0.6–0.8. The peak stress ratio is obtained at 1–1.2 mm horizontal displacement for lower normal stresses (12.5 & 50 kPa), whereas it is obtained at the higher horizontal displacement of 1.5–2.5 mm for higher normal stresses (200 & 400 kPa). However, there is no significant post–peak degradation in the moist samples. The stress ratio becomes nearly constant after reaching the peak stress ratio at around 1–1.5 mm of horizontal displacement for the moist samples. Wei et al. (2018) also showed that the post–peak degradation of stress ratio for the compacted soil–rock mixtures with higher moisture is less significant.

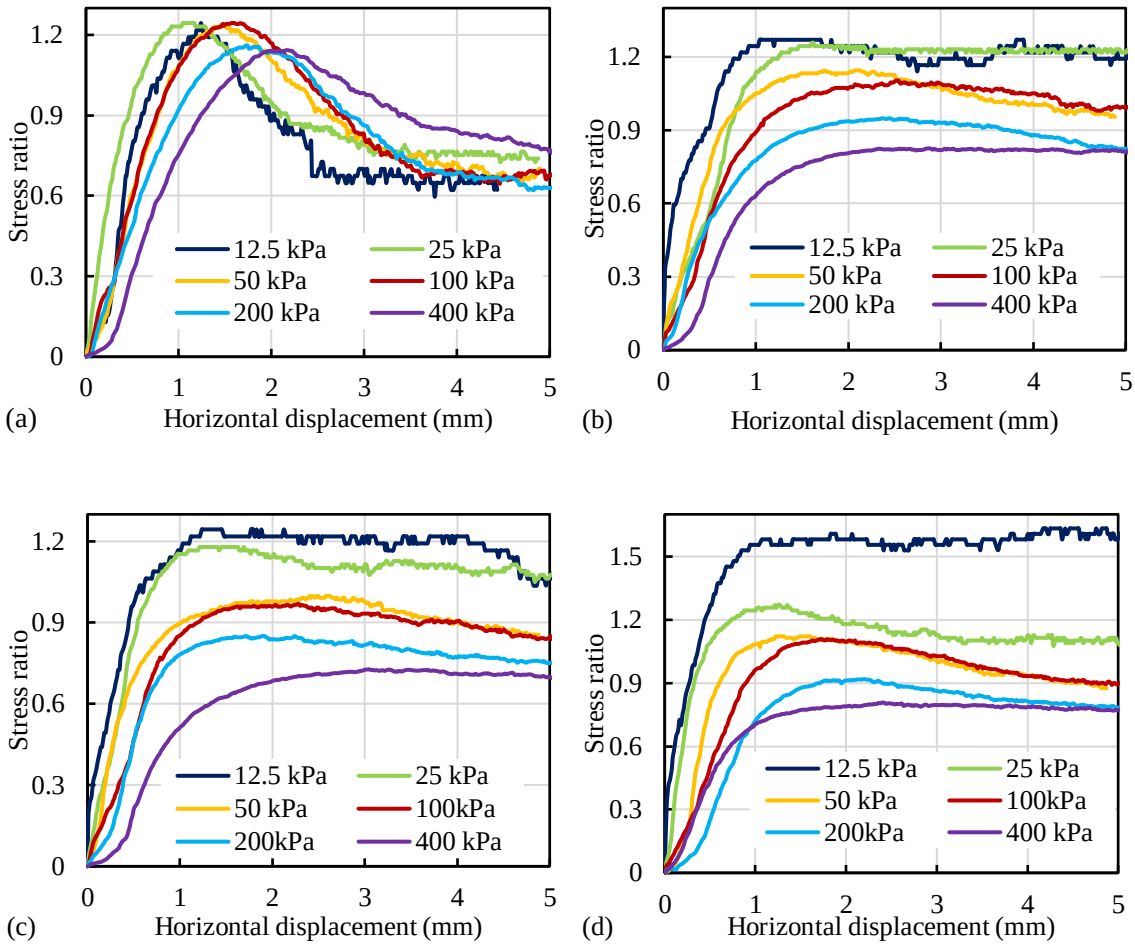


**Figure 3-23**: Stress ratio for compacted sand sample for varying moisture contents a) 0% (Dry), b) 1.5%, c) 3%, and d) 6%.

Figure 3-24 shows the stress (ratio)–displacement behavior of the uncompacted (loose) sand samples. The moist sand samples reach the peak stress ratio at a higher horizontal displacement (~5 mm) for the loose condition than for the dry sand samples. The peak stress ratio for loose dry sand is around 0.7–0.9, which is close to the critical state value (0.6–0.8) of the compacted dry sand discussed earlier. The post–peak degradation of stress ratio is noticed for dry sand in higher normal stress of 100 kPa, which may be due to densification of the sample during the application of normal stress before shearing. As

observed above, the peak stress ratio is the highest at 12.5 kPa of normal stress that decreases with the increase in normal stress.

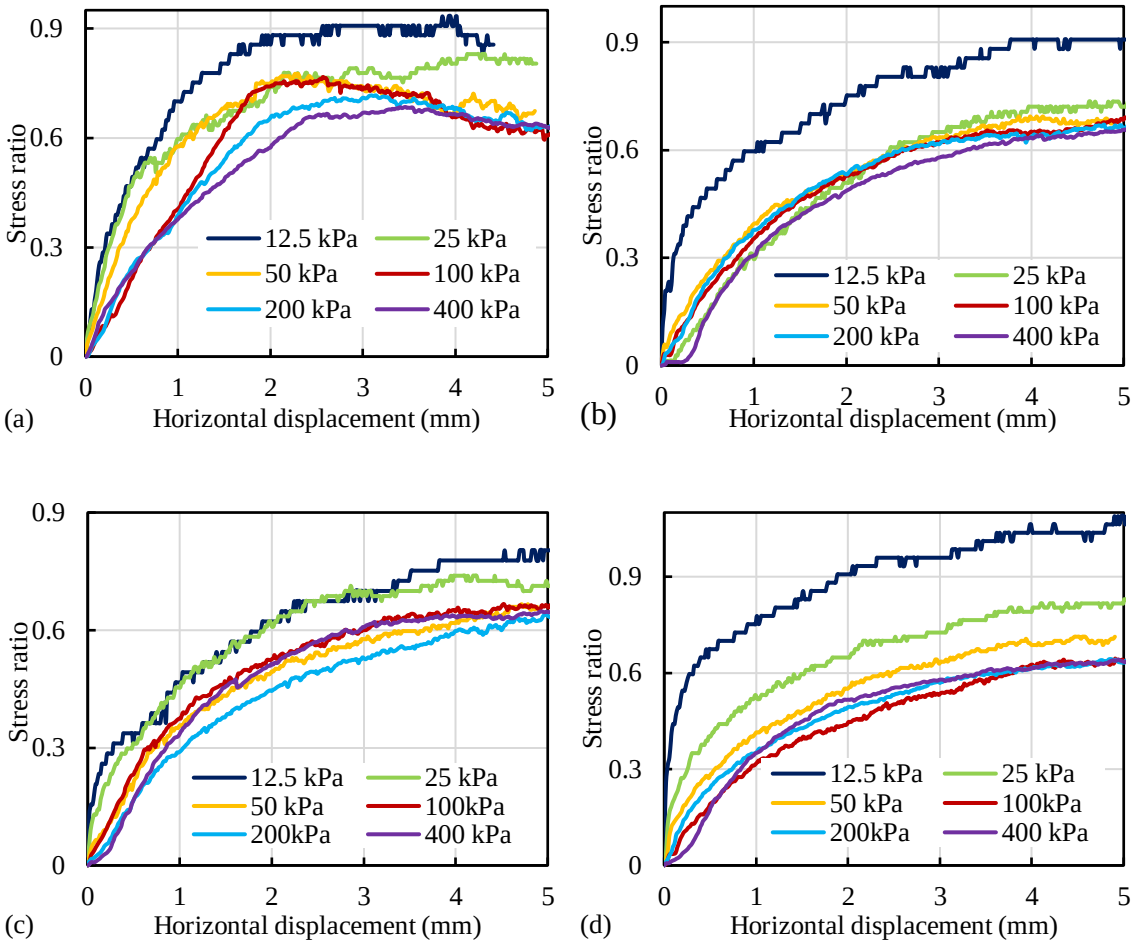


**Figure 3-24**: Stress ratio for uncompacted sand sample for varying moisture contents a) 0% (Dry), b) 1.5%, c) 3%, and d) 6%.

Figure 3-25 plots the calculated dilation rate against the horizontal displacement for the compacted samples. Dilation rate is calculated as discussed in section 3.6.2. Moving average values of the dilation rate are plotted in the figure to minimize the noise in the measured values. The post–peak degradation in the dilation rate is found to be more

significant for the dry sample in the figure (Figure 3-25). A similar scenario is observed in the case of peak stress ratio (Figure 3-23). The peak dilation rate for the dry sample is around 0.47–0.5 for all normal stresses except 400 kPa, where it is 0.36 (Figure 3-25(a)). There is a rapid drop in the dilation rate after reaching the peak values. The compacted moist samples show different peak dilation rates at different normal stresses. There is a gradual reduction of the peak dilation rate from 0.6 to 0.14 with the increase of normal stress from 12.5 kPa to 400 kPa for the sample with 6% of moisture contents (Figure 3-25 (d)).

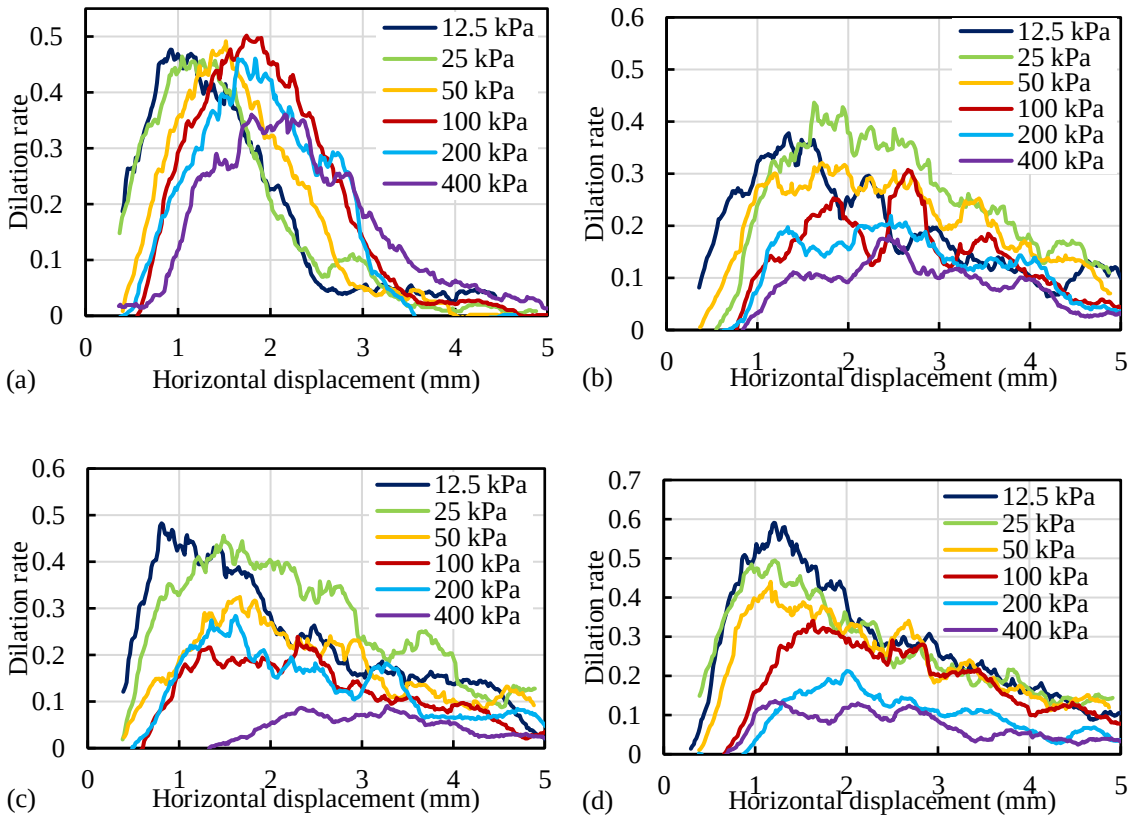


**Figure 3-25**: Dilation rate for compacted sand sample for varying moisture contents a) 0% (Dry), b) 1.5%, c) 3%, and d) 6%.

Dilation rates for the uncompacted loose sand samples are shown in Figure 3-26. The dry loose sands show some positive dilation rate with a maximum value of 0.1 over a shearing range (Figure 3-26 (a)), which denotes an increase in volume. However, the moist sample shows a negative dilation rate corresponding to the contraction that reaches close to zero dilation rate at high shear displacement.

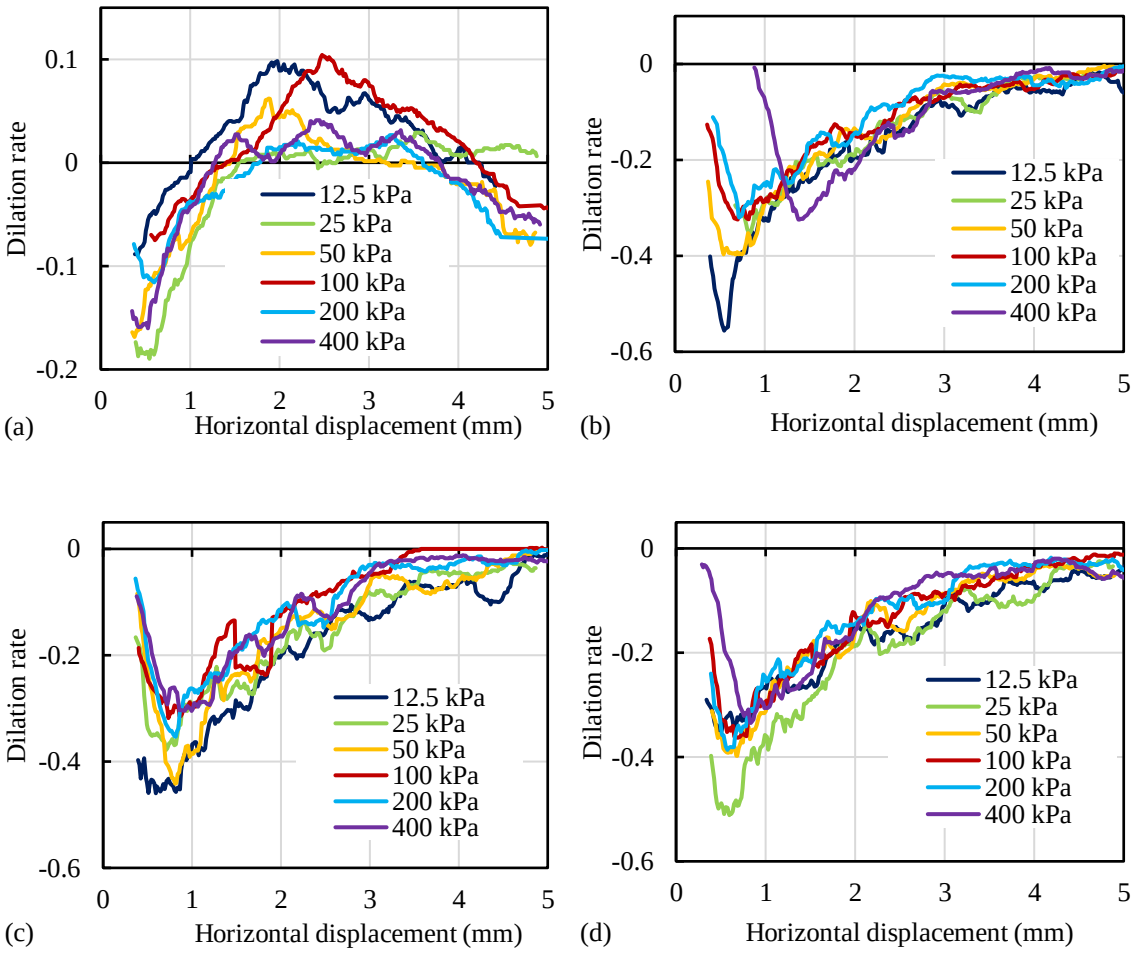


**Figure 3-26**: Dilation rate for uncompacted sand sample for varying moisture contents: a) 0% (Dry), b) 1.5%, c) 3%, and d) 6%.

### 3.7.2 Peak Stress Ratio

Figure 3-27 shows the variation of peak stress ratio with normal stress for the compacted samples. Again, the peak stress ratio decreases with the increase in normal stress. The peak stress ratio at the lowest normal stress of 12.5 kPa is ~1.25 for all samples except for the sample with 6% of moisture content. The difference in peak stress ratio between the dry sample and moist sample increases with the increase in normal stress as the rate of changing stress ratio with normal stress is more in the moist sands. The Peak stress ratio is less in the moist samples, indicating a lower shear strength.

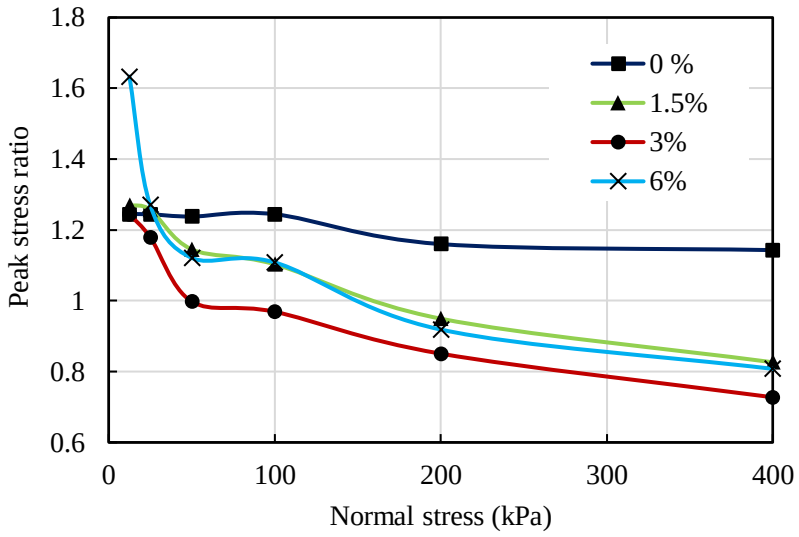


**Figure 3-27**: Effects of moisture content and normal stress on peak stress ratio for compacted sand samples.

The variation of the peak stress ratio with normal stress for loose sand is shown in Figure 3-28. The peak stress ratio is reduced gradually from 0.93 to 0.68, with the increase of normal stress from 12.5 kPa to 400 kPa for the dry samples. However, the peak stress ratio of the moist samples remains almost constant (~0.67) for normal stresses between 100

and 400 kPa, indicating a less effect of normal stress on the peak stress ratio of loose samples. A similar phenomenon was observed in Taylor (1948) from the triaxial tests on Ottawa sand where the angle of internal friction for loose condition decreased from 30° to 27° with an increase of confining pressure from 48 kPa to 766 kPa whereas, for dense condition, it decreased from 34.5° to about 29° due to the same increase in confining pressure.

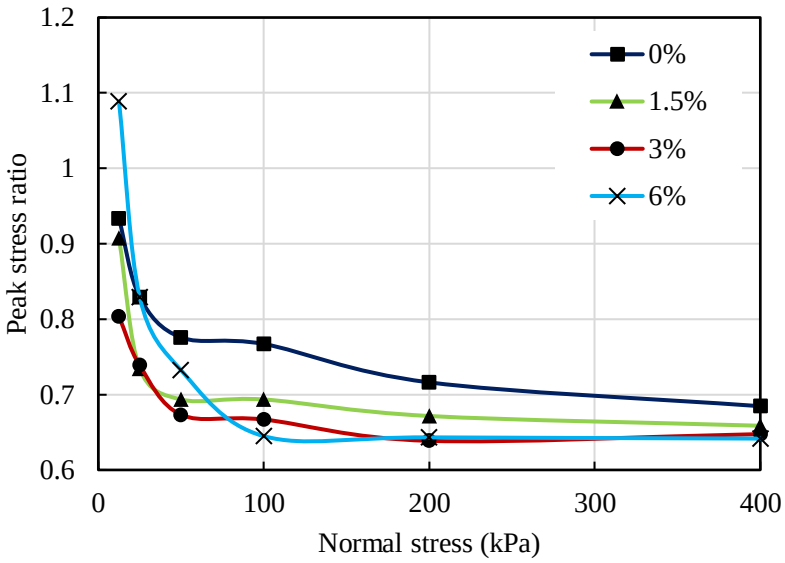


**Figure 3-28**: Effects of moisture content and normal stress on peak stress ratio for uncompacted sand sample.

### 3.7.3 Effect of Shearing Rate

The effect of the rate of shearing on the stress ratio is studied under four normal stresses 50,100, 200, and 400 kPa for dry sand samples only. Figure 3-29 shows the variation of stress ratio with horizontal displacement for the compacted samples. The peak stress ratio is obtained at 1.5 mm of horizontal displacement for each of the displacement rates with

50 kPa of normal stress, whereas for 400 kPa of normal stress, it is obtained at 2.5 mm of horizontal displacement. There is no significant difference in the peak stress ratio and the post–peak degradation for different displacement rate in Figure 3-29.

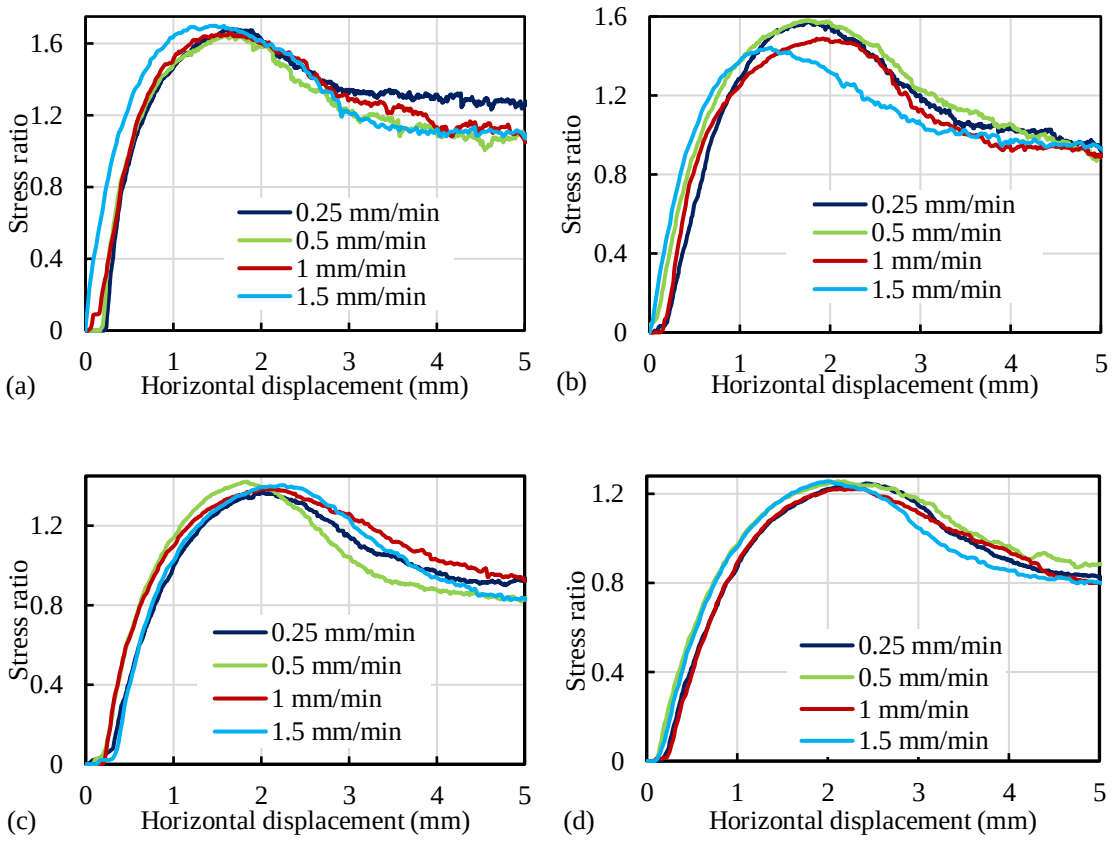


**Figure 3-29**: Stress ratio for compacted sand sample for varying shear displacement rates (mm/min) at normal stresses a) 50 kPa, b) 100 kPa, c) 200 kPa, and d) 400 kPa

Similar behavior is observed for the uncompacted samples, as seen in Figure 3-30. Lade and Nam (2009) also reported no effect of shearing on the shear strength of the dry sand.

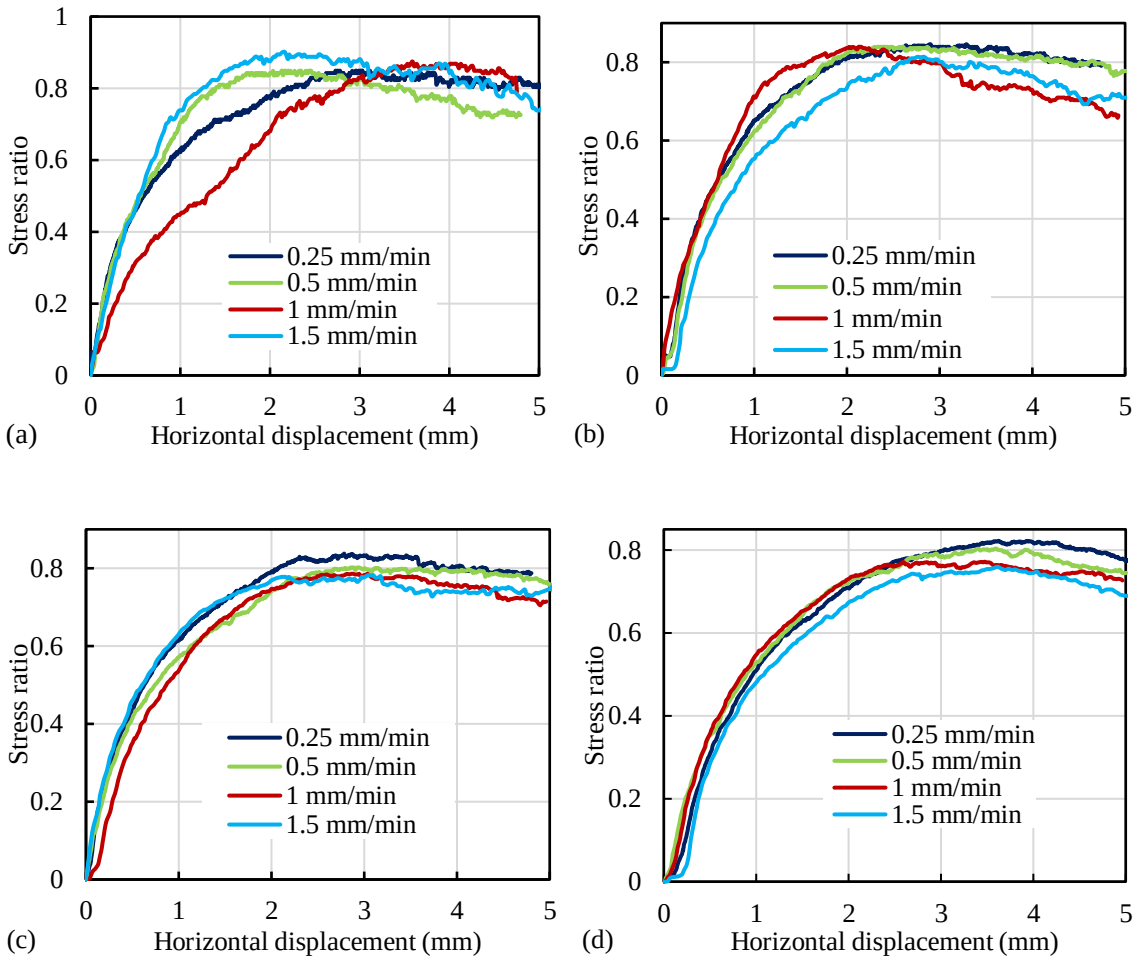


**Figure 3-30**: Stress ratio for uncompacted sand sample for varying shear displacement rates (mm/min) at normal stresses a) 50 kPa, b) 100 kPa, c) 200 kPa, and d) 400 kPa

### 3.7.4 The Angle of Internal Friction

The above study revealed that the angle of internal friction depends on the density, stress level, and moisture content of the sand. To examine these further, the peak shear stresses from the tests are plotted against the normal stresses in Figure 3-31. Results of two additional tests (w = 5.6% and 0% with dry densities of 18.6 kN/m$^3$ and 18.1 kN/m$^3$, respectively) conducted as a part of the study are also included in Figure 3-31. Test results

showed that the peak shear stress versus normal stress response is almost linear at low densities of the soil (Figure 3-31a). Beyond the density of 17 kN/m$^3$, the responses are nonlinear (Figure 3-31b). Thus, at lower densities (or unit weights) of the soil, the effect of the normal stress on the friction angle (the slope) is insignificant. However, at the higher unit weights of the soil, the friction angle is higher at lower stress levels and relatively lower at higher stress levels. In both cases, the intercepts of the shear strength versus normal stress plot are negligible even for the soil with the moisture contents of 1.5% to 6% or under submerged conditions. Thus, the effect of suction on the shear strength (i.e., apparent cohesion) of the soils negligible during the direct shear tests.

Figure 3-31 reveals that the shear strength of the soil is higher for a higher density of the soils. The rate of increase of shear strength with density is relatively less for the sand with a density of less than 17 kN/m$^3$. For an increase of the density from 11.5 kN/m$^3$ to 16.1 kN/m$^3$, the shear strength increases from 256.6 kPa to 273.8 kPa at the normal stress of 400 kPa. However, for the increase of density from 17 kN/m$^3$ to 19 kN/m$^3$, the shear stress increases from 290.1 kPa to 578.8 kPa at the same normal stress (i.e., 400 kPa). Thus, the effect of density on the shear strength (hence, the angle of internal friction) is very significant at the dense condition of the soil (>17 kN/m$^3$).

Note that even at different moisture contents, the shear strengths are the same for the same levels of densities. In Figure 3-31b, the responses for the moisture contents of 1.5% (with $\gamma_d$ = 17.4 kN/m$^3$) and 6% (with $\gamma_d$ = 17.2 kN/m$^3$) match with each other. Similarly, the test results with dry unit weights of 18~19 kN/m$^3$ match reasonably (less than 10%

difference) with each other. Thus, the contribution of the moisture contents is considered insignificant to the shear strength.

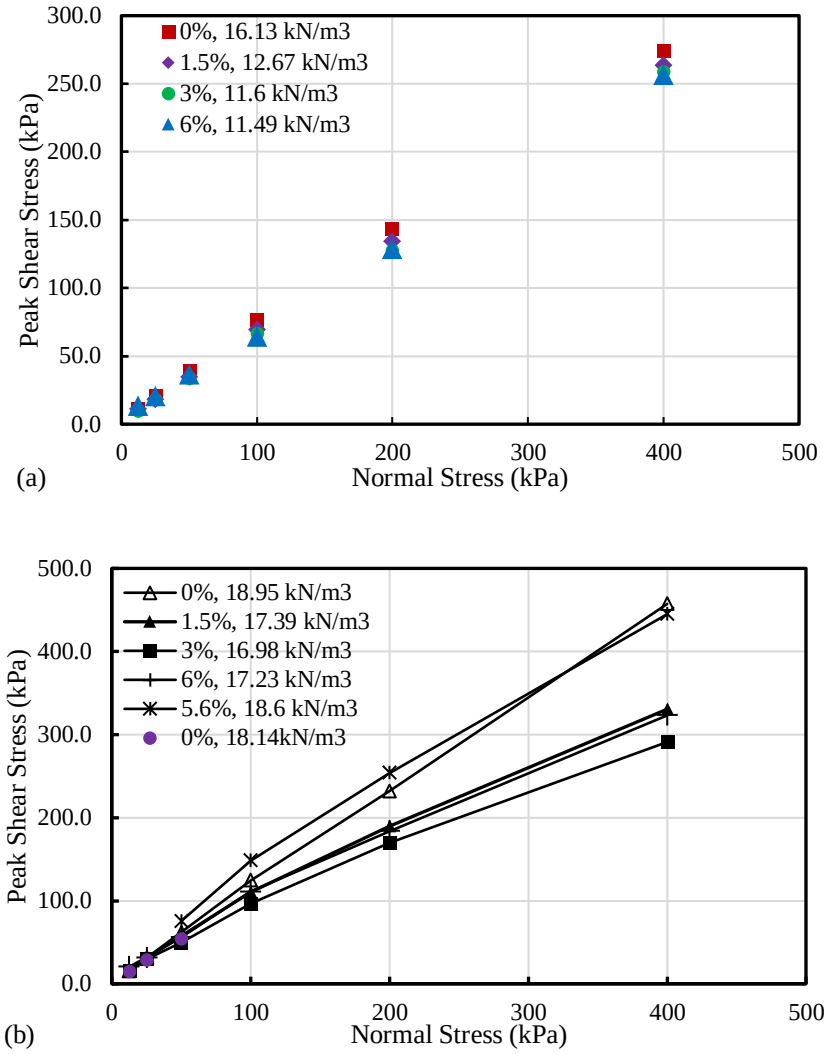


**Figure 3-31**: Shear stress-Normal stress plot of sample A for (a) Low dry unit weight and (b) High dry unit weight

The angles of internal friction of the sand are calculated from the slope of linear trendlines of the peak shear stress versus normal stresses data from the tests. The calculated angles of internal friction and the dry densities are plotted against the water contents in

Figure 3-32. The maximum angle of internal friction of 49° is found for the compacted dry samples, which is reduced with the increase of moisture content. For the uncompacted sample, the maximum angle of internal friction is ~34.5° for the dry sand that is reduced with the moisture contents. Dry unit weights of the sand are also reduced with the increase of moisture content for both compacted and uncompacted soil. This observation confirms that the reduction of the angle of internal friction with moisture content in the tests is due to the reduction of the density (dry unit weight). Thus, the degree of compaction is the most significant controlling parameter for the shearing resistance of the soil. Note that the peak shear stress of the dry sand is close to that of the moist sand with 5.6% moisture in Figure 3-31(b), as the dry unit weights of the soils are similar.

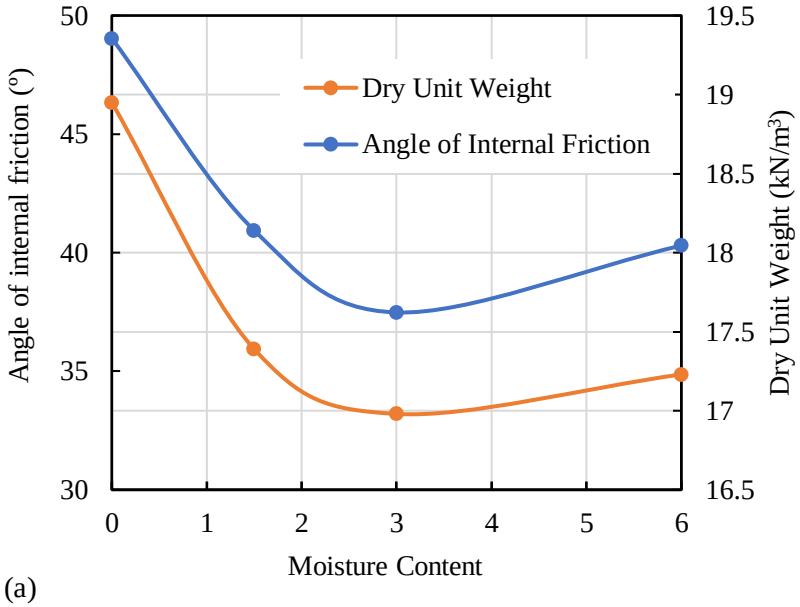


(a)

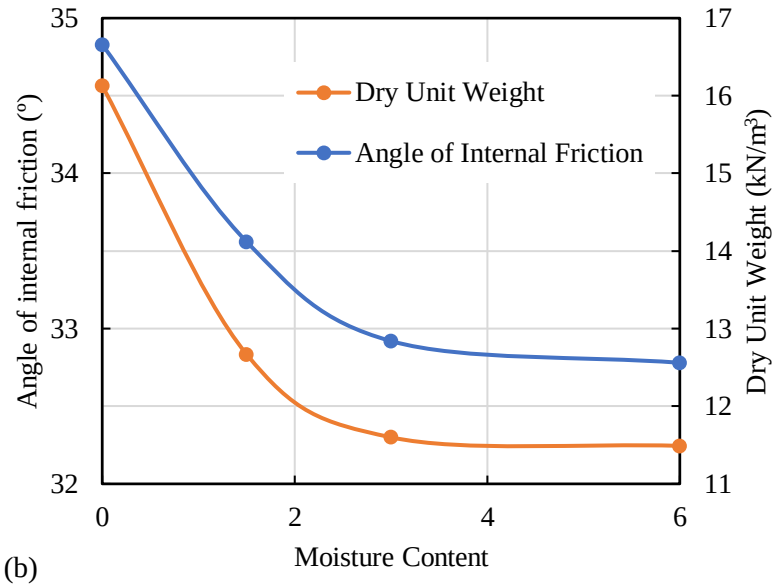


**Figure 3-32**: Effects of moisture content on the angle of internal friction and dry unit weight for (a) compacted sand and (b) Uncompacted Sand.

Figure 3-33 plots the friction angles against the relative compaction calculated using the maximum dry density obtained from the Standard Proctor Compaction tests. As expected, the friction angle increases with the increase of the relative compaction. The rate of increase is less at lower relative compactions (loose condition), which is significantly high at high relative compactions.

The friction angles for sample A and sample B are similar in Figure 3-33, indicating that the removal of coarse particles may not significantly affect the friction angle of the soil. The poorly graded silica sand is found to have a lower friction angle at the same level of relative compactions.

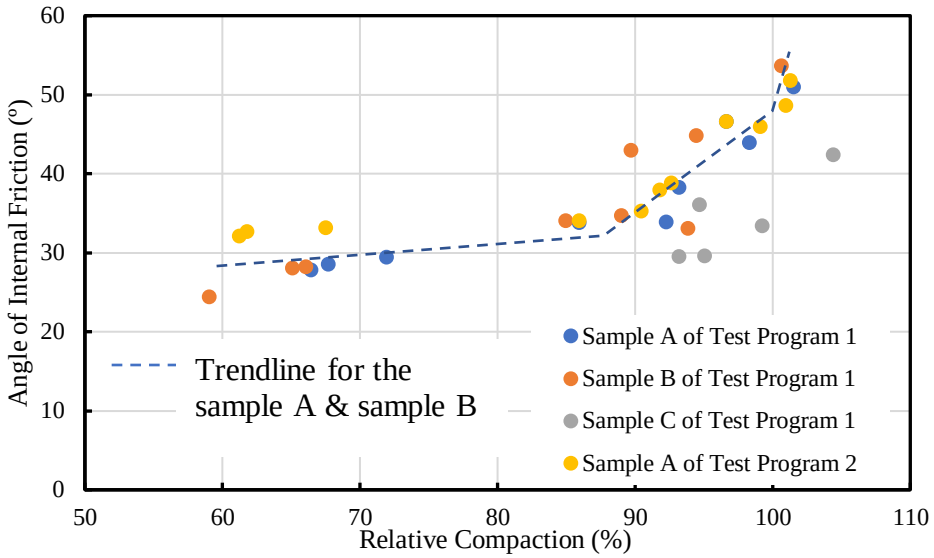


**Figure 3-33**: Variation of peak friction angle with relative compaction

### 3.8 Summary

The behavior of sands is studied using direct shear tests with varying moisture content, compaction level, and stress level. It reveals that the cohesion resulting from matric suction is negligible for the range of moisture content considered (1% to 6%). This is attributed to the fact that the air voids in the granular soil are connected in the direct shear apparatus, causing the air pressure to be the same as the atmospheric pressure. Thus, the negative pore-water pressure in the soil was negligible. The sand considered here also falls within the low suction effect zone according to the grain-size distribution plot in Jung et al. (2016). The soil-moisture characteristic reveals the soil to have negligible matric suction at the water content of 8.5% (degree of saturation of 51%) and 95.5 kPa of matric suction at ~

1% of water content (6~7% degree of saturation). A very low air entry value of 0.3 kPa is estimated based on the fitting of data with Van Genuchten's model.

The friction angle of the soil was found to depend significantly on the density of the soil. In general, the friction angle was higher for dry soil that changed with the increases of moisture content in the soil. The change in the friction angle matches well with the change in the dry density of the soil. Thus, the variation of the friction angle with moisture content is attributed to the changes in the dry unit weight. Although a similar approach of soil compaction is used in each of the tests, the degrees of compaction of the soil samples in the test box was different due to the presence of different moisture contents. The rate of increase of the friction angle with relative density is less at lower relative compactions and very high at high relative compaction (>85%). The rate of shearing within the range of 0.25 mm/min to 1.5 mm/min was found to have an insignificant effect on the behavior of the dry soil.

The dense sand samples showed the post–peak degradation of stress ratio. The peak stress ratio is higher for lower normal stress, indicating a higher friction angle for the soil at the lower confining pressure. The higher friction angle is due to dilation of the soil at lower confining stress. A high confining pressure can suppress the dilation, reducing the angle of internal friction and the post–peak softening behavior. The friction angle was reduced with the increase of normal stress for both dry and moist sands. However, this phenomenon was more pronounced for the dense condition of the soil. The effect of normal stress on the friction angle was insignificant for uncompacted (loose) sands.

The comparison of the behavior of different soil samples from Test Program 1 revealed that the behaviors of sample A (Local sand passing the #4 sieve) are similar to the behavior of sample B (Local sand passing the #8 sieve) and sample C (Silica sand). The removal of coarse particles retained on the #8 sieve from the local sand does not affect the peak friction angle significantly. The strength parameter (friction angle) for poorly graded silica sand is found to be less than the parameter for the well-graded local sand at the same level of relative compaction.

### 3.9 References


Duncan, J. M., Wright, S. G., and Brandon, T. L. 2014. *Soil Strength and Slope Stability*. 2nd ed. John Wiley & Sons, Incorporated.

Lade, P. V., and Nam, J. 2009. 2009. "Strain Rate , Creep , and Stress Drop-Creep Experiments on Crushed Coral Sand." *Journal of Geotechnical and Geoenvironmental Engineering* 135 (7): 941–954.

Lu, N., Wu, B., and Tan, C.P.C. 2007. "Tensile strength characteristics of unsaturated sands." J*ournal of Geotechnical and Geoenvironmental Engineering*. 133 (2): 144–154.

Lu, N., & Likos, W. J. (2013). "Origin of Cohesion and Its Dependence on Saturation for Granular Media. " *Poromechanics V* 1669–1675.

Natural Resources (2004) "Geological Map of Newfoundland", Geological Survey, Newfoundland and Labrador. https://www.gov.nl.ca/nr/files/mines-investments-

geology-map-nl.pdf.

Ravindran, S., and Gratchev, I. 2020. “Estimation of Shear Strength of Gravelly And Sandy Soils from Shallow Landslides.” *International Journal of GEOMATE* 18 (70): 130–137.

Simoni, A., and Houlsby, G. T. 2006. “The Direct Shear Strength and Dilatancy of Sand-Gravel Mixtures.” *Geotechnical and Geological Engineering* 24 (3): 523–549. https://doi.org/10.1007/s10706-004-5832-6.

Al Tarhouni, M. A., Fouzder, A., Hawlader, B., and Dhar, A. 2017. “Direct Simple Shear and Triaxial Compression Tests on Dense Silica Sand at Low Effective Stress.” 70th Canadian Geotechnical Conference, Geoottawa 2017, Ottawa, ON, Oct. 1-4.

Taylor, D. W. 1948. *Fundamentals of Soil Mechanics*. J. Wiley, New York.

Terzaghi, K., Peck, R.B., and Mesri, G. 1996. *Soil Mechanics in Engineering Practice*. John Wiley and Sons, Inc., New York.

Tiwari, B., and Al-Adhadh, A. R.2014. “Influence of Relative Density on Static Soil-Structure Frictional Resistance of Dry and Saturated Sand.” *Geotechnical and Geological Engineering* 32 (2): 411–427. https://doi.org/10.1007/s10706-013-9723-6.

Wang, J., Zhang, H., Tang, S., and Liang, Y. 2013. “Effects of Particle Size Distribution on Shear Strength of Accumulation Soil.” *Journal of Geotechnical and Geoenvironmental Engineering* 139 (11): 1994–1997.

Wei, H. Z., Xu, W. J., Wei, C. F., and Meng. Q. S. 2018. “Influence of Water Content and Shear Rate on the Mechanical Behavior of Soil-Rock Mixtures.” *Science China Technological Sciences* 61 (8): 1127–1136.

# CHAPTER 4 Sand Characterization using Triaxial Tests

## 4.1 General

Characterization of sand using direct shear tests is discussed in Chapter 3. The study revealed that the removal of particles retaining on the #8 sieve does not affect the soil parameters significantly. Particles passing the #8 sieve are used for the triaxial tests to comply with the size of the test facility. Tests with both moist (unsaturated) and saturated sands were conducted. The testing of moist or unsaturated sand requires special considerations as the conventional two-phase solid-water system of saturated sand is changed into a three-phase air-solid-water system. The mutual interaction of air, water, and solid phase introduces capillary forces due to surface tension and disintegrate pore pressure into pore air pressure and pore water pressure. The difference between pore air pressure and pore water pressure is termed as matric suction. The control of the matric suction during test increases complicacy in the testing of unsaturated soil (Tarantino 2010).

Different experimental techniques are used to determine the parameters for the Mohr-Coulomb model and assessment of the shear strength of unsaturated soil. The most rigorous approach involves modification of conventional triaxial apparatus to accommodate independent measurement and control of pore-air and pore-water pressures and the resolution of air and water components of volume change (Wulfsohn et al. 1998; Fredlund and Vanapalli 2002). Researchers also employed a modification of direct shear and triaxial apparatus to perform testing on soils under constant suction (Gan and Fredlund 1988; Nam et al. 2011; Maleki and Bayat 2012; Gallage and Uchimura 2016 and others). However,

the modification of conventional triaxial and direct shear apparatus is complex and prohibitive for application in engineering practice. Testing using the modified equipment also requires skilled personnel and consumes a longer time to conduct the test under desired matric suction (Bai and Liu 2012; Al-Khazaali and Vanapalli 2019). An alternative method is using an indirect approach where the suction related information is separately obtained using soil-water characteristic curves (SWCC). Then, the shear strength of unsaturated soil considering the suction is predicted from the extension of total stress approach accumulating the SWCC data, saturated soil property, and conventional shear strength test data (Fredlund et al. 1996; Vanapalli et al. 1996; Khalili and Khabbaz 1998; Oh et al. 2008). However, this method is only applicable to the soils for which the SWCC is developed. The practicing engineers seek a method suitable for testing unsaturated soil using laboratory equipment employed in conventional geotechnical engineering practice.

This chapter presents a test program undertaken using a conventional triaxial testing system for examining the responses of the sand in an attempt to understand the behavior under triaxial stress conditions. A locally manufactured sand, discussed in Chapter 3, is used in this investigation. Triaxial tests are conducted at various initial densities and moisture contents. Based on the test results, soil parameters are obtained to assess the shear strength using the total stress approach in the continuum mechanics framework.

Depending on the moisture content, the granular media can be at four different states of unsaturated conditions, namely, pendular, funicular, capillary, and slurry states (Mitarai and Nori 2006). The pendular state occurs at very low moisture contents when the soil particles are held together by lens-shaped liquid (liquid bridges) at their contact points.

Voids in the soil are filled with air. At the funicular state, some voids are fully saturated while the others include air. All voids between particles are filled with air at the capillary state when the surface liquid is under capillary action. The slurry state refers to fully immerged particles in liquid. Typically, the pendular state occurs at the degree of saturation of 20%, the funicular state occurs at a degree of saturation between 20 and 90%, and the capillary state occurs at the degree of saturation of 90 to 100% (Lu et al. 2009). The objective of the current study is to examine the behavior of the sand at its pendular and funicular states. The capillary state can occur in almost saturated soil. A set of tests with a saturated condition of the sand was also conducted.

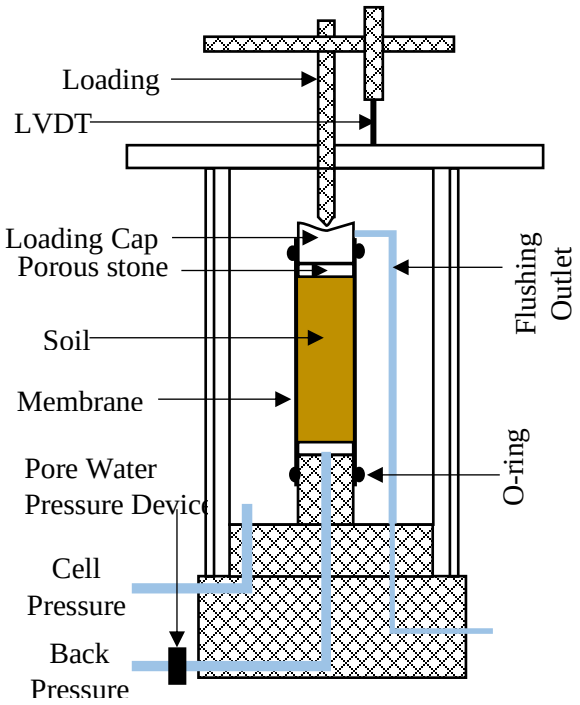


**Figure 4-1**: Schematic diagram of a triaxial setup

## 4.2 Testing equipment

A Standard Automated GDS Triaxial System available at Memorial University was used in this study. The testing system has a cell with a capacity of 3.5 MPa pressure and a base pedestal for a 38 mm diameter sample. The backpressure and cell pressure transducer has a capacity of 3 MPa with a volume controller. The pore water pressure transducer has a capability of 3.44 MPa. Figure 4-1 shows a schematic view of the apparatus. Using the loading frame, the axial load could be applied at a velocity of 0.00001 to 10 mm/min. An LVDT with a capacity of 50 mm is used to measure axial displacements. A 16-bit standard GDS 8-channel data acquisition device is used to collect the system data into a computer.

## 4.3 Testing Methodology

Triaxial tests were conducted on saturated and unsaturated sand samples. For the unsaturated samples, the moisture content is varied from 0 to ~12% that provided a degree of saturation of 0 to 60.5% for the samples. Details of the test program are listed in Table 4-1.

**Table 4-1**: Test Program

| Test No. | Sample Condition | Average Moisture Content (%) | Dry Unit Weight ($kN/m^3$) | Initial Void Ratio | Confining Pressure (kPa) |
|---|---|---|---|---|---|
| 1–3 | Unsaturated | 2.93 | 17.58 | 0.46 | 50,100, & 200 |
| 4–6 | Unsaturated | 6.98 | 15.98 | 0.61 | |
| 7–9 | Unsaturated | 11.88 | 17.10 | 0.50 | |
| 10–12 | Saturated | 17.60 | 18.25 | 0.41 | |

Oven-dried sand was used to prepare the samples with the addition of water. A porous stone sandwiched between two filter papers was seated on the pedestal of the base plate of the triaxial apparatus. The pedestal with porous stone and filter papers was inserted inside a membrane with O-ring. The membrane was stretched and fitted inside a split cylindrical mold. The sample was then poured inside the membrane in five layers of equal thickness. Each layer was compacted using 25 blows of a compaction hammer. After compaction, filter paper, porous stone, and the loading cap were placed on compacted sand and fitted inside the membrane with O-ring.

For testing of saturated sand, conventional consolidated undrained tests are conducted. An oven-dry soil is first placed into the mold, as discussed above. The specimen was subjected to de-aired water and $CO_2$ flushing from bottom to top for saturating. The $CO_2$ flushing was performed for 3–4 hours, whereas the water flushing was performed until water volume in is equal to volume out. The split mold was then dispatched from the mold after applying suction with backpressure into the sample to hold the sample (Figure 4-2).

**Figure 4-2**: Prepared sample

The height and diameter of the sample were then measured. The specimen is then subjected to saturation with de-aired water at high pore-water pressures (back pressure) in several stages to remove dissolved air bubbles from the water. Backpressure in the range of 580 kPa to 670 kPa was applied, while a cell pressure of 20 kPa higher than the backpressure was maintained. This procedure provided a B value of around 0.93. While the B value should ideally be 1 for saturated soil, a maximum value of around 0.93 could be obtained during tests. After completion of saturation, consolidation was conducted on the sample at predefined confining pressures. Then, shearing was applied with a loading velocity of 0.065mm/min under undrained conditions.

For the unsaturated specimen, the mixture of oven-dried sand with a predetermined amount of de-aired water was placed and compacted within the mold. No $CO_2$ and de-aired water flushing were applied to the specimens. No attempt to remove dissolved air bubbles was made. A small back pressure of –5 kPa was applied to the sample to hold it straight with minimum impact on the specimen. The backpressure valve was then closed to make it in an undrained condition before applying confining pressure. Immediately after the application of confining pressure, shearing was applied in undrained conditions to ensure the constant water content of the specimen during the tests. The moisture content of the sample was measured after the completion of each test for confirmation of the water contents. The loading was applied at the same velocity as that used for the saturated sample.

Figure 4-3 shows a typical shearing mechanism observed during the test. The height and diameter of the samples were 73–73.5 mm and 38.8–38.9 mm, respectively.

**Figure 4-3**: Sample after shearing

## 4.4 Results

The stress–strain responses during shearing in the triaxial tests for various conditions of the sand are shown in Figure 4-4. The confining pressures (i.e., 50 kPa, 100 kPa, and 200 kPa) include the backpressure applied to the sample during preparation. Thus, the applied pressure was 45 kPa to obtain a total confining pressure of 50 kPa with a 5 kPa of backpressure. Shearing was applied in undrained conditions (with a closed pore water valve) in all tests. Confining pressures were also applied with the closed pore pressure valve (undrained consolidation) for unsaturated soil to restrict any water flow into and out of the samples. Although undrained consolidation does not increase the shear strength of saturated soil, an increase of shear strength is expected for the unsaturated soil (Vanapalli et al. 1999). For the saturated soil, the confining pressure during consolidation was applied under drained conditions (CU tests) that contribute to the increase of shear strength of the saturated soil (similar to the unsaturated soil).

Figure 4-4 shows a significant increase of deviatoric stresses with the increase of confining pressure in all samples. Thus, shear strength in unsaturated moist soil is increased under the undrained confining pressures. The deviatoric stress reaches its peak at 2–4% of axial strain for unsaturated sand, whereas the deviatoric stress reaches its peak at 4–6% axial strain for the saturated sand. Degradation of deviatoric stresses after peak values is observed, indicating a dense sand behavior. Shear strength degradation is more significant at higher confining pressures. Within the strain level considered during the tests (9%), the residual stress condition was not reached.

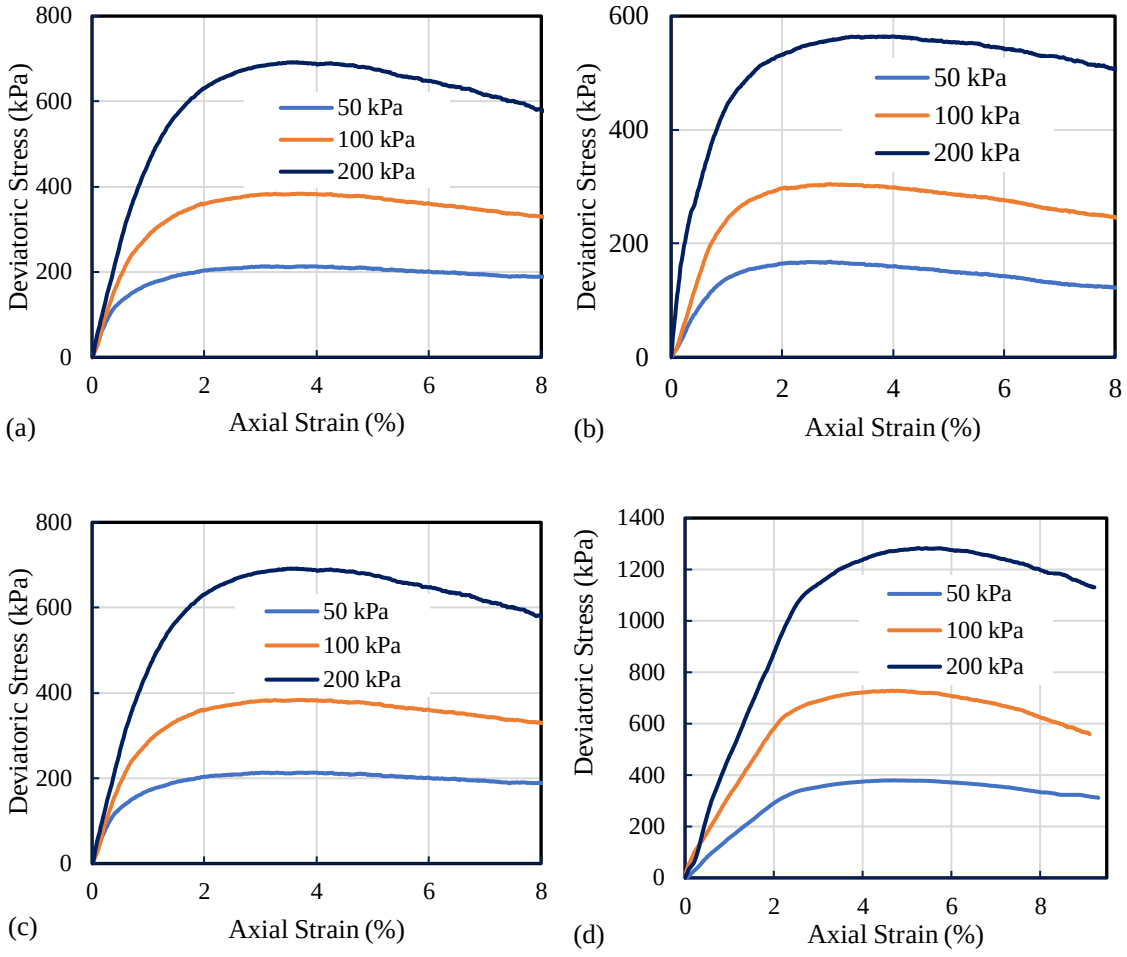


**Figure 4-4**: Stress–strain behavior for sand samples for varying moisture contents (a) 2.93% (b) 6.98%, (c) 11.88% and (d) Saturated

To examine the effect of moisture content on the shear strength, the deviatoric stresses under each confining pressure are plotted in Figure 4-5. For each confining pressure, the maximum deviatoric stresses of saturated soil are higher than the stresses in the unsaturated soil with different moisture contents. The unsaturated soil with 6.98% of moisture has the lowest deviatoric stress among all samples, which is almost half of the maximum deviatoric stress of the saturated sample. These discrepancies are associated with differences in the

densities of the soil specimens. Note that all samples are compacted using the same compaction effort. The same compaction effort in soil samples with different moisture contents can provide different compaction levels, which was also observed in direct shear tests discussed in Chapter 3. For the saturated soil, an oven-dry sample was placed and compacted in the mold before water flushing and saturation was applied. Therefore, the dry unit weights of saturated specimens are higher than the unit weights of the unsaturated specimens. As a result, the shear strength of the saturated soil is higher. Robert (2010) also found higher shear strengths of fully saturated Cornell and Tokyo gas sands than their unsaturated conditions due to higher dry unit weights obtained applying the same level of compaction effort. However, suction was externally applied and controlled in most of the past research on the unsaturated soil test. This suction is key to provide unsaturated soil higher strength than saturated soil (Houston et al. 2008; Maleki and Bayat 2012).

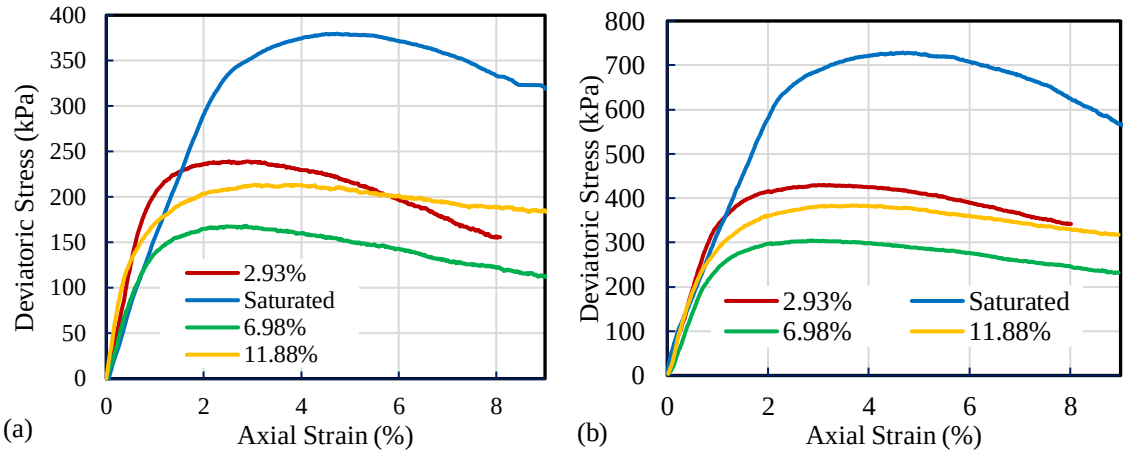

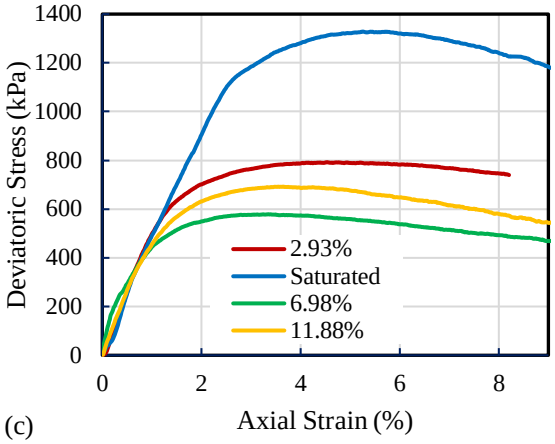

(c)

**Figure 4-5**: Stress–strain behavior for sand samples for varying confining pressure (a) 50 kPa (b) 100 kPa (c) 200 kPa

To determine the shear strength parameters, such as the angle of internal friction and apparent cohesion, the Mohr-Coulomb failure envelope is plotted as a tangent to the total stress Mohr circles corresponding to the failure points (Figure 4-6). The conventional straight-line approach was found to reasonably represent the Mohr-Coulomb failure envelop for each test, where the slope of the straight is the angle of internal friction, the intercept of the y-axis is the apparent cohesion and the intercept on the x-axis is the suction stress (Lu et al. 2009). The shear strength parameters obtained at different moisture contents are summaries in Table 4-2.

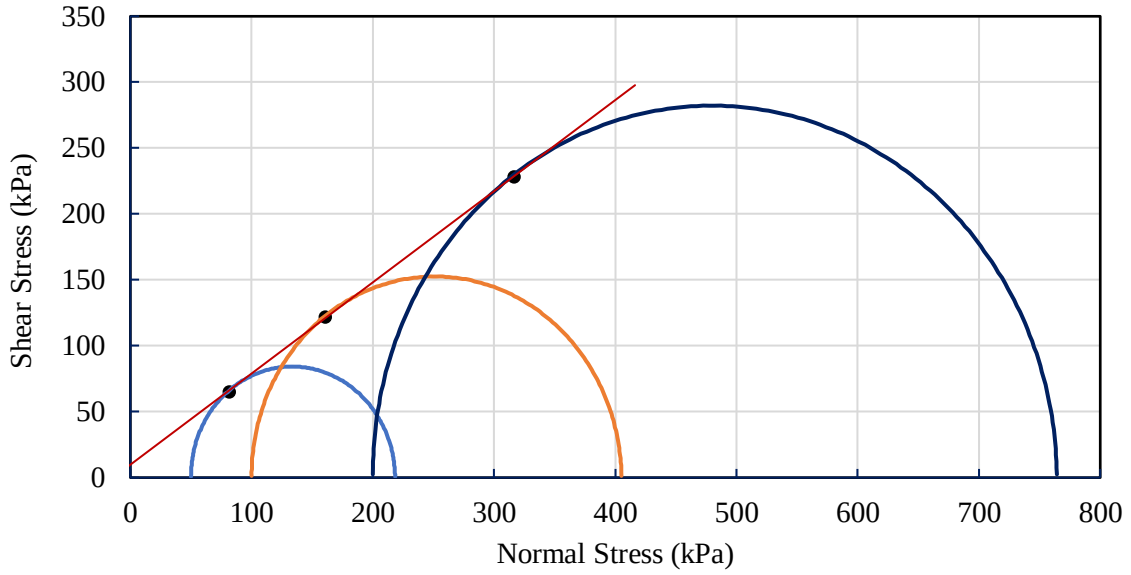


**Figure 4-6**: Mohr-Coulomb failure envelope

**Table 4-2**: Shear strength parameters

| Moisture Content (%) | Apparent Cohesion (kPa) | Angle of Internal Friction (°) | Suction stress (kPa) |
|---|---|---|---|
| 2.93 | 15.5 | 40.3 | 18.2 |
| 6.98 | 9.8 | 34.7 | 14.1 |
| 11.88 | 14.3 | 37.9 | 18.4 |
| Saturated | 12.6 | 49.5 | 10.8 |

Table 4-2 shows that the apparent cohesion of the saturated soil is non-zero. This may be because the soil sample could not be fully saturated using the method employed. The B value of 0.93 was obtained during the test, which does not represent the full saturation condition. A suction of around 10.8 kPa is estimated for the saturated sample used in the tests. The apparent cohesion in the unsaturated soil ranged from 9.8 kPa to 14.3 kPa, which

correspond to suction stresses of 14.1 kPa to 18.4 kPa. The magnitudes of apparent cohesion (and suction stress) for the most sand are not significantly high. The soil-water characteristic curve presented in Chapter 3 reveals that at the moisture contents of 2.9%, 7%, and 11.9% considered here, the matric suctions in the soil are 5 kPa, 2.5 kPa, and <1 kPa, respectively, which are less than the suction stresses obtained from the tests.

As expected, the angle of internal friction for the saturated sample is the highest in Table 4-2, which is due to a higher relative density. Among the moist soils, the angle of internal friction is the highest at the moisture content of 2.93% and lowest at the moisture content of 6.98%. To examine if the variation of the angle of internal friction is due to the variation in the density of soil, dry densities of the soil specimens are plotted along with the angles of internal friction in Figure 4-7. The variation of the angle of internal friction with moisture content for unsaturated sand is found to follow the variation of dry unit weight with the moisture content of the samples (Figure 4-7). Thus, the changes in the angle of internal friction are likely due to the changes in the dry density (or relative density) of the sand, not due to suction resulting from partial saturation. Schnellmann et al. (2013) also revealed from the direct shear test of unsaturated silty sand with the same moisture content and density, but different suctions that the effective angle of internal friction did not increase significantly with the matric suction. However, the apparent cohesion increased with an increase in suction.

The suction within unsaturated soil depends on the moisture content and the degree of saturation. The apparent cohesion (a measure of the effect of soil suction) is plotted against the water content in Figure 4-8. It appears that the apparent cohesion of the unsaturated

sand decreases with the increase in moisture content up to 6.98% and increases with a further increase of moisture content up to 11.88%, which is close to the optimum. It also shows that the variation of the apparent cohesion follows the variation of dry unit weight with the moisture content of the samples. Thus, the relative density has a significant contribution to the apparent cohesion.

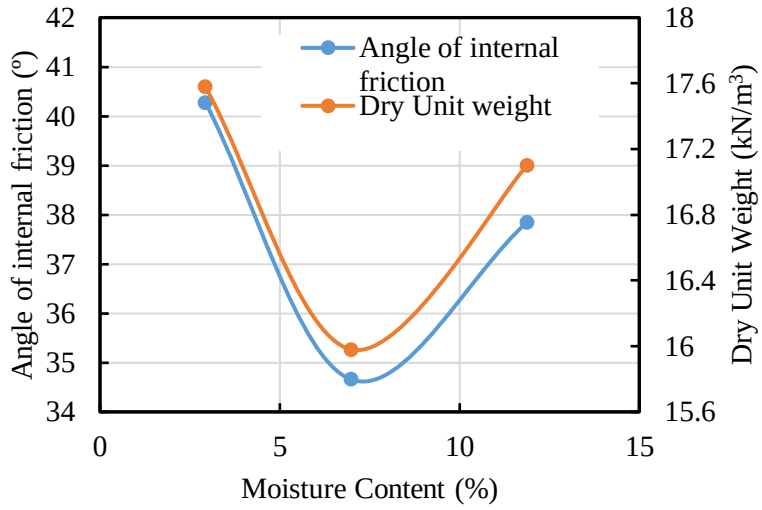


**Figure 4-7**: Variation of angle of internal friction for unsaturated soil

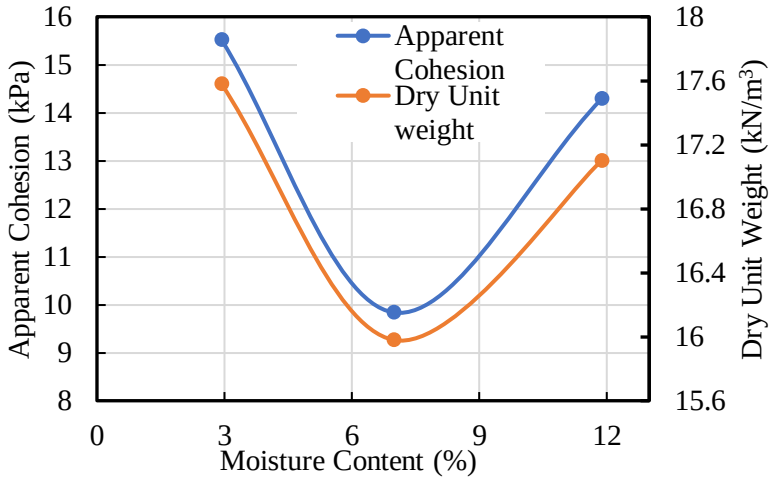


**Figure 4-8**: Variation of apparent cohesion for unsaturated soil

Figure 4-9 represents the variation of shear strength parameter (apparent cohesion, angle of internal friction) with the degree of saturation for unsaturated soil. The changes of apparent cohesion with the degree of saturation are similar to the variations of angle of internal friction. Both the apparent cohesion and angle of internal friction are the lowest at the degree of saturation of 29.5%, which is attained at 6.98% moisture content. However, both the suction stress and dry unit weight is lowest at this moisture content (see Table 4-1 & Table 4-2).

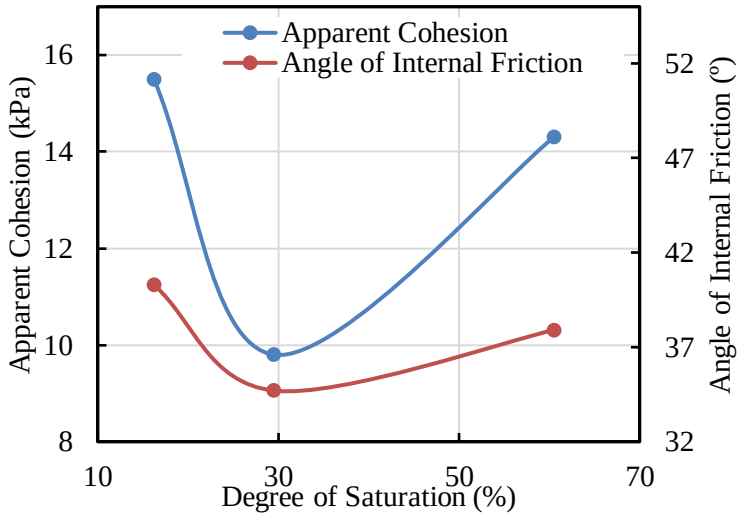


**Figure 4-9**: Effect of degree of saturation on shear strength parameter

### 4.5 Summary

Triaxial tests were conducted on a locally manufactured sand under unsaturated and saturated conditions using a conventional triaxial machine. The findings from the study are summarised below:

- The shear strength parameters of the sand significantly depend on the dry density of the sand regardless of the moisture contents. A similar conclusion was drawn from the results of direct shear tests discussed in Chapter 3.

- Both apparent cohesion and angle of internal friction of the sand vary with the moisture contents, which initially decreased and then increased with the increase of moisture content. The change in the apparent cohesion and the angle of internal friction was found to have a strong correlation with the dry density of the soil. The saturated soil sample showed the highest magnitudes of shear strength parameters, which had the highest relative density.

- Apparent cohesion, resulting from suction stress, was not significantly high for the soil (ranged from 9.8 kPa to 15.5 kPa). The corresponding isotropic tensile strengths (suction stress) are 10.8 kPa to 18.4 kPa.

- Obtaining full saturation (with B values of 1) of the soil during the test is very challenging. As a result, the effect of suction (apparent cohesion) was observed for the saturated soil.

- The effect of the degree of saturation on the shear strength parameter coincides with the dry unit weight and suction stress.

- It was challenging to obtain the same density level in multiple triaxial tests. Testing with similar densities of the soil would be required to identify the effect of degree of saturation on the shear strength parameters.

## 4.6 References


Al-Khazaali, M., and Vanapalli, S. K. 2019. “Axial Force-Displacement Behaviour of a Buried Pipeline in Saturated and Unsaturated Sand.” *Geotechnique* 69 (11): 986–1003. https://doi.org/10.1680/jgeot.17.P.116.

Bai, F. Q., and Liu, S. H. 2012. “Measurement of the Shear Strength of an Expansive Soil by Combining a Filter Paper Method and Direct Shear Tests.” *Geotechnical Testing Journal* 35 (3): 451–459. https://doi.org/10.1520/GTJ103342.

Fredlund, D. G., and Vanapalli, S.K. 2002. *Methods of Soil Analysis. Part 4, Physical Methods*. Edited by J.H. Dane and G.C. Topp. Madison: Soil Science Soc. of America.

Fredlund, D. G., Xing, A., Fredlund, M. D., and. Barbour, S. L.1996. “The Relationship of the Unsaturated Soil Shear Strength to the Soil-Water Characteristic Curve.” *Canadian Geotechnical Journal* 33 (3): 440–448.

Gallage, C., and Uchimura, T. 2016. “Direct Shear Testing on Unsaturated Silty Soils to Investigate the Effects of Drying and Wetting on Shear Strength Parameters at Low Suction.” *Journal of Geotechnical and Geoenvironmental Engineering* 142 (3): 1–9. https://doi.org/10.1061/(ASCE)GT.1943-5606.0001416.

Gan, K. J., and Fredlund, D. G. 1988. “Multistage Direct Shear Testing of Unsaturated Soils, Geotechnical Testing Journal.” *Geotechnical Testing Journal* 11 (2): 132–138.

Houston, S. L., Perez-garcia, N., and Houston, W.N. 2008. “Shear Strength and Shear-

Induced Volume Change Behavior of Unsaturated Soils from a Triaxial Test Program." *Journal of Geotechnical and Geoenvironmental Engineering* 134 (11): 1619–1632. https://doi.org/10.1061/(ASCE)1090-0241(2008)134.

Khalili, N., and Khabbaz, M. H. 1998. "A Unique Relationship for the Determination of the Shear Strength of Unsaturated Soils." *Geotechnique* 48 (5): 681–87.

Lu, N., Kim, T., Sture, S., and Likos, W. J. 2009. "Tensile Strength of Unsaturated Sand." *Journal of Geotechnical and Geoenvironmental Engineering* 135 (12): 1410–1419.

Maleki, M., and Bayat, M. 2012. "Experimental Evaluation of Mechanical Behavior of Unsaturated Silty Sand under Constant Water Content Condition." *Engineering Geology* 141–142: 45–56. https://doi.org/10.1016/j.enggeo.2012.04.014.

Mitarai, N., and Nori, F. 2006. "Wet Granular Material." *Advances in Physics* 55: 1–45.

Nam, S., Gutierrez, M., Diplas, P., and Petrie, J. 2011. "Determination of Shear Strength of Unsaturated Soils Using Multistage Direct Shear Test." *Engineering Geology* 122: 272–280.

Oh, W. T., Garga, V. K., and Vanapalli, S. K. 2008. "Shear Strength Characteristics of Statically Compacted Unsaturated Kaolin." *Canadian Geotechnical Journal* 45 (7): 910–922. https://doi.org/10.1139/T08-032.

Robert, D. J. 2010. "Soil–Pipeline Interaction in Unsaturated Soils." The University of Cambridge. https://doi.org/https://doi.org/10.17863/CAM.11686.

Schnellmann, R., Rahardjo, H., and Schneider, H.R. 2013. "Unsaturated Shear Strength of

a Silty Sand." *Engineering Geology* 162: 88–96.

Tarantino, A. 2010. *Basic Concepts in the Mechanics and Hydraulics of Unsaturated Geomaterials*. Edited by Lyesse Laloui. *Mechanics of Unsaturated Geomaterials*. John Wiley & Sons, Incorporated.

Vanapalli, S. K., Fredlund, D. G., Pufahl, D. E., and Clifton, A. W. 1996. "Model for the Prediction of Shear Strength Respect to Soil Suction." *Canadian Geotechnical Journal* 33 (3): 379–392.

Vanapalli, S. K., Pufahl, D. E., and Fredlund, D.G. "Interpretation of the Shear Strength of Unsaturated Soils in Undrained Loading Conditions." In *52th Canadian Geotechnical Conference*, 643–650. Regina,Saskatchewan.

Wulfsohn, D., Adams, B.A., and Fredlund, D.G. "Triaxial Testing of Unsaturated Agricultural Soils." *Journal of Agricultural Engineering Research* 69: 317–330.

# CHAPTER 5 Tests at Constant Densities

## 5.1 General

The direct shear tests and triaxial tests conducted at different moisture contents with the same compaction effort revealed the shear strength parameters depend significantly on the conditions of the soil (discussed in Chapters 3 and 4). The differences in the shear strength parameters are attributed to the relative compaction of the soil, as the changes in the soil's density with the moisture content were similar to the changes in the shear strength parameters. However, testing at the same density of the soil is required for understanding the effects of moisture content on the shear strength parameters. This chapter presents a test program carried out at the same soil densities but with different moisture contents. Two series of direct shear tests and triaxial tests were conducted on the sand samples maintaining two different dry unit weights of 17 kN/m$^3$ and 18.5 kN/m$^3$, respectively. A comparison of the soil parameters obtained from the direct shear tests and triaxial tests is also presented.

## 5.2 Experimental Program

Direct shear tests and triaxial tests were conducted using the local sand (Sample A, discussed in Chapter 3). Moisture contents of the soil were varied, keeping the dry unit weights the same for all specimens in each series of tests. The methodologies employed for the tests, including the maintenance of constant dry unit weights, are described below.

### 5.2.1 Direct Shear Test

The direct shear tests were conducted on oven-dry, moist, and submerged sand samples under three normal stresses of 50 kPa, 100 kPa, and 200 kPa. The shear box of the direct shear device allows testing of a specimen with a 63.5 mm diameter and 26 mm thickness. For each sample, the amount of dry sand was calculated to fill the fixed volume of the direct shear box and obtain the fixed dry unit weights (17 $kN/m^3$ and 18.5 $kN/m^3$, respectively). For testing of oven-dry soil, the predetermined amount of dry sand was directly placed and compacted in the shear box of constant volume, and then shearing was applied. For the moist samples, the predetermined amount of dry sand was first mixed with a specified amount of moisture. The sample is then put inside an airtight Ziploc bag for 24 hours to allow thorough soaking. After 24 hours, the moist samples were placed and compacted in the shear box (of constant volume) before the shearing was applied. Moisture contents from 2% to 10% were considered for the moist samples.

For testing of saturated/submerged samples, the dry sand was first placed in the shear box as mentioned above, which was then submerged in water for 24 hours. Then, the shearing was applied. The shearing was applied at a displacement rate of 1 mm/min in each test.

The thickness of each sample after compaction was recorded to determine the final dry unit weights. After completion of each test, the actual moisture content of each soil sample is determined. The test program of the direct shear test for two densities of the soil considered is shown in Table 5-1 and Table 5-2, respectively.

**Table 5-1**: The direct shear test program for dry unit weight of 17 kN/m$^3$

| Target Moisture Content (%) | Average Moisture Content after tests (%) | Dry Unit Weight, $\gamma_d$ (kN/m$^3$) | Normal Stress (kPa) |
|---|---|---|---|
| 0 | 0 | 17.01 | 50,100, & 200 |
| 2 | 1.78 | 17.02 | |
| 4 | 3.79 | 16.97 | |
| 6 | 5.75 | 17.01 | |
| 8 | 7.72 | 17.04 | |
| 10 | 9.80 | 17.12 | |
| Submerged | 16.41 | 17.10 | |

**Table 5-2**: The direct shear test program for dry unit weight of 18.5 kN/m$^3$

| Target Moisture Content (%) | Average Moisture Content after tests (%) | Dry Unit Weight, $\gamma_d$ (kN/m$^3$) | Normal Stress (kPa) |
|---|---|---|---|
| 0 | 0 | 18.70 | 50,100, & 200 |
| 2 | 1.50 | 18.59 | |
| 6 | 5.71 | 18.46 | |
| 10 | 9.02 | 18.70 | |
| Submerged | 14.12 | 18.65 | |

### 5.2.2 Triaxial Test

Triaxial tests were conducted on the moist and saturated samples under three confining pressures of 50 kPa, 100 kPa, and 200 kPa. The test specimens have a diameter of 38–38.5 mm and a height of 72–73 mm. As in the direct shear test, a predetermined amount of dry sand is used to fill the triaxial mold of known volume, maintaining a constant dry unit weight of the samples. The moist samples were put in airtight ziplock bags for 24 hours for proper soaking. The triaxial test setup is shown in Figure 4-1 in Chapter 4.

The procedure discussed in Chapter 4 was employed for the preparation of the samples. The pedestal with porous stone sandwiched between two filter papers and the split cylindrical mold were fitted inside a membrane. The samples were poured inside the membrane in five layers of equal thickness. Each layer was compacted using a compaction hammer as required to place a predetermined amount of soil within a fixed volume of mold (to ensure constant unit weights). For the saturated sample, dry sand was placed, and the specimen was subjected to deaired water and $CO_2$ flushing from the bottom to the top. The $CO_2$ flushing was performed for 3–4 hours, and the water flushing was performed until the water volume in is equal to volume out. The split mold was then dispatched from the specimen after applying suction with the back-pressure valve to hold the sample. The height and diameter of the sample were then measured to check the dry unit weight of the soil. The specimen was then subjected to saturation with deaired water at high pore-water pressures (back pressure) in several stages for dissolving of any air bubbles into the water. Backpressure in the range of 580 kPa to 670 kPa was applied with a cell pressure of 20 kPa higher than the backpressure. This procedure provided a B value of around 0.93. While the B value should ideally be 1 for saturated soil, a maximum value of around 0.93 could be obtained during tests. After completion of saturation, consolidation was conducted on the sample at predefined confining pressures. Then, shearing was applied with a loading velocity of 0.065 mm/min under undrained conditions.

For the unsaturated specimen, no $CO_2$, de-aired water flushing, saturation, and consolidation were applied to the samples. A small back pressure of $-5$ kPa was applied to the sample to hold it straight with minimum impact on the specimen initially. The

backpressure valve was then closed to make it in an undrained condition. After the filling of the triaxial cell with water that provided support to the specimen, the back-pressure valve was opened to reduce the backpressure to zero, and then the valve was again closed. Then, the confining pressure was applied. After the application of confining pressure, shearing was applied in undrained conditions to ensure the constant moisture content of the specimen during the tests. The loading was applied at the same velocity as that used for the saturated sample. The moisture content of each sample was measured after the completion of each test for confirmation of the moisture contents. Details of triaxial test programs are shown in Table 5-3 and Table 5-4, respectively.

**Table 5-3**: Triaxial test program for dry unit weight of 17 kN/m$^3$

| Target Moisture Content (%) | Average Moisture Content after tests (%) | Dry Unit Weight, $\gamma_d$ (kN/m$^3$) | Confining Pressure (kPa) |
|---|---|---|---|
| 2 | 1.98 | 16.95 | 50,100 & 200 |
| 4 | 3.91 | 16.96 | |
| 6 | 6.05 | 17.18 | |
| 8 | 8.11 | 16.96 | |
| 10 | 10.10 | 17.11 | |
| Saturated | 17.58 | 17.12 | |

**Table 5-4**: Triaxial test program for dry unit weight of 18.5 kN/m$^3$

| Target Moisture Content (%) | Average Moisture Content after tests (%) | Dry Unit Weight (kN/m$^3$) | Confining Pressure (kPa) |
|---|---|---|---|
| 2 | 2.36 | 18.48 | 50,100 & 200 |
| 6 | 6.44 | 18.43 | |
| 10 | 10.39 | 18.48 | |
| Saturated | 14.61 | 18.49 | |

## 5.3 Results

### 5.3.1 Direct Shear Test

The stress–displacement behavior of the samples from the direct shear tests with dry unit weight of 17 kN/m$^3$ and 18.5 kN/m$^3$ are shown in Figure 5-1 and Figure 5-2, respectively. The figures show that the peak stress ratios of the samples are different for different moisture contents, although the dry unit weight of the soils is the same. Thus, the moisture content influences the shear strength of the soil, contrary to that reported in Chapter 3. Note that the dry densities of the moist sand discussed in Chapter 3 were less.

The post–peak degradations in the stress ratios are observed for the dry soils, while the post–peak degradation is not evident for the moist soil at 17 kN/m$^3$ of dry unit weight (Figure 5-1). As a result, the peak stress ratios are less for the moist soils, indicating lower shear strengths. However, the moist samples with 10% moisture contents showed post–peak degradation for 18.5 kN/m$^3$ of dry density (Figure 5-2) and at lower normal stresses (e.g., 50 kPa) for 17.0 kN/m$^3$ of dry density. Thus, the effects of moisture content on the soil behavior also depend on the relative compaction.

At both densities of the soil, the dry soils and the submerged soils showed similar peak stress ratios, with slightly higher stress ratios for the submerged soil. The peak stress ratio is higher at low normal stress of 50 kPa than those at higher stresses for all samples, which is in general agreement with the observations discussed in Chapter 3.

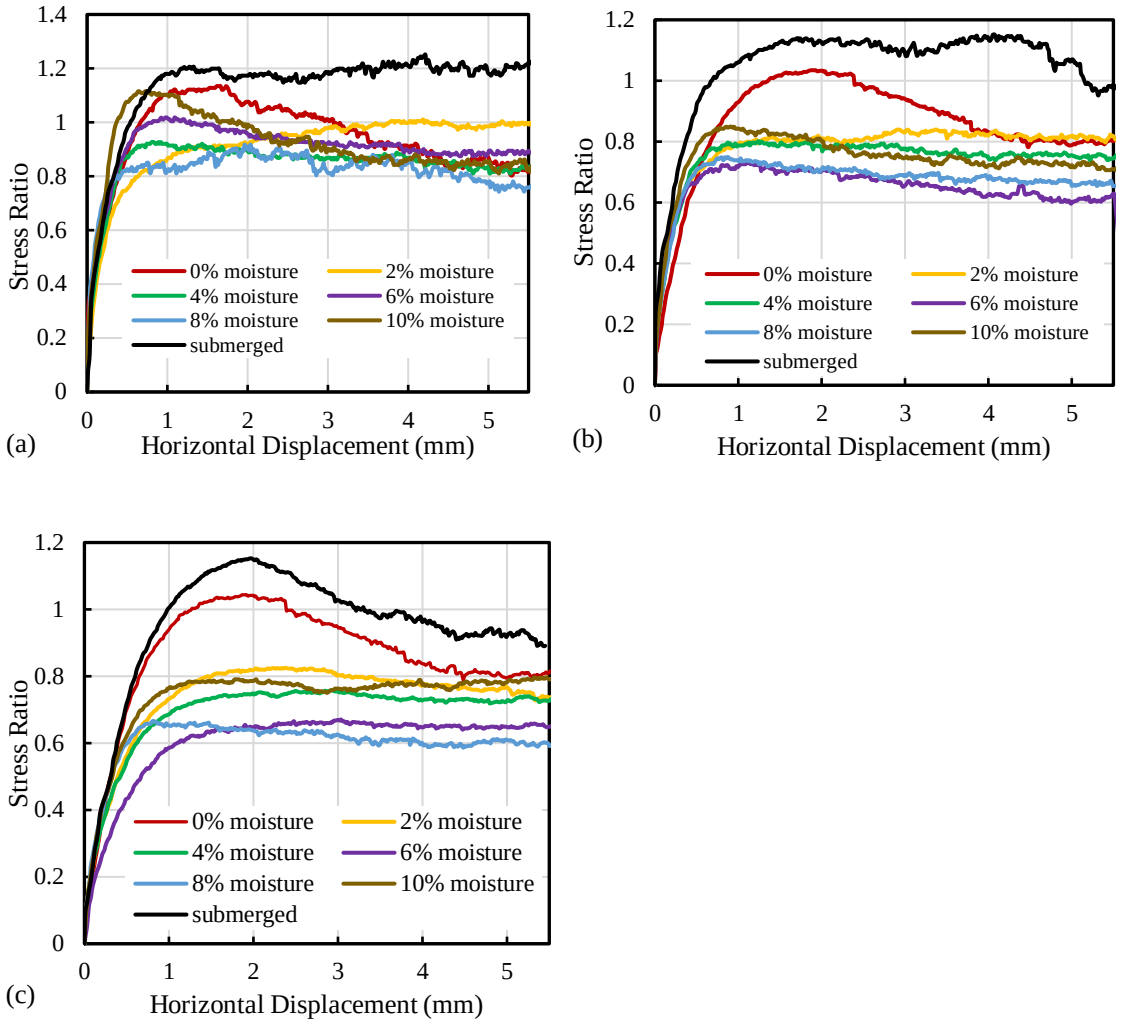


**Figure 5-1**: Effect of moisture content on stress–displacement responses for dry unit weight of 17 kN/m$^3$: (a) 50 kPa (b) 100 kPa (c) 200 kPa

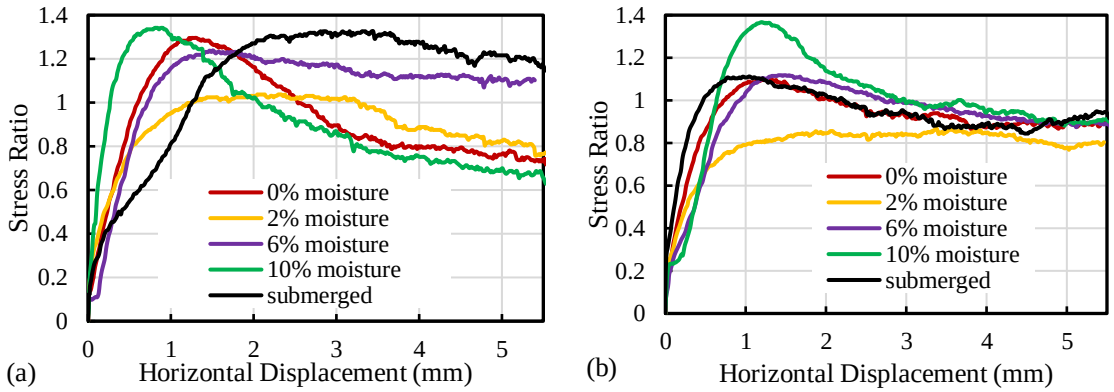

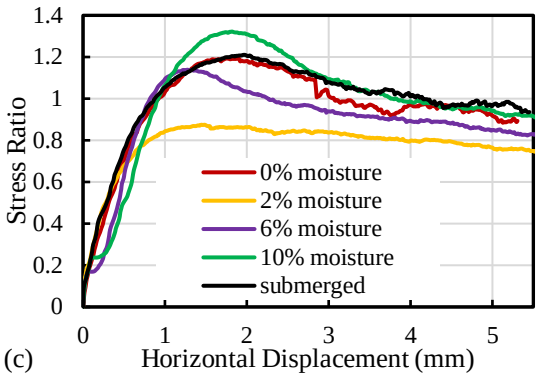


**Figure 5-2**: Effect of moisture content on stress–displacement responses for dry unit weight of 18.5 kN/m$^3$: (a) 50 kPa (b) 100 kPa (c) 200 kPa

Figure 5-3 plots the peak shear stresses against the normal stresses obtained from the direct shear tests. It shows that the peak shear stresses for the dry soil match those for submerged soil for $\gamma_d$ = 18.5 kN/m$^3$ and are close to each other for $\gamma_d$ = 17 kN/m$^3$. The dry/submerged soil strengths are higher than the moist soil strength, except for the soil with 10% moisture at $\gamma_d$ = 18.5 kN/m$^3$. The moist sample with 10% moisture is in the transition regime, where a further increase of moisture changes the state from funicular to capillary regime. Linear trendlines with the relations in Figure 5-3 are used to determine the strength parameters for the different conditions of the soil (additional plots are included in Appendix A). The resulting angles of internal friction were calculated to range from 30° to 48° for $\gamma_d$ = 17 kN/m$^3$ and from 40° to 52.5° for $\gamma_d$ = 18.5 kN/m$^3$. The corresponding apparent cohesions for the soils range from 4.8 kPa to 16.7 kPa for $\gamma_d$ = 17 kN/m$^3$ and from 2.2 kPa to 7.8 kPa for $\gamma_d$ = 18.5 kN/m$^3$.

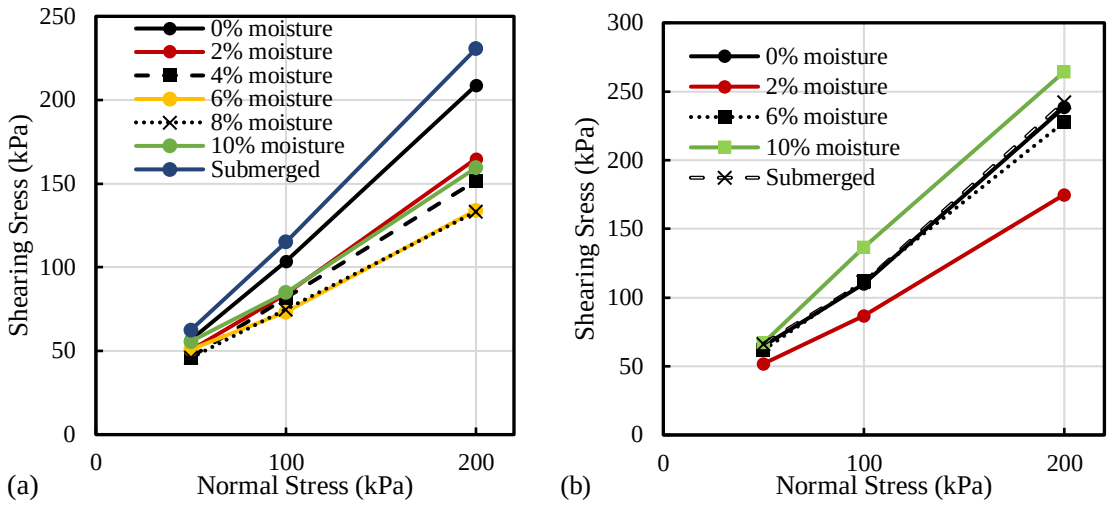


**Figure 5-3**: Peak shear stress versus normal stress: a) $\gamma_d$ = 17 kN/m$^3$; b) $\gamma_d$ = 18.5 kN/m$^3$

### 5.3.2 Triaxial Test

Figure 5-4 and Figure 5-5 represents the stress-strain behavior from the triaxial tests with the dry unit weight of 17 kN/m$^3$ and 18.5 kN/m$^3$, respectively. The saturated samples show significantly higher strength than the moist sample for both cases. In both figures, the peak deviatoric stresses are the highest for the saturated samples that occur at the larger axial strains. The peak deviatoric stresses for the moist samples do not change significantly for the changes in the moisture contents. Mohr-circles with the peak deviatoric stresses and the corresponding confining pressure are plotted to fit with the linear Mohr-Coulomb's failure criteria to determine the strength parameters. Total stress Mohr circles are drawn for the moist soils as the pore-water pressure was not available (please in Appendix B).

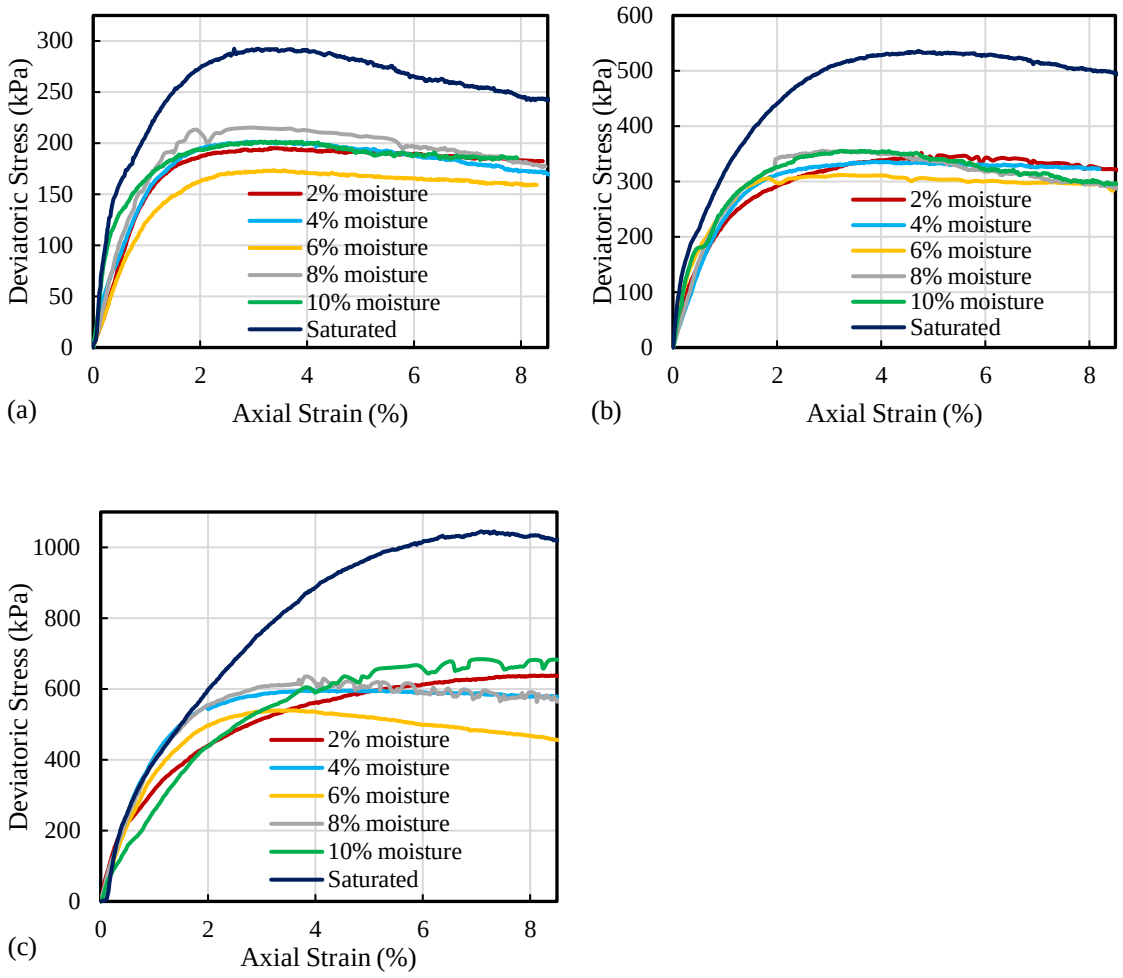


**Figure 5-4**: Stress-strain behavior from triaxial tests for samples with dry unit weight of 17 kN/m$^3$: (a) Confining pressure = 50 kPa (b) Confining pressure = 100 kPa (c) Confining pressure = 200 kPa

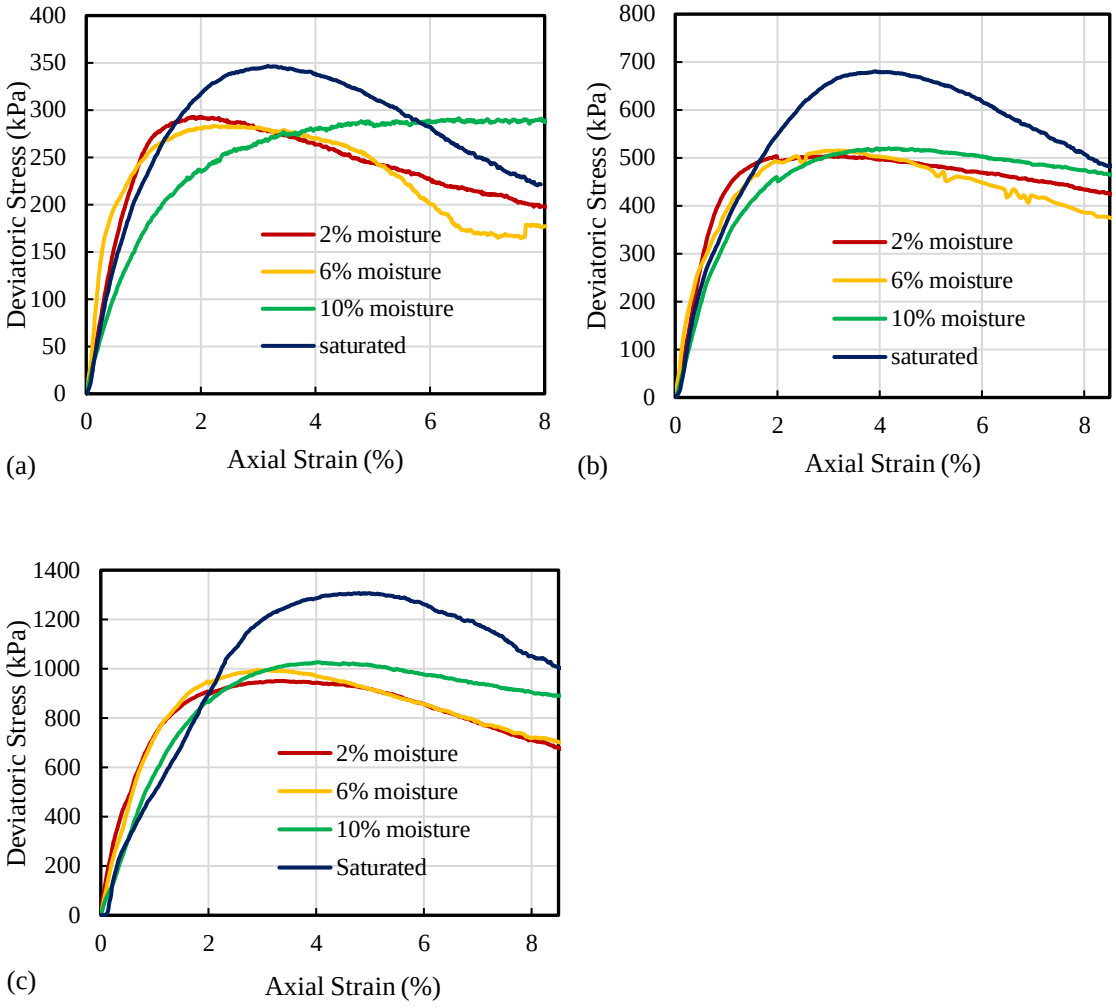


**Figure 5-5:** Stress–strain behavior from triaxial tests for samples with dry unit weight of 18.5 kN/m$^3$: (a) Confining pressure = 50 kPa (b) Confining pressure = 100 kPa (c) Confining pressure = 200 kPa

For the saturated soils, the total stress and effective stress Mohr circles are drawn, as shown in Figure 5-6. At failure, negative pore water pressure was measured during the tests due to dilation of the dense soils, which resulted in higher effective stresses than the total stresses in the figure. The strength parameters for the saturated soil are obtained as below.

For $\gamma_d$ = 17 kN/m$^3$:

Total stress parameters: apparent cohesion, c = 6.5 kPa and the angle of internal friction, ∅ = 45.8°.

Effective stress parameters: apparent cohesion, c = 26.0 kPa and the angle of internal friction, ∅ = 39.4°.

For $\gamma_d$ = 18.5 kN/m$^3$:

Total stress parameters: apparent cohesion, c = 5.5 kPa and the angle of internal friction, ∅ = 49.6°.

Effective stress parameters: apparent cohesion, c = 19.6 kPa and the angle of internal friction, ∅ = 44.2°.

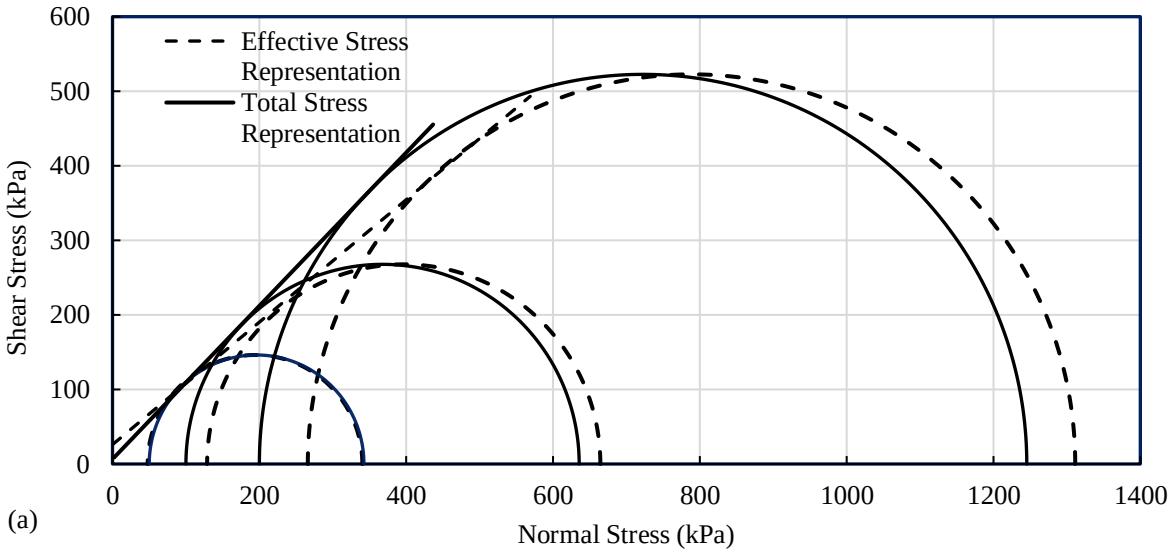

(a)

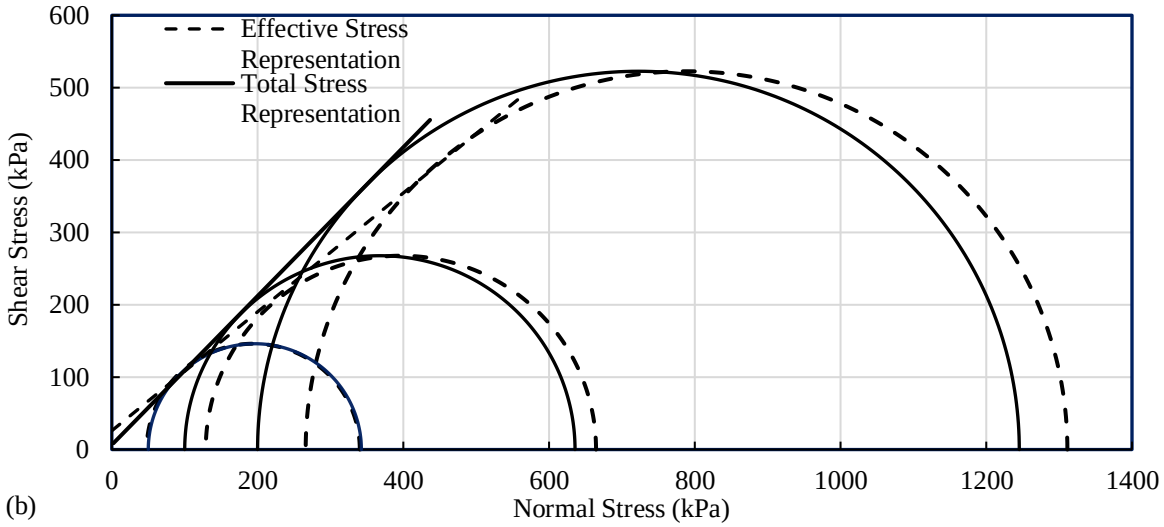


**Figure 5-6**: Mohr circles for determination of strength parameters: a) $\gamma_d$ = 17 kN/m$^3$; b) $\gamma_d$ = 18.5 kN/m$^3$

### 5.3.3 Comparison of Strength Parameters

The shear strength parameters obtained from the direct shear tests and triaxial tests are compared for different moisture contents to demonstrate the influence of moisture content on the strength parameters. As mentioned earlier, the strength parameters from the direct shear tests are calculated using the linear trendline with the peak shear stress versus normal stress data. For the triaxial tests, a linear Mohr-Coulomb failure envelope is plotted as a tangent to the Mohr circles stresses corresponding to the peak deviatoric stress. The conventional straight-line approach was found to reasonably represent the Mohr-Coulomb failure envelop for each test. The slope of the straight line represents the angle of internal friction, and the intercept of the y-axis represents the apparent cohesion.

The obtained angle of internal friction and the apparent cohesion is plotted against the degree of saturation in Figure 5-7 and Figure 5-8, respectively. Figure 5-7 shows that the angle of internal friction from the direct shear tests is the highest at the dry and saturated conditions and less at the unsaturated conditions. The friction angle decreases with the increase of moisture contents from the dry state, reaches the lowest value, and then increases, achieving the highest value at the submerged condition. For the dry density of 17 kN/m$^3$, the friction angle is 45.5$^o$ at the dry state, the lowest (i.e., 29.3$^o$) at around 30% degree of saturation, and 48$^o$ at the submerged condition. The results from the triaxial test follow the test results from the direct shear tests, except that test data for the dry condition is not available. The changes in the friction angle with the degree of saturation are consistent with those reported in Lu and Wu (2005). Lu and Wu (2005) found the angle of internal friction of fine sand to decrease from 41$^o$ to 36$^o$ for an increase of the degree of saturation from 0% to 4%, and then return to 40$^o$ at 100% saturation. However, greater shear strength of unsaturated soil is often reported in the literature where external matric suction is applied during the tests to maintain constant suction. The external matric suction is likely the cause for the higher shear strength (Gallage and Uchimura 2016; Maleki and Bayat 2012; Schnellmann et al. 2013; Likos et al. 2010). However, the external suction is not present in the soil used as the backfill material in the field. The shear strength for these materials is expected to be less under unsaturated condition.

For the soil with a dry unit weight of 18.5 kN/m$^3$, the angle of internal friction from the direct shear tests was 50° in the dry state that reached the lowest value of 40° at the degree of saturation of around 10%. Beyond the 10% degree of saturation, the friction angle

increases with the increase of the degree of saturation. However, the angle of internal friction from the triaxial tests increases from the minimum value of 43.4° at the degree of saturation of 16% to the maximum value of 49.6° in the saturated state. Triaxial tests were not conducted for dry condition. Figure 5-7 shows that the angle of internal friction is minimum at the degree of saturation of 10-15% for dry unit weight of 18.5 kN/m$^3$ and 30–35% for dry unit weight of 17 kN/m$^3$.

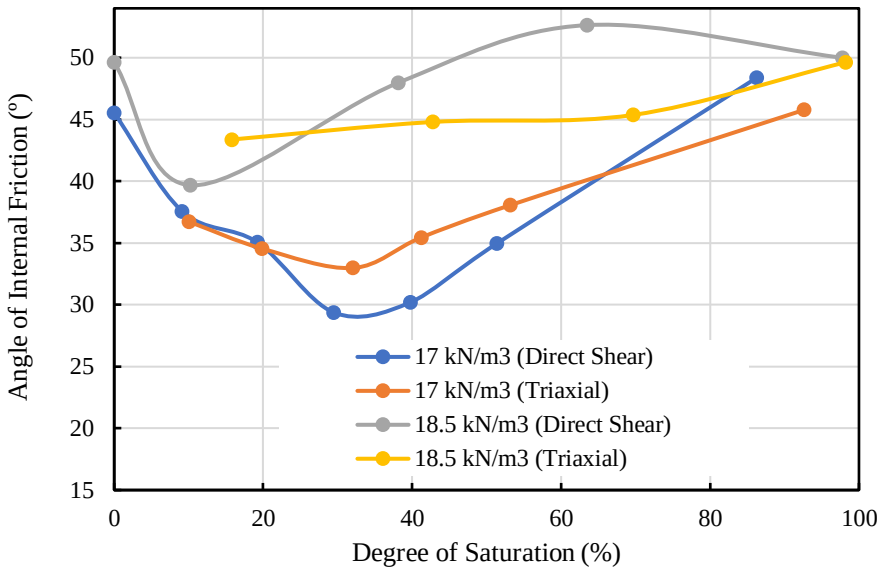


**Figure 5-7**: Effect of degree of saturation on the angle of internal friction

The apparent cohesion is higher for the unsaturated sands due to the suction but almost negligible for the dry and the saturated conditions (Figure 5-8). For the dry unit weight of 17 kN/m$^3$, the apparent cohesion increases with the increase of the degree of saturation from the dry state and reaches the maximum apparent cohesion of 20 kPa at the 30% to 40% degree of saturation. Lu and Wu (2005) also showed that the apparent cohesion of

fine sand reaches the peak value at an intermediate degree of saturation (20–30%) and reduces to the minimum value at the fully saturated and dry conditions. A similar observation was also reported for gravelly soil in Ravindran and Gratchev (2020). For the dry unit weight of 18.5 kN/m$^3$, the maximum apparent cohesion of 7.7 kPa was observed at a 10% degree of saturation from direct shear tests beyond which the apparent cohesion was reduced. A reduction of apparent cohesion for the increase of the degree of saturation beyond 15% was observed from the triaxial tests as no test at a lower degree of saturation was conducted.

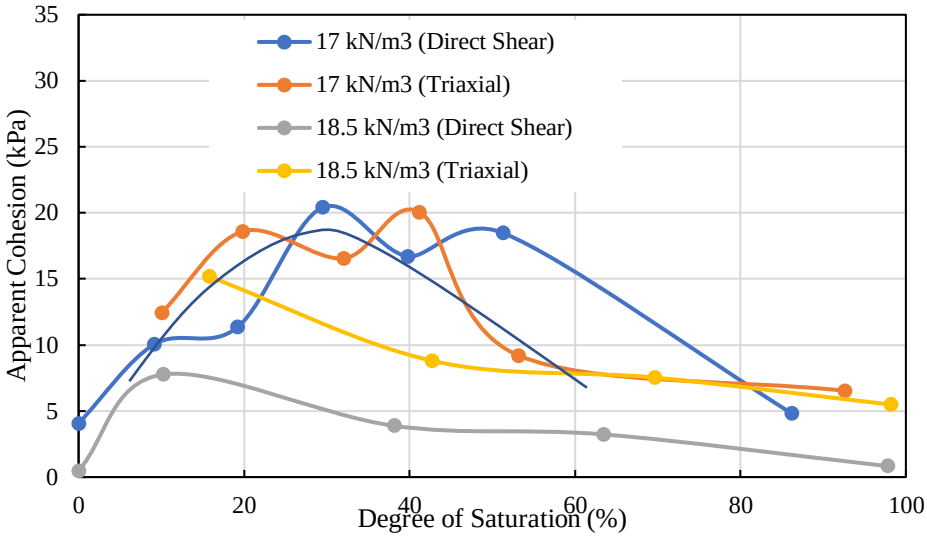


**Figure 5-8**: Effect of degree of saturation on apparent cohesion

### 5.3.4 Suction Stress

Lu and Likos (2006) defined suction stress as the resultant macroscopic intraparticle stress such as cementation, van der Waals attraction, double layer repulsion, capillary stress, which is developed in unsaturated soil due to surface tension, and negative pore-

water pressure. It is a function of the degree of saturation or matric suction. Lu and Likos (2006) modified Terzaghi's (1936) effective stress (see Eq. (5.1)), incorporating suction stress for unsaturated soil,

$$\sigma' = (\sigma - u_a) - \sigma^s$$

$$\text{Or, } \sigma' = (\sigma - u_a) - (u_a - u_w)S_e \quad [5.1]$$

Where, $S_e$ is the effective degree of saturation, $(\sigma - u_a)$ is net normal stress, $(u_a - u_w)$ is matric suction, and $\sigma^s$ is suction stress.

Suction stress is also defined as isotropic tensile stress arising from capillary mechanisms in unsaturated sand, which has an equivalent meaning of the "apparent cohesion." The isotropic tensile strength ($\sigma_{ti}$) can be obtained through a linear extension of the Mohr-Coulomb failure envelope with total stress Mohr circles to the horizontal axis (Figure 2-6, in Chapter 2) (Lu et al. 2009).

As the variation of the suction stress with the degree of saturation has intrinsic relation with the soil water characteristics curve, it can be estimated from the soil water characteristics curve (SWCC) (Lu et al. 2014; Oh et al. 2012). According to van Genuchten (1980) mathematical model for SWCC,

$$S_e = \frac{\theta - \theta_r}{\theta_s - \theta_r} = \left[\frac{1}{1+[\alpha(u_a - u_w)]^n}\right]^m \quad [5.2]$$

Where, $\theta$ is volumetric water content, $\theta_r$ residual volumetric water content, $\theta_s$ is saturated volumetric water content, $\alpha$ is inverse of air entry value, n and m are fitting parameters.

Lu et al. (2010) described suction stress as the function of the effective degree of saturation or matric suction (see Eq. (5.3) and Eq. (5.4)) incorporating $\alpha, n,$ and $m$ from the SWCC fitting.

$$\sigma^s = -\frac{S_e}{\alpha}\left(S_e^{\frac{n}{1-n}} - 1\right)^{1/n} \quad [5.3]$$

Or

$$\sigma^s = -\frac{(u_a - u_w)}{[1+(\alpha(u_a - u_w))^n]^{n-1/n}} \quad [5.4]$$

The suction stresses at various moisture contents are calculated using SWCC relations for the soil (Eq. (5.3) and Eq. (5.4)) and from the results of direct shear tests and triaxial tests (extension of Mohr-Coulomb envelop to the normal stress axis). The results are compared in Figure 5-9. It reveals that the suction stress calculated from SWCC relations decreases from a high value (41 kPa for $\gamma_d$ = 17 kN/m$^3$ and 13 kPa for $\gamma_d$ = 18.5 kN/m$^3$) to a low below for increase of the degree of saturation from around 6% to 15%, beyond which the suction stresses are negligible. However, suction stress obtained from direct shear tests and triaxial tests increases initially with the increase of the degree of saturation and then decreases, which could not be calculated using the SWCC relation. Similar behavior was also observed in Maleksaeedi et al. (2017), where the suction stress is determined from both suction test and conventional direct shear test of granular material. The suction stress obtained from the direct shear and triaxial tests are significantly higher than those calculated from SWCC for dry unit weight of 17 kN/m$^3$. For the dry unit weight of 18.5 kN/m$^3$, the difference is less significant. The suction stresses for $\gamma_d$ = 17 kN/m$^3$ are higher

than those for $\gamma_d$ = 18.5 kN/m$^3$. Song (2014) also reported that the suction stress for sand reduces with the increase of dry unit weight.

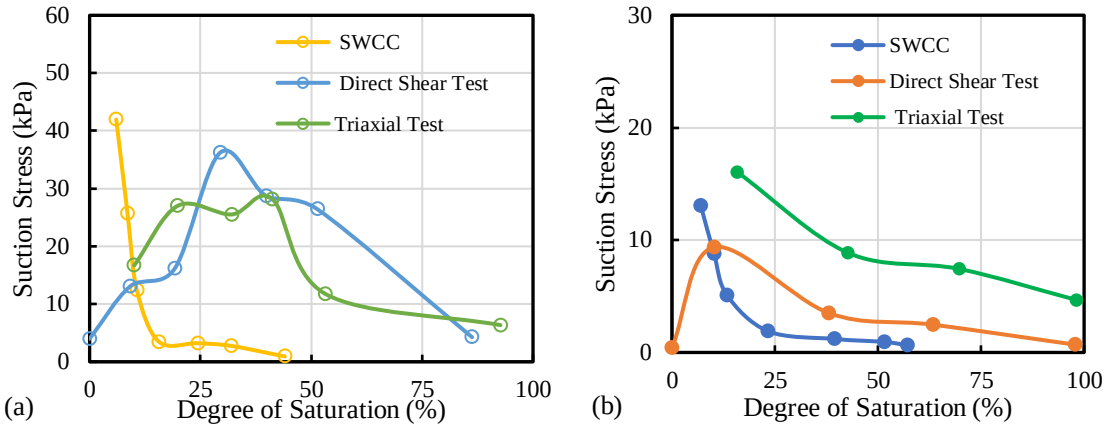


**Figure 5-9**: Comparison of suction stresses: a) $\gamma_d$ = 17 kN/m$^3$; b) $\gamma_d$ = 18.5 kN/m$^3$

## 5.4 Summary

This chapter presents the direct shear tests and triaxial tests conducted with different moisture contents but at two constant dry unit weight of 17 kN/m$^3$ and 18.5 kN/m$^3$. The followings are major conclusions from these tests.

- The strength parameters depend on the degree of saturation of the soil. The angle of internal friction decreases with the increase of the degree of saturation from its maximum value at the dry state of the soil and reaches the minimum value at the degree of saturation of 10 to 30%. Beyond that, the angle of internal friction increases with the increase of the degree of saturation, reaching the maximum value at the submerged condition.

- The apparent cohesion is negligible for dry and saturated soil. It increases with the increase of the degree of saturation from the dry condition and reaches a maximum value beyond which it decreases with the minimum value at the saturated condition. The highest cohesion of around 20 kPa was obtained for the dry unit weight of 17 kN/m$^3$ of the soil. The maximum apparent cohesion for the dense soil (the dry unit weight of 18.5 kN/m$^3$) was less (~10 kPa).
- The suction stress calculation method from the SWCC generally provides higher suctions stress at the lower moisture contents and cannot account for the reduction of the suction stress at very low degrees of saturation. Although the suction stresses calculated using the SWCC show a similar trend as those obtained from the results of direct shear and triaxial tests for the sand with the dry unit weight of 18.5 kN/m$^3$, these were significantly different for the sand with the dry unit weight of 17 kN/m$^3$.

## 5.5 References

Gallage, C., and Uchimura, T. 2016. Direct Shear Testing on Unsaturated Silty Soils to Investigate the Effects of Drying and Wetting on Shear Strength Parameters at Low Suction, *Journal of Geotechnical and Geoenvironmental Engineering,* 142 (3): 1–9.

van Genuchten, M.T. 1980. "A Closed-Form Equation for Predicting the Hydraulic Conductivity of Unsaturated Soils." *Soil Science Society of America Journal* 44: 892–898.

Likos, W. J., Wayllace, A., Godt, J., and Lu, N. 2010. "Modified Direct Shear Apparatus for Unsaturated Sands at Low Suction and Stress." *Geotechnical Testing Journal* 33

(4): 286–298.

Lu, N., Godt, J. W., and Wu, D. T. 2010. "A Closed-form Equation for Effective Stress in Unsaturated Soil." *Water Resources Research* 46 (5): W05515.

Lu, N., Kaya, M., and Godt, J.W. 2014. "Interrelations among the Soil-Water Retention , Hydraulic Conductivity , and Suction-Stress Characteristic Curves," no. 1983: 1–10. https://doi.org/10.1061/(ASCE)GT.1943-5606.0001085.

Lu, N., Kim, T., Sture, S., and Likos, W. J. 2009. Tensile strength of unsaturated sand, Journal of Engineering Mechanics, ASCE, 135(12): 1410-1419.

Lu, N., and Likos, W.J. 2006. "Suction Stress Characteristic Curve for Unsaturated Soil." *Journal of Geotechnical and Geoenvironmental Engineering* 132 (2): 131–142.

Lu, N., and Wu, B. 2005. "Unsaturated Shear Strength Behavior of a Fine Sand." In *Second Japan-U.S. Workshop on Testing, Modeling, and Simulation in Geomechanics*, 488–499. Kyoto, Japan: ASCE.

Maleki, M., and Bayat, M. 2012. Experimental Evaluation of Mechanical Behavior of Unsaturated Silty Sand under Constant Water Content Condition, Engineering Geology, 141–142: 45–56. https://doi.org/10.1016/j.enggeo.2012.04.014

Maleksaeedi, E., Nuth, M., Sarlati, S., and Chekired, M. 2017. "Experimental Study of Suction Stress Characteristic Framework for Granular Materials Using Conventional Direct Shear Test." In *PanAm Unsaturated Soils 2017*, 289–298. Dallas, Texas: ASCE. https://doi.org/https://doi.org/10.1061/9780784481684.030.

Oh, S., Lu, N., Kim, Y. K., Lee, S. J., Lee, S. R. 2012. “Relationship between the Soil-Water Characteristic Curve and the Suction Stress Characteristic Curve : Experimental Evidence from Residual Soils” 138 (January): 47–57. https://doi.org/10.1061/(ASCE)GT.1943-5606.0000564.

Ravindran, S., and Gratchev, I. 2020. “Estimation of Shear Strength of Gravelly And Sandy Soils from Shallow Landslides.” *International Journal of GEOMATE* 18 (70): 130–137.

Schnellmann, R., Rahardjo, H., and Schneider, H.R. 2013. Unsaturated Shear Strength of a Silty Sand, Engineering Geology, 162: 88–96.

Song, Y. 2014. “Suction Stress in Unsaturated Sand at Different Relative Densities.” *Engineering Geology* 176: 1–10. https://doi.org/10.1016/j.enggeo.2014.04.002.

Terzaghi, K. 1936. “The Shear Resistance of Saturated Soils.” In *Ist International Conference Soil Mechanics and Foundation Engineering, Cambridge*, MA, 1, 54-56.

# CHAPTER 6 Conclusion and Future Recommendation

## 6.1 General

The strength and deformation characteristics of the backfill material significantly govern the behavior of the buried structures. The backfill material can be in dry, unsaturated, and saturated conditions depending upon the climatic conditions. The behavior of the soil subjected to various moisture condition is very complex. This thesis presents an investigation of the behavior of a manufactured sand under various moisture contents. Conventional direct shear tests and triaxial tests were conducted to investigate the soil under various densities, moisture contents, and stress levels. In this chapter, the overall findings from this research are discussed. The specific conclusions related to different aspects are discussed in Chapters 3, 4, and 5.

## 6.2 Major Findings from the Direct Shear Test Program

- Although the same compaction effort was applied during sample preparation, the dry density of the sand was different for different moisture contents. Thus, the test results were influenced by the densities of the soil, in addition to the moisture contents and the stress levels considered in the test programs.
- The effect of matric suction on the apparent cohesion is negligible for the range of moisture content considered (1% to 6%) during the direct shear tests. It is likely because the air voids in the granular soil are connected in the direct shear apparatus, resulting in the air pressure the same as the atmospheric pressure.

- The friction angle of the moist soil was found to change due to changes in the dry unit weight (or relative compaction) during the tests. The soil with higher relative compaction had a higher friction angle. However, the rate of increase of the friction angle was less at lower relative compactions and was very high at high relative compactions (>90%).
- At low normal stresses (<50 kPa), the peak friction angles were higher than those at higher normal stresses for dense conditions of the soil. The effect of normal stress on the friction angle was insignificant for uncompacted (loose) sands.
- The rate of shearing within the range of 0.25 mm/min to 1.5 mm/min was found to have insignificant effects on the behavior of the dry soil.
- The removal of around 18% of coarse particles (retained on #8 sieve) from the sand did not affect the peak friction angle significantly.

## 6.3 Major Findings from the Triaxial Test Program

- Apparent cohesion, resulting from suction stress, was observed from the triaxial tests. However, the magnitude of the apparent cohesion was not significantly high for the soil (ranged from 9.8 kPa to 15.5 kPa). The corresponding isotropic tensile strengths (suction stress) are 10.8 kPa to 18.4 kPa.

- Similar to the results obtained from the direct shear test program, the shear strength parameters were found to vary with the degrees of saturation due to the changes in the dry unit weights. The saturated soil sample had the highest magnitudes of shear strength parameters, which also had the highest relative density.

- Both the apparent cohesion and angle of internal friction are the lowest at the degree of saturation of 29.5%, which is attained at 6.98% moisture content. The suction stress and dry unit weight were also the lowest at this moisture content. Obtaining full saturation (with B values of 1) of the soil during the test was a challenge during the triaxial tests. It may cause suction (apparent cohesion) in the saturated sand.

### 6.4 Tests at Constant Densities

- The strength parameters of soil with constant dry density varies with the degree of saturation.
- The angle of internal friction initially decreases with the increase of the degree of saturation from its maximum value in the dry soil and then increases. The minimum friction angle was observed at the degree of saturation of 10 to 30%.
- The apparent cohesion is negligible for dry and saturated soil. The apparent cohesion increases initially with the degree of saturation from the dry condition and then decreases with a further increase of the degree of saturation. The highest cohesion of around 20 kPa was obtained for the dry unit weight of 17 $kN/m^3$ of the soil. The maximum apparent cohesion for the dense soil (the dry unit weight of 18.5 $kN/m^3$) was less (10 kPa).
- The suction stress calculation method from the SWCC cannot account for the low suction stress at lower degrees of saturation observed during the direct shear and triaxial tests.

## 6.5 Recommendation for Future Study

The soil is a very complex natural material whose behavior is influenced by various conditions. Laboratory investigation can provide an improved understanding of the behavior of the soil. In this thesis, an investigation was conducted to understand the behavior of a locally manufactured sand. The following presents a list of recommendations for further improvement in the understanding of the behavior of the sand.

- Testing in soil mechanics is subject to random errors, resulting in variabilities in the test results. The random errors can be measured by the scatter in the results from repeated tests (Selig and Ladd 1973). A statistical approach can be undertaken to correctly identify soil parameters by minimizing random errors.
- Structural backfill materials are often subjected to low stresses. Testing of soil at low stresses is difficult using conventional test apparatus. Research can be undertaken to identify the concerns with the application of low confining pressure and address the concerns.
- In the current study, the conventional testing apparatus was used to investigate the soil behavior. The findings from the tests with the conventional device should be compared with the test results using specially designed equipment for unsaturated soil. Particularly, the measurement of suction during the tests would provide valuable information to interpret the observed behaviors.

- Based on a detailed study, different correlations of soil parameters for dry, unsaturated, and saturated soils can be developed for use in the design.
- Mineralogical analysis of the sand is also recommended to characterize the soil grains.

## 6.6 References

Selig, E.T., and Ladd, R.S. 1973. "Evaluation of Relative Density Measurements and Applications." In *Evaluation of Relative Density and Its Role in Geotechnical Projects Involving Cohesionless Soils*, 487–504. Los Angeles, USA: ASTM STP523-EB.7744-1.

## APPENDIX A  Direct Shear Test

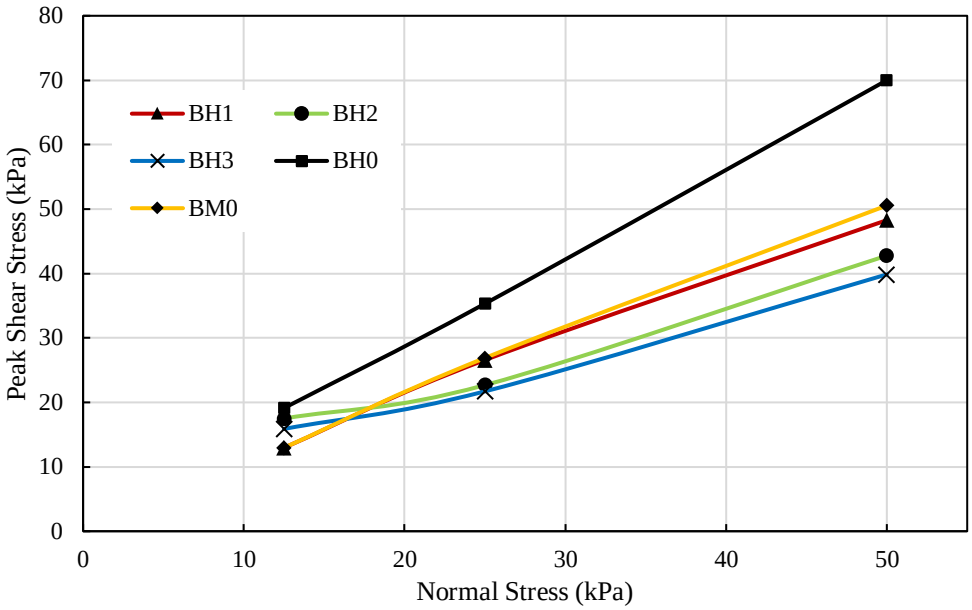


**Figure A-1**: Shear stress–Normal stress plot for sample B with compaction

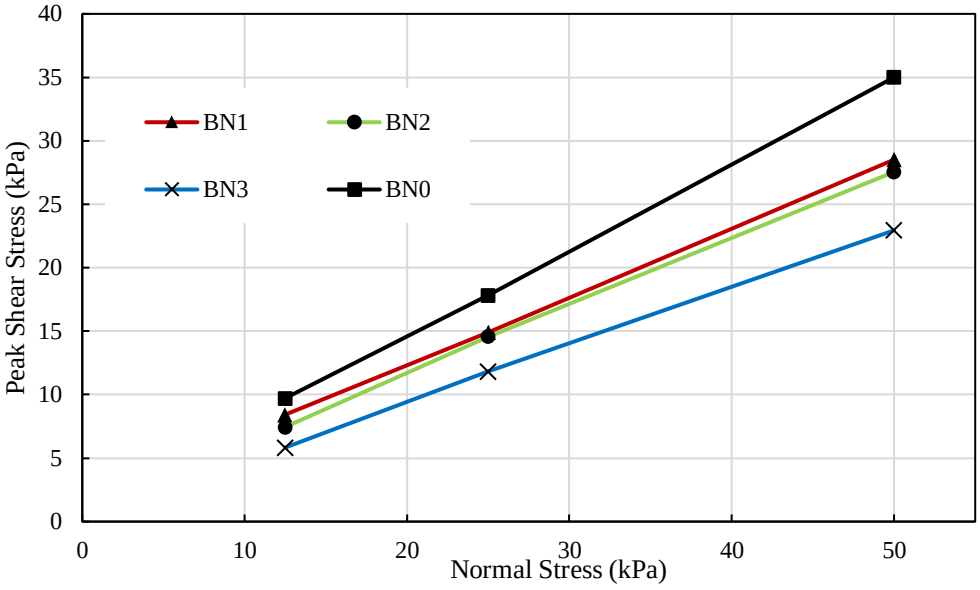


**Figure A-2**: Shear stress–Normal stress plot for sample B without compaction

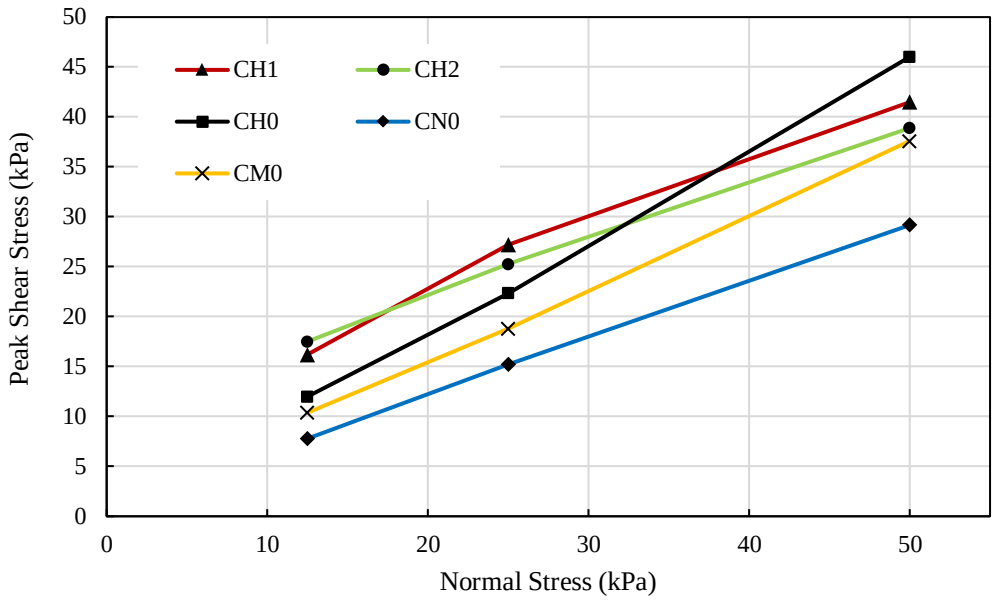


**Figure A-3**: Shear stress–Normal stress plot for sample C

## APPENDIX B  Triaxial Test

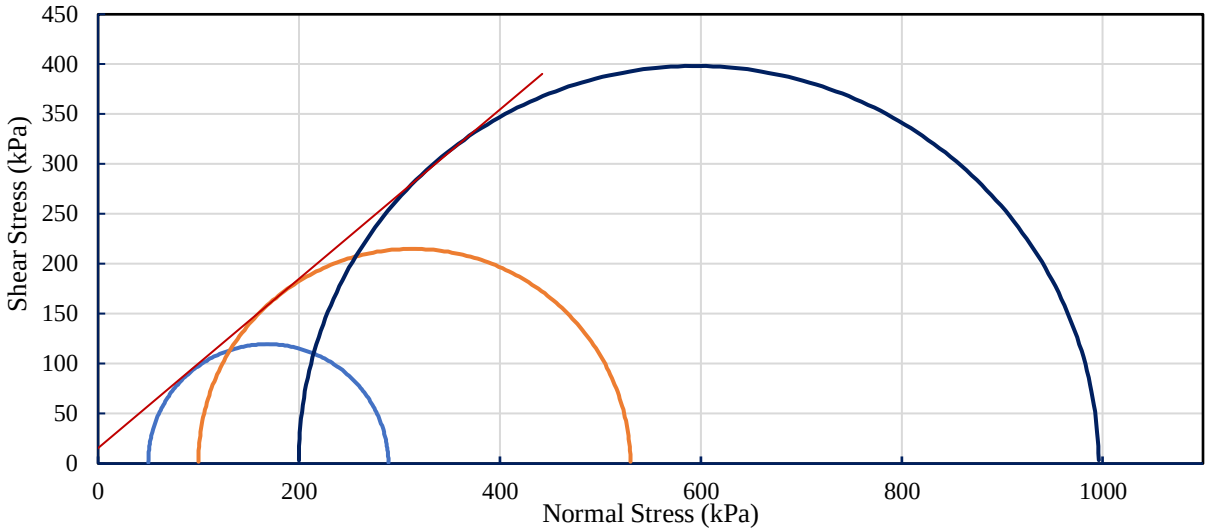


**Figure B-1**: Mohr-Coulomb failure envelope for sand sample with 2.93% moisture and $\gamma_d$ of 17.58 kN/m$^3$

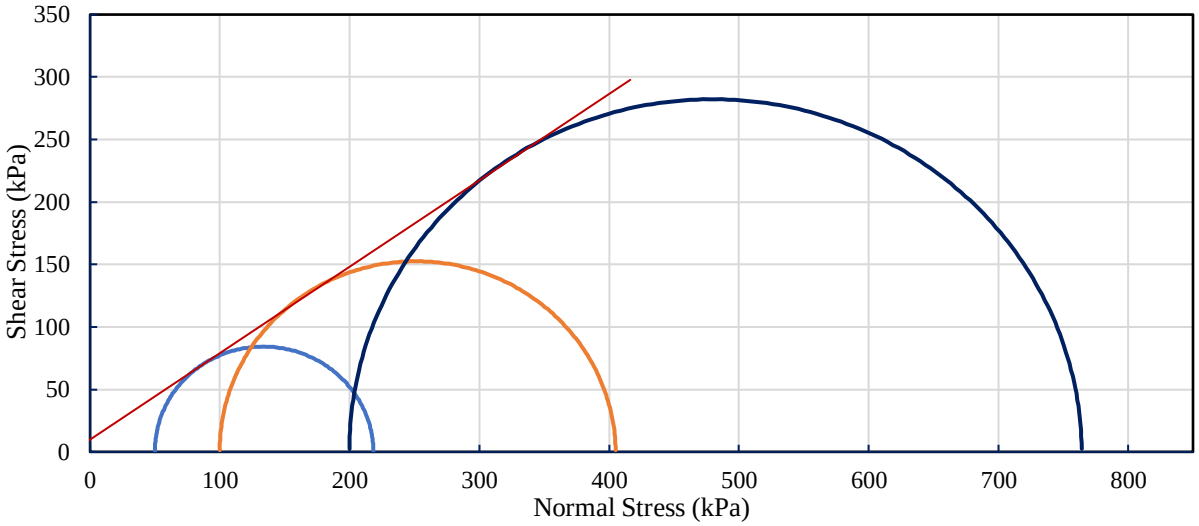


**Figure B-2**: Mohr-Coulomb failure envelope for sand sample with 6.98% moisture and $\gamma_d$ of 15.98 kN/m$^3$

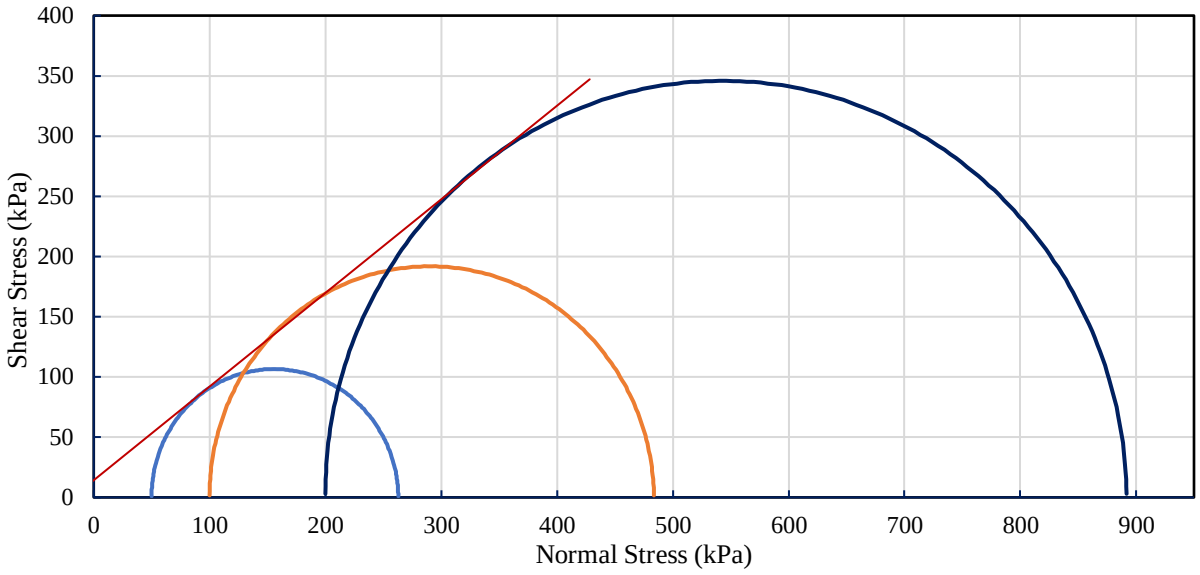


**Figure B-3**: Mohr-Coulomb failure envelope for sand sample with 11.88% moisture and $\gamma_d$ of 17.10 kN/m$^3$

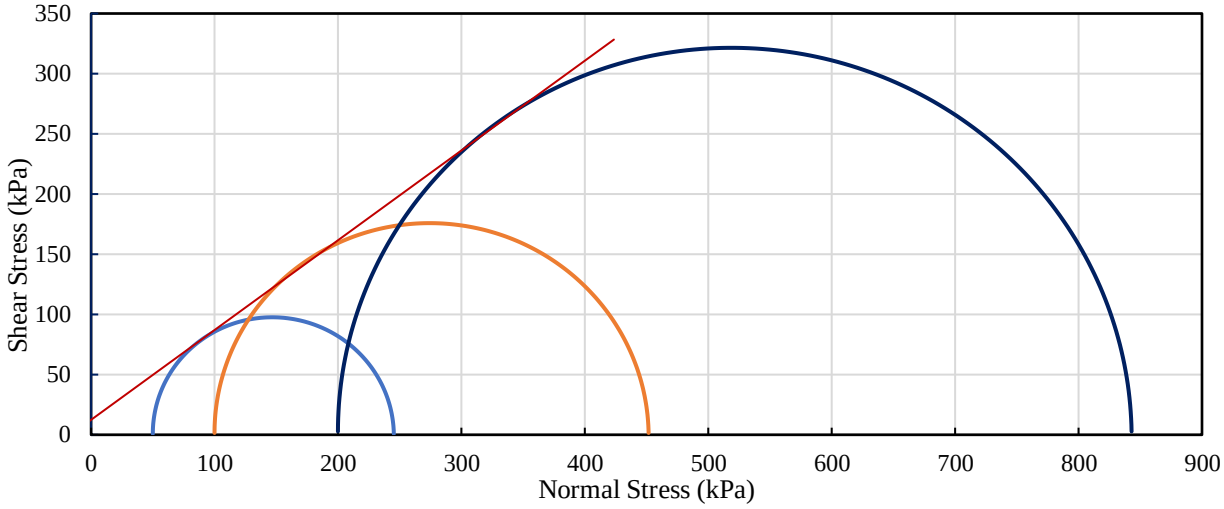


**Figure B-4:** Mohr-Coulomb failure envelope for sand sample with 2% moisture and $\gamma_d$ of 17 kN/m$^3$

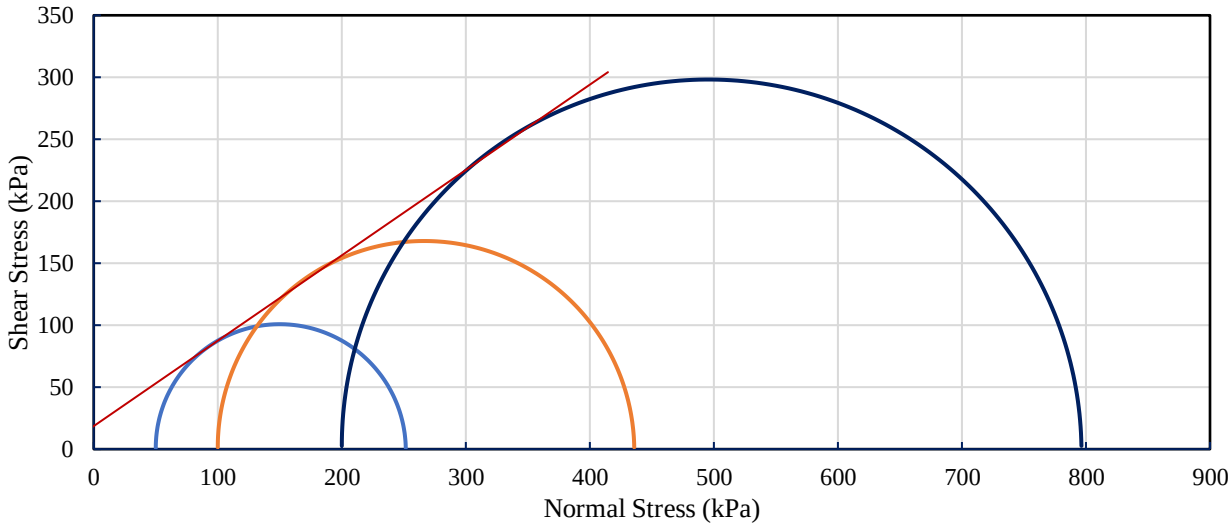


**Figure B-5**: Mohr-Coulomb failure envelope for sand sample with 4% moisture and $\gamma_d$ of 17 kN/m$^3$

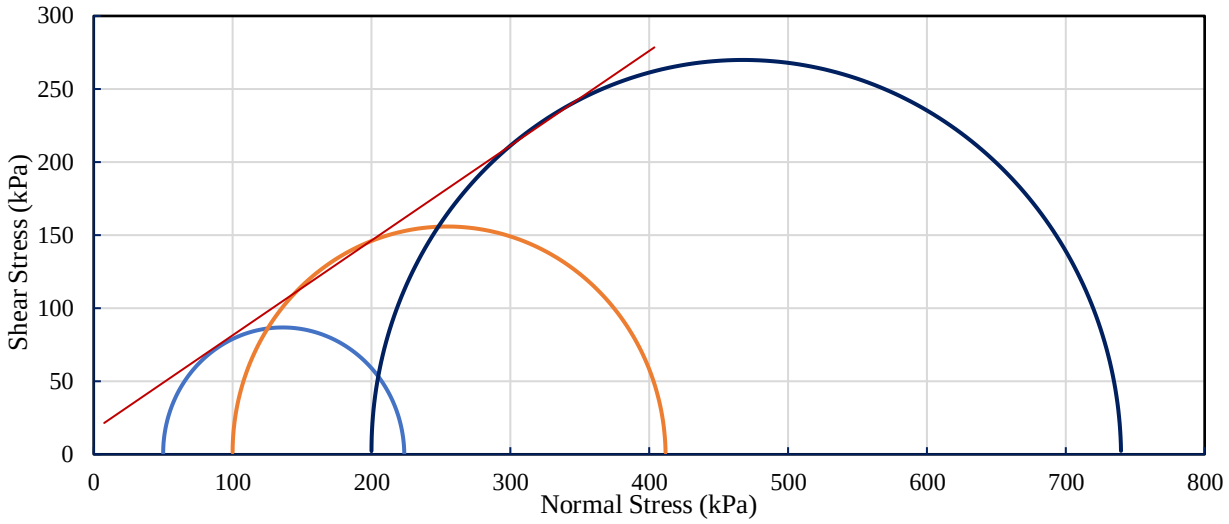


**Figure B-6**: Mohr-Coulomb failure envelope for sand sample with 6% moisture and $\gamma_d$ of 17 kN/m$^3$

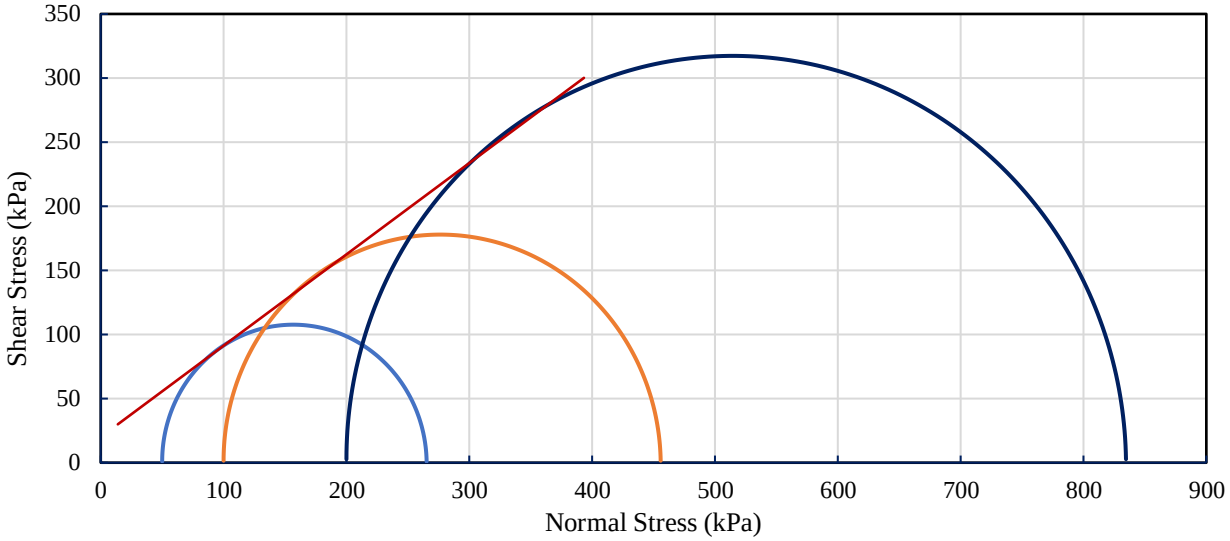


**Figure B-7**: Mohr-Coulomb failure envelope for sand sample with 8% moisture and $\gamma_d$ of 17 kN/m$^3$

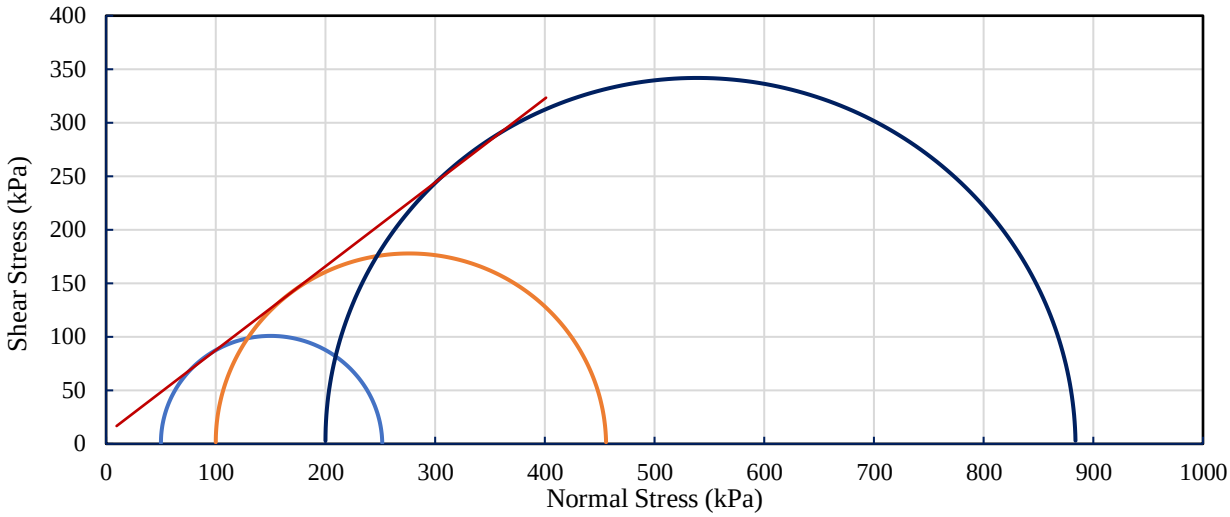


**Figure B-8**: Mohr-Coulomb failure envelope for sand sample with 10% moisture and $\gamma_d$ of 17 kN/m$^3$

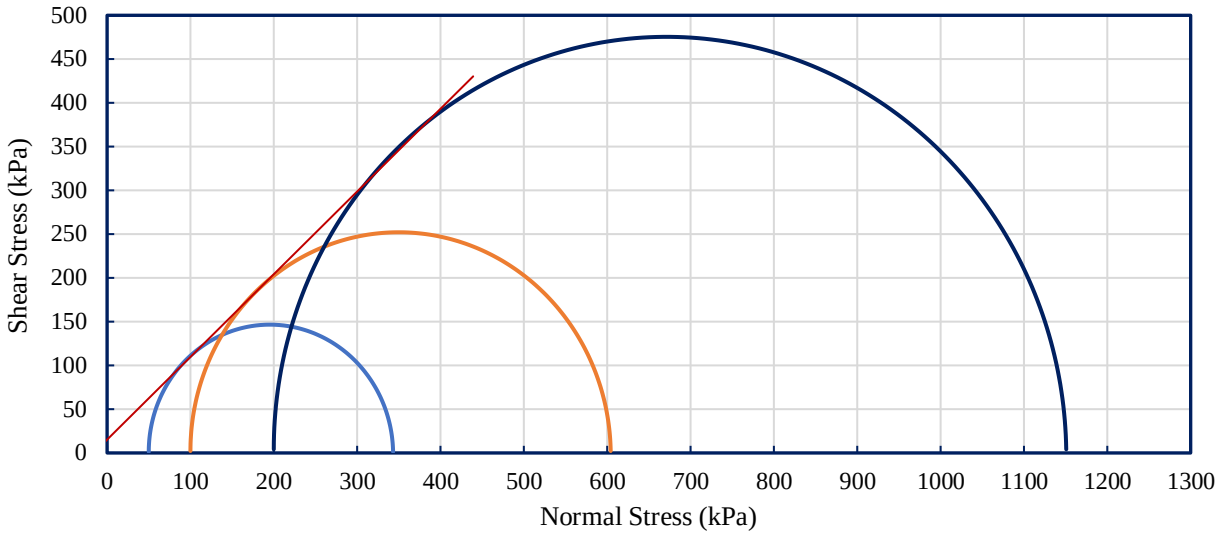


**Figure B-9**: Mohr-Coulomb failure envelope for sand sample with 2% moisture and $\gamma_d$ of 18.5 kN/m$^3$

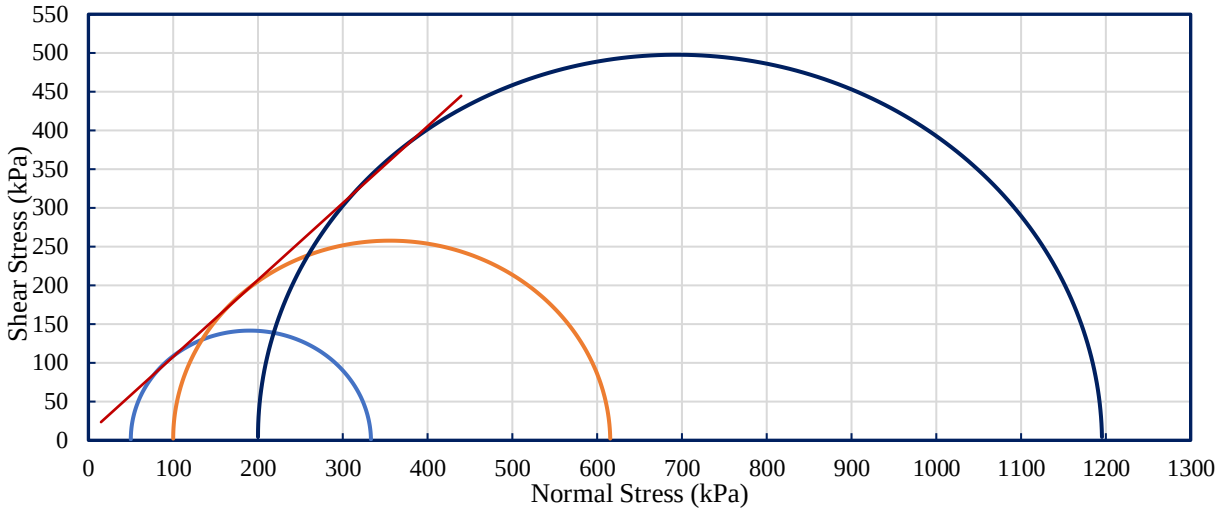


**Figure B-10**: Mohr-Coulomb failure envelope for sand sample with 6% moisture and $\gamma_d$ of 18.5 kN/m$^3$

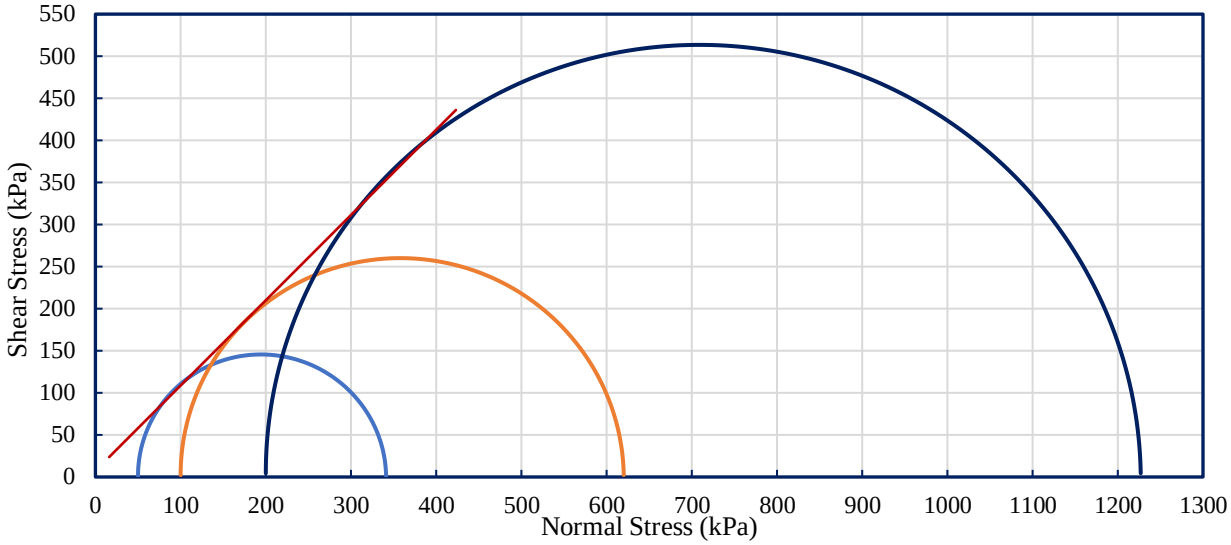


**Figure B-11**: Mohr-Coulomb failure envelope for sand sample with 10% moisture and $\gamma_d$ of 18.5 kN/m$^3$